CONVENTIONAL AND OFFSET QUADRATURE PHASE-SHIFT KEYING (QPSK & O-QPSK) FOR DIGITAL COMMUNICATIONS BY SATELLITE *

ELIAS PSARRAS

A MAJOR TECHNICAL REPORT

IN

THE DEPARTMENT

OF

ELECTRICAL ENGINEERING

Presented in Partial Fulfillment of the Requirements

for the Degree of Master of Engineering at

Concordia University

Montreal, Quebec, Canada

April 1980

ABSTRACT

CONVENTIONAL AND OFFSET QUADRATURE PHASE-SHIFT KEYING (QPSK & O-QPSK) FOR DIGITAL COMMUNICATIONS BY SATELLITE :

Elias Psarras

Conventional and offset phase-shift keying (QPSK & O-QPSK) modulation techniques are often considered for use in nonlinear bandlimited satellite channels, because both techniques have efficient detection performances.

The objective of this report is to examine the performance of QPSK and O-QPSK modulation formats for nonlinear channels having bandwidths approximately equal to the data rate bandwidth. Theoretical aspects of both modulation schemes are analytically presented. Non-filtered and filtered modulated waveforms, bandwidth occupancy, band-limiting and non-linearity effects on both signals, carrier recovery techniques and phase ambiguity resolution are treated in particular. The behaviour of QPSK and O-QPSK in nonlinear bandlimited environments is examined extensively. Although O-QPSK has less overall amplitude variations than QPSK, and seems to behave better, it has larger amplitude variations at the sampling instants. This implies that O-QPSK suffers more from nonlinearities than QPSK, and consequently its overall performance degrades more.

The paper is enriched with computer simulation and test results [1], [2], [3], [4], on the comparative performance of QPSK and O-QPSK along with MSK. The results indicate that the bit error performance

of QPSK is superior to the others, when the signal is transmitted through a narrowband channel. In a wideband channel, however, O-QPSK performs slightly better than QPSK and MSK.

ACKNOWLEDGEMENT

I wish to express my gratitude and appreciation to Dr. D.T. Gibbons for supervising this study, and for his valuable guidance and suggestions throughout the course of this investigation. I would also like to express my appreciation to Canadian National Canadian Pacific (CNCP) Telecommunications, Montreal, for the support and facilities given to me in preparing this report.

Finally, I wish to thank my wife, Eva, whose devotion and understanding encouraged me and gave me the time to complete this report.

TABLE OF CONTENTS

LIST OF FIGURES

LIST OF TABLES

LIST OF SYMBOLS AND ABBREVIATIONS

A	Amplitude of the Carrier Signal
ASK	Amplitude Shift Keying
B_sT	Normalized Baseband Bandwidth
BER	Bit Error Rate
BPSK	Binary Phase Shift Keying
BTR	Bit Timing Recovery
CTR	Carrier Timing Recovery
γ	Bit Energy Ratio
d_k	Bit Stream
$d_I(t)$	Symbol Stream that Modulates the In-phase Carrier
$d_Q(t)$	Symbol Stream that Modulates the quadrature phase carrier
E	Bit energy
f	Frequency Offset from the Carrier
f_b	Bit Rate
f_c	Carrier Frequency
FSK	Frequency Shift Keying
FFSK	Fast Frequency Shift Keying
ϕ	Phase of Received Signal Plus Noise
ϕ_T	Random Phase of the Carrier
$\phi\{r(t)\}$	Phase Distortion introduced by a TWTA
G(f)	Power Spectral Density
$G_{MSK}(f)$	Power Spectral Density of MSK
$G_{O\text{-}QPSK}(f)$	Power Spectral Density of O-QPSK
$G_{QPSK}(f)$	Power Spectral Density of QPSK
h(t)	Impulse Response

K_o	Optimum Threshold Value
N_ϕ	Power Spectral Density of Noise
n(t)	Narrowband Additive White Gaussian Noise
NRZ	Non Return to Zero (Data)
O-QPSK	Offset Quadrature Phase Shift Keying
PSK	Phase Shift Keying
P(e)	Error Probability
QPSK	Quadrature Phase Shift Keying
$R(\tau)$	Autocorrelation Function
RZ	Return to Zero(Data)
R{r(t)}	Amplitude Distortion introduced by a TWTA
ρ	Correlation Coefficient
$S_{O\text{-}QPSK}(t)$	The O-QPSK Signal
$S_{QPSK}(t)$	The QPSK Signal
$S_i(t)$	Transmitted Signal
T	Bit Period
t	Time
U_m	Message Signal(Data)
ω	Radiation Frequency.
ω_c	Radiation Carrier Frequency
X(f)	Fourier Transform of x(t)
$W_o(f)$	Power Spectrum at the output of a TWTA

CHAPTER ONE

1. INTRODUCTION

Digital communications via digital satellite systems is expanding at an ever increasing rate. The reason is that satellite communications offers efficient and economic means of communicating digital data, when it is compared with terrestrial microwave and cable systems. The desire also to use more efficiently the power and bandwidth of available channels, and the evolution of integraded circuit technology as well as the case of transmitting signals using digital techniques, have contributed to the initiation of intensive work, during the past few years, towards the improvement of satellite communications.

In the past, analog FM techniques have been used on satellite communications systems. To accommodate a large number of simultaneous messages frequency division multiplexing (FDM) has been used from any given ground station. Such earth terminals produce FDM/FM signals. Early communications satellites were severely power limited but the occupied bandwidth was more than sufficient. Thus, the use of large modulation index FM was a good trade-off of power at the expense of bandwidth. Modern high capacity satellite systems were considered to be bandwidth-limited rather than power limited [5]. In these systems, a large number of ground stations, with a different volume of message traffic, simultaneously access a satellite channel or transponder. This is known as a multiple access satellite system. Two well-known digital multiple access techniques are, the Time Division Multiple Access System

(TDMA) and the Single Channel Per Carrier System (SCPC).

The ever increasing demand for digital transmission requires the implementation of transmission techniques that can handle as high and as accurate a data rate as possible. This implies the necessity of developing transmission systems which can transmit a given data rate over a long distance, using as little bandwidth as possible while achieving a small bit error rate for a given transmitted power, which is limited in satellite communications systems. This ever increasing demand for more efficient digital transmission channels has stimulated the investigation of advanced modulation techniques.

As will be seen in Chapter Two, Phase Shift-Keying (PSK) is the optimum digital modulation method. For this reason, Binary Phase Shift-Keying (BPSK) is a very popular digital transmission technique that is most frequently used in its quadrature format. Quadrature Phase Shift-Keying (QPSK) is a combination of two BPSK data channels that results in the ability to transmit two information bits/sec (theoretically) in a unit of the occupied bandwidth.

Studies have shown that the use of either BPSK or QPSK modulation is particularly suitable for digital data transmission via a satellite link. The power spectrum of PSK signals, however, contain sidelobes that may interfere with other communication systems. To suppress the out-of-band interference, the sidelobes must be removed by filtering at the transmitter.

As a result of such filtering, an AM component arises which produces undesired results when the signals pass through nonlinear devices such as a Traveling Wave Tube Amplifier (TWTA) in the satellite transponder. Because of the limited available power in the satellite

transponder, the TWTA is usually operated at, or near, saturation where its maximum peak output exists. In this operating mode, the TWTA exhibits two types of nonlinear effects. First, there is a nonlinear output envelope versus input envelope relationship (AM/AM conversion) and secondly, there is a nonlinear output phase versus input envelope relationship (AM/PM conversion). Owing to the aforementioned amplitude fluctuations, the performance of the PSK systems deteriorates, especially, if AM is converted into PM. Moreover, if after a conventional PSK modulator followed by a suitable filter, a hardlimiter is inserted, the power spectrum of the PSK signal at the output of the limiter appears to be about the same as that before the filtering. Hence, after the signal has passed through nonlinear devices, additional filtering will be required to reduce interference into adjacent channels.

In conventional QPSK, the in-phase and quadrature data streams are synchronously aligned. An instantaneous carrier phase shift at 180° occurs when both binary components change state simultaneously. Such transitions of 180° in the carrier phase plane results in the most severe amplitude fluctuation of the carrier envelope caused by bandlimiting. This envelope amplitude fluctuation of a QPSK signal causes distortion and power spectrum spreading when it passes through a nonlinear device.

Recently, modulation formats similar to QPSK format have evolved. Offset-Quadrature Phase Shift-Keying (O-QPSK) and Minimum Shift Keying (MSK) have gained increasing popularity for use in band-limited nonlinear channels as alternatives to conventional QPSK format. Both of them have the same bandwidth efficiency with QPSK, that is, theoretically 2b/s/Hz, and their envelope fluctuation is smaller in comparison with that of the QPSK signal. As a result, less power spectrum spreading occurs

when they pass through a nonlinear device. Thus, it has been foreseen that the use of O-QPSK and MSK over nonlinear satellite channels will improve transmission performance over that of QPSK.

O-QPSK is derived from conventional QPSK by applying a delay of half the symbol period ($T_s/2$) to one of the data streams. By this method, the instantaneous phase shift of 180° is avoided and the band-limited O-QPSK signals does not go through zero. Thus the envelope variation is smaller in comparison with that of QPSK signal and therefore less spectrum spreading will occur when it passes through a nonlinear device. The same advantage is met with MSK signals.

MSK can be viewed either as a form of coherent frequency shift-keyed modulation with spectral spacing between the two transmitted tones (mark and space) equal to half the bit rate, or as a special case of O-QPSK. In the latter case, MSK is simply an O-QPSK modulation with sinusoidal weighting of the symbols which modulate the two quadrature carriers. Thus, the difference between O-QPSK and MSK lies in baseband data pulse shape. The shape of the baseband data pulses are rectangular in O-QPSK, whereas they are half cosine in MSK. Due to its sinusoid pulses, MSK has a smoother phase transition than the O-QPSK signal. However, its main spectral lobe is 50% wider than that of QPSK or O-QPSK and its transmitted spectrum would have to be severely filtered in applications with closely spaced channels (narrowband channels). This would reintroduce signal envelope fluctuation and because of that its use in narrowband nonlinear channels is not preferred.

Although O-QPSK and MSK have less overall envelope variations than QPSK, they have much larger envelope variations at the times it matters, i.e. the sampling points. Because of this, O-QPSK and MSK

signals suffer more from nonlinearities than QPSK signal, and as a result, their overall system performance will degrade more.

The subject of this report focusses on the presentation and analysis of QPSK and O-QPSK signals in nonlinear channels. It is organized around the principles of PSK signalling, the analysis of the QPSK and O-QPSK waveforms along with their filtered envelope fluctuation, the implementation of a quaternary PSK modem and finally the presentation of computer simulation and test results on the comparative performance of QPSK and O-QPSK for systems including nonlinear device.

CHAPTER TWO

2. PRINCIPLES OF PHASE SHIFT-KEYING (PSK)

2.1 SIGNAL OPTIMIZATION

2.1.1 Optimum Receiver Structure and Error Probability

When a bit stream is to be sent over a channel, it is either transmitted directly or indirectly (i.e. using a modulation process), depending upon the application.

Since in this report only binary digital communication systems are considered, it implies that the message signal consists of only two levels. Thus, it will be assumed that the message signal (data) is a bit stream of a bit rate R, related to the bit period T by R = 1/T, and is of the form

$$U_m(t) = \begin{cases} V_1 \text{ for logic "0"} \\ V_2 \text{ for logic "1"} \end{cases} \tag{2.1.1}$$

The transmitted signal $S_i(t)$ is of the form

$$S_i(t) = \begin{cases} S_1(t) \text{ for } U_m(t) = V_1 \\ S_2(t) \text{ for } U_m(t) = V_2 \end{cases} \tag{2.1.2}$$

with the only restriction that both $S_1(t)$ and $S_2(t)$ have finite energy in the bit period T. The bit energies E_1 and E_2 are:

$$E_1 = \int_{kT}^{(k+1)T} S_1^2(t)\, dt$$

$$E_2 = \int_{kT}^{(k+1)T} S_2^2(t)\, dt \tag{2.1.3}$$

The transmitter structure is such that it can generate and transmit the signals $S_1(t)$ and $S_2(t)$ as requested by (2.1.2) and (2.1.3).

The receiver should detect the message $U_m(t)$ from the received signal in the presence of noise with the minimum possible probability of error. Thus, it must be capable of minimizing the effect of noise in the first place. Therefore the first stage of the receiver should be a detection device with noise reduction properties. This device is called a "Receiving Filter". The output of this device is identical to the transmitted data stream, $U_m(t)$, except for the resulted errors owing to noise corruption on the received signal. To further minimize the probability of error, P(e), a sample of each detected bit is taken, at a well defined instant of each bit period. This sample is then fed into a threshold device, which decides about the value of the bit by comparing it with a threshold value K_o. Such a receiver is depicted in Fig. 2.1.1, in which the input (received) signal is

$$r(t) = S_i(t) + n(t) \qquad (2.1.4)$$

where the noise is assumed white with power spectral density $N_o/2$. The error probability for such a generalized system has been derived [6] and is given by

$$P(e) = \frac{1}{2}\,\mathrm{erfc}\left[\frac{S_{02}(T) - S_{01}(T)}{2\sqrt{2}\ \sigma_o}\right] \qquad (2.1.5)$$

where erfc(.) is the complementary error function which equals to 1-erf(.), $S_{01}(T)$ and $S_{02}(T)$ are the transmitted signals $S_1(t)$ and $S_2(t)$ at the output of the sampler (refer to Fig. 2.1.1) and σ_o is the standard deviation of the signal at the sampler output.

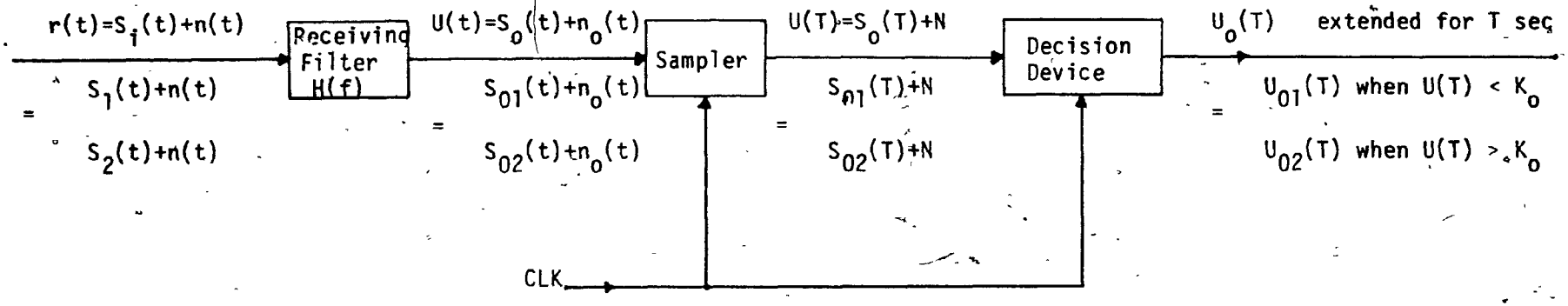

Fig. 2.1.1 Generalized Receiver for the Recovery of a Binary Data Stream

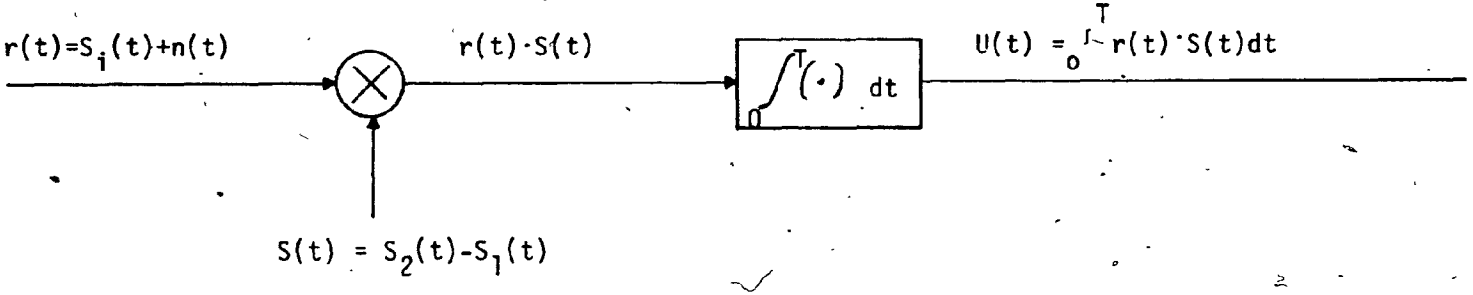

Fig. 2.1.2 Optimum Receiving Filter

Evidently, the argument of the erfc in (2.1.5) should be maximized in order for P(e) to become minimum. In other words, minimization of P(e) can be obtained by optimizing the characteristics of the receiving filter, which is then called a Matched Filter, and the receiver is called Optimum Receiver. It can be shown that the optimum receiving filter may be implemented as illustrated in Fig. 2.1.2. This implementation is sometimes referred to as a Correlator Receiver.

Referring to Fig. 2.1.2, it can be shown that the output of the receiving filter U(t) can be written in the form

$$U(t) = \int_0^T S_i(t) \, [S_2(t) - S_1(t)] \, dt \qquad (2.1.6)$$

which in turn can be expressed as

$$U_1(T) = S_{01}(T) = \rho\sqrt{E_1 E_2} - E_1 \text{ for } S_i(t) = S_1(t)$$

and (2.1.7)

$$U_2(T) = S_{02}(T) = E_2 - \rho\sqrt{E_1 E_2} \text{ for } S_i(t) = S_2(t)$$

where ρ is the correlation coefficient of $S_1(t)$ and $S_2(t)$ defined by

$$\rho = \frac{1}{\sqrt{E_1 E_2}} \int_0^T S_1(t) \, S_2(t) \, dt \qquad (2.1.8)$$

Since $S_1(t)$ and $S_2(t)$ have equal probabilities and the conditional probability density functions of the filter output are symmetrical, the optimum threshold value, K_o, is

$$K_o = \frac{1}{2} \, [S_{01}(T) + S_{02}(T)] \qquad (2.1.9)$$

Applying equations (2.1.7), K_o, can be rewritten in the form

$$K_o = \frac{1}{2}[E_2 - E_1] \qquad (2.1.10)$$

The bit error rate performance of the optimum receiver in a White Gaussian Noise environment and for infinite bandwidth is given by [6]

$$P(e) = \frac{1}{2}\,\mathrm{erfc}\left[\frac{E_1 + E_2 - 2\sqrt{E_1 E_2}\,\rho}{4N_o}\right]^{1/2} \qquad (2.1.11)$$

where N_o is the power spectral density of the noise.
By noting

$$E = \frac{E_1 + E_2}{2} \qquad (2.1.12)$$

as the average received bit energies, and

$$\gamma^2 = \frac{E_2}{E_1} \qquad (2.1.13)$$

as the bit energies ratio, eq. (2.1.11) becomes

$$P(e) = \frac{1}{2}\,\mathrm{erfc}\left[\frac{E}{2N_o}\left(1 - \frac{2\gamma}{1+\gamma^2}\,\rho\right)\right]^{1/2} \qquad (2.1.14)$$

2.1.2 Optimum and Suboptimum Signalling

Once the receiver optimization is accomplished and the bit error performance for the optimum receiver is evaluated as in Equ. (2.1.14) the values of the parameter γ and ρ, which affect P(e), are then optimized. By doing so, the signal $S_i(t)$ is actually optimized and therefore the transmitter itself.

First, the parameter γ^2 can be optimized by differentiating the term

$$1 - \frac{2\gamma}{1+\gamma^2}\,\rho$$

of equation (2.1.14), with respect to γ and equating the derivative to zero. Thus, the optimum value of γ^2 is found to be unity

$$\gamma_o = 1 \tag{2.1.15}$$

This means that for optimum performance the bit energies E_1 and E_2 should be equal

$$E_1 = E_2 \tag{2.1.16}$$

As a result the value of the optimum threshold, K_o, from (2.1.10) becomes

$$\text{Optimum threshold: } K_o = 0 \tag{2.1.17}$$

Applying (2.1.15) to (2.1.14) the bit error performance of the optimum receiver can be written as

$$P(e) = \frac{1}{2} \operatorname{erfc}\left[\sqrt{\frac{E}{2N_o}(1-\rho)}\right] \tag{2.1.18}$$

It is apparent from (2.1.18) that P(e) also depends on the similarity between $S_1(t)$ and $S_2(t)$ through ρ, and the value of ρ that minimizes P(e) is

$$\rho_o = -1 \tag{2.1.19}$$

for which the optimum bit error rate is obtained as

$$P(e) = \frac{1}{2} \operatorname{erfc}\left(\sqrt{\frac{E}{N_o}}\right)$$

$$= \frac{1}{2} \operatorname{erfc}\sqrt{\frac{V^2T}{2N_o}} \tag{2.1.20}$$

From the definition of ρ, equation (2.1.8), it becomes evident that, should ρ be -1 when $E_1 = E_2$, the following relation must hold:

$$E = -\int_0^T S_1(t) \cdot S_2(t)\, dt \qquad (2.1.21)$$

which is satisfied only when

$$S_1(t) = -S_2(t) \qquad (2.1.22)$$

This signal pair consists of two signals, $S_1(t)$ and $S_2(t)$, identical to each other but they differ by a phase reversal of 180°. Such signals are said to be "Antipodal" between each other and constitute the optimum signal pair for the matched filter receiver. A realizable pair of this type is:

$$S_1(t) = A \cos \omega_c t$$
$$S_2(t) = A \cos (\omega_c t + \pi) = -A \cos \omega_c t \qquad (2.1.23)$$

The transmitted signal $S_i(t)$ is, therefore, a signal of constant carrier frequency and of phase 0° or 180° to represent the mark (binary one) and space (binary zero) states respectively. Such a signal can be generated by multiplying a carrier by a Non-Return to Zero (NRZ) data stream at the transmitter. This signalling is referred to as Phase Shift-Keying (PSK). Figure 2.1.3 depicts the transmitted waveform $S_i(t)$ in relation the message signal $U_m(t)$.

Although the optimum signal choice is that of PSK, there are some practical reasons which raise the necessity of employing other suboptimum techniques. These techniques result by assigning different values to the parameters ρ and γ, and maintaining always the relation $f_1 = nR$, with n an integer, which is very critical for the threshold stability. This constraint allows only three values of ρ, namely, -1, 0 and +1. Following the same procedure and using different values of

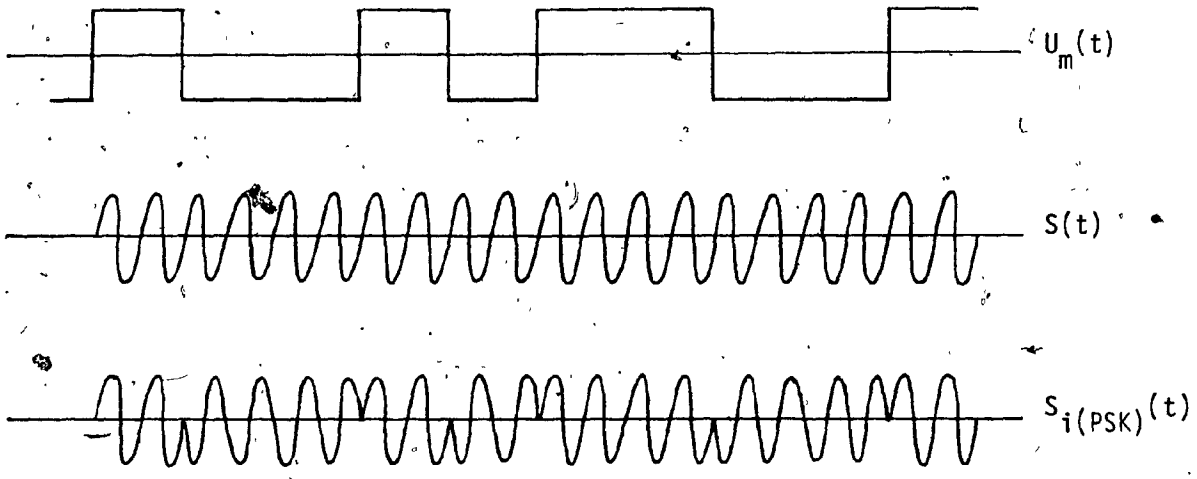

Fig. 2.1.3 The PSK System Waveforms

	$\lvert\alpha\rvert$	ρ	Signal Type	Error Probability P(e)	Comments
ASK	0	0	Orthogonal	$\frac{1}{2}\text{erfc}\sqrt{\frac{E}{2N_0}} = \frac{1}{2}\text{erfc}\sqrt{\frac{V^2T}{8N_0}}$	Suboptimum
FSK	1	0	Orthogonal	$\frac{1}{2}\text{erfc}\sqrt{\frac{E}{2N_0}} = \frac{1}{2}\text{erfc}\sqrt{\frac{V^2T}{4N_0}}$	Suboptimum
PSK	1	-1	Antipodal	$\frac{1}{2}\text{erfc}\sqrt{\frac{E}{N_0}} = \frac{1}{2}\text{erfc}\sqrt{\frac{V^2T}{2N_0}}$	Optimum

Table 2.1.1 Basic Digital Signalling Schemes

ρ and γ whose value is restricted to 1 (optimum value) and 0 ($E_1 \neq 0$, $E_2 = 0$), the bit error performances of Frequency Shift-Keying (FSK) and Amplitude Shift-Keying (ASK) are also obtained from equation (2.1.14). The error probabilities of the three basic coherent digital signalling schemes are shown in Table 2.1.1.

From this table, it becomes evident that coherently detected PSK systems require exactly 3 dB less Signal-to-Noise ratio, for any error rate compared to coherent FSK systems. This represents the advantage of using antipodal signals, as opposed to orthogonal signals. In addition, since coherent FSK involves essentially the same circuitry complexities as coherent PSK, the latter is considered as the most popular modulation method. Actual systems performance results have also proven that binary FSK requires an excess of 3 dB signal-to-noise ratio than binary PSK, for any specified bit error rate.

2.2 BINARY PHASE SHIFT KEYING (BPSK) MODULATION

In the previous section, it was seen that the PSK system is the optimum binary system using two signals which have a cross-correlation coefficient of -1, or the two signals are the negatives of each other, which means that in a carrier system the two signals differ from each other only by a phase reversal of the carrier.

A generalized PSK waveform can be represented by

$$S_{PSK}(t) = A \sin \{\omega_c t + \theta(t)\} \qquad kT \leq t \leq (k+1)T \qquad (2.2.1)$$

The digital modulation is carried in the angle of the carrier ω_c by $\theta(t)$, which assumes discrete values from a set of M equally spaced points in $[0,2\pi]$ at the sample times. Thus, the kth message or baud is

modulated by

$$\theta(t) = \phi_T + \frac{2i\pi}{M} \cdot d_k, \; i = 0,1,2\ldots M-1 \qquad (2.2.2)$$

where ϕ_T is the random phase of the carrier which is constant and independent of time. It can assume any discrete value in $[0,2\pi]$ without loss of generality. The assumption which will be used throughout this report is that

$$\phi_T = \frac{\pi}{M} \qquad (2.2.3)$$

M represents the modulation levels which are assumed to be equally probable, $d_k = \pm 1$ the bipolar data being transmitted at a rate $R = 1/T$, and A is the amplitude of the carrier. Hence,

$$S_{PSK} = A \sin \{\omega_c t + \frac{\pi}{M} + \frac{2i\pi}{M} d_k\}, \; kT \leq t \leq (k+1)T \qquad (2.2.4)$$

This general expression of a phase shift keying(PSK) signal can be expanded, using well-known trigonometric identities, as follows:

$$S_{PSK}(t) = A \left[\sin (\frac{2i\pi}{M} d_k) \cos (\omega_c t + \frac{\pi}{M}) + \cos(\frac{2i\pi}{M} d_k) \cdot \sin(\omega_c t + \frac{\pi}{M})\right] \qquad (2.2.5)$$

$$kT \leq t \leq (k+1)T$$

By substituting the modulation levels for binary PSK signalling, it can be seen that any such signal is composed of two antipodal components as was mentioned above

$$S_{PSK}(t)_{[M=2]} = S_{BPSK}(t) = A \left[\sin(d_K \cdot i\pi) \cdot \cos (\omega_c t + \frac{\pi}{2}) + \cos(d_K \cdot i\pi) \cdot \sin (\omega_c t + \frac{\pi}{2})\right] = A \cdot d_K \cos (i\pi) \cdot \cos \omega_c t \qquad (2.2.6)$$

$$kT \leq t \leq (k+1)T$$

The information, d_k, is conveyed in the phase of the carrier, as the value of $d_k \cdot \cos(i\pi) = \pm 1$ ($i=0$ for $d_k = +1$ and $i = 1$ for $d_k = -1$). Thus, the last expression can be rewritten as:

$$S_{BPSK}(t) = A\, d_k \cos \omega_c t \qquad kT \le t \le (k+1)T \tag{2.2.7}$$

From equation (2.2.7), it follows that for a bit of +1 the modulated BPSK signal equals $A\cos\omega_c t$ and for a bit of -1 equals $-A\cos\omega_c t = A\cos(\omega_c t + 180°)$, and equation (2.1.23) is verified. It is obvious that one matched filter or one correlator receiver, as shown in Fig. 2.2.1, is required to detect the data optimally in additive white noise environment.

Since the term $\cos(i\pi)$ is invariant in a baud interval, the modulating signal can be represented by a "square-pulse", and equation (2.2.7) can take the form

$$S_{BPSK}(t) = A \sum_{K=-\infty}^{\infty} d_k\, p(t-KT) \cos \omega_c t \tag{2.2.8}$$

where

$$p(t) = \begin{cases} \text{rectangular pulse for } |t| \le T \\ 0 \qquad\qquad\qquad \text{elsewhere} \end{cases}$$

The normalized (one ohm resistance) power spectrum of a BPSK signal is given by:

$$G_{BPSK}(f) = A^2 T \left[\frac{\sin \pi(f-fc)\, T}{\pi(f-fc)\, T}\right]. \tag{2.2.9}$$

where,

f_c = carrier frequency

and

f = frequency offset from the carrier.

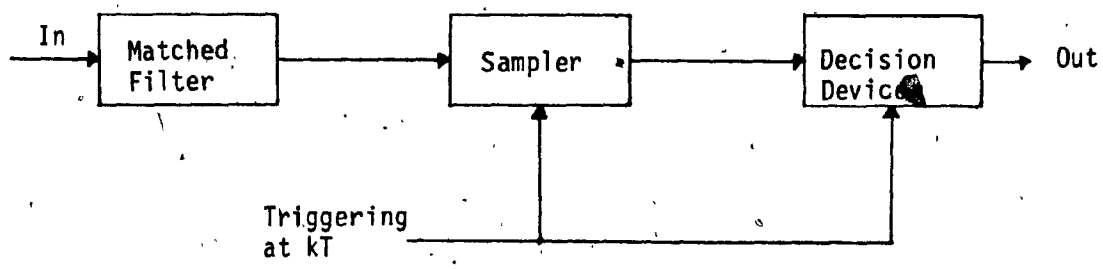

(a) Matched Filter Detector

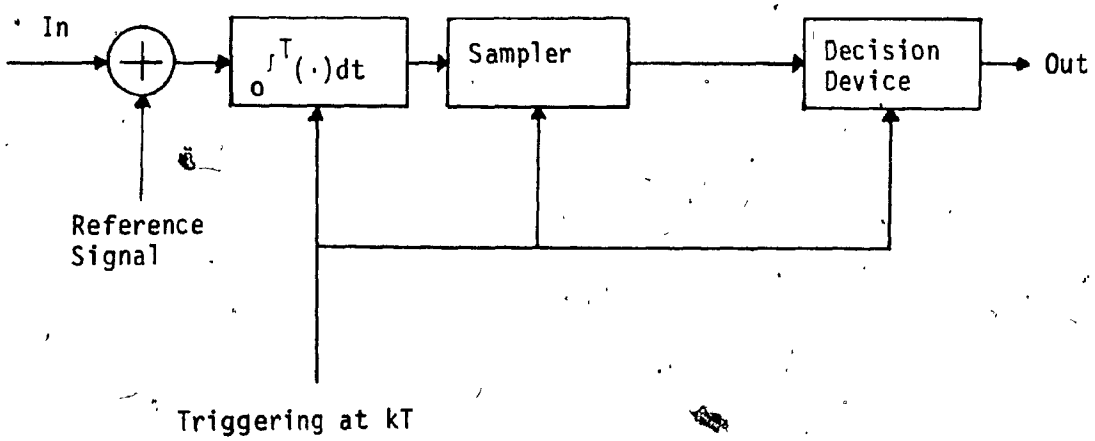

(b) Correlating Detector

Fig. 2.2.1 PSK Matched Filter and Correlating Detectors

It is known that the operation of a matched filter is to coherently combine the spectral components of the received signal, so that the ratio of the peak output signal voltage to the rms noise output voltage is maximized at a specific instant in time. By definition, a matched filter has an impulse h(t) which is the time reverse of the input signal s(t).

The output signal of the matched filter for the Kth sent pulse is given by:

$$U(t) = \int_{kT}^{(k+1)T} S(\tau) \cdot S(t-kT + \tau)\, d\tau \qquad (2.2.10)$$

where τ is the independent variable in the convolution integral. Equation (2.2.10) also represents the autocorrelation function of the input signal S(t).

Evidently, at time t = kT and while the kth pulse has been accommodated in the filter, the input autocorrelation function has its maximum value. The output autocorrelation function always has twice the duration of the input matched signal. However, although the output matched signal is dispersed in time over twice the duration of the input signal, there is no intersymbol interference (ISI) between adjacent signals (pulses). This is due to the fact that the envelope of the output autocorrelation function is decayed to zero when the subsequent signal is sampled at its maximum value, which occurs at t = kT and is given by

$$U(t) = \int_{kT}^{(k+1)T} S^2(\tau)\, d\tau \qquad (2.2.11)$$

Therefore, for optimum BPSK detection sampling must occur at the symbol rate. Differentially coherent detection is assumed for the purpose of this report.

2.3 BANDWIDTH CONSERVATION NEED - QPSK

In most applications the transmission system is considered to be more cost effective if in a given bandwidth more bits/sec are transmitted. Usually, the system efficiency is characterized in terms of transmitted bits per second per Hertz (b/s/Hz).

In binary transmission, as was mentioned previously, one transmitted symbol conveys only one information (source) bit. Hence, the data rate in bits per second equals the keying rate in bands, that is $f_b = f_s$. In a quaternary PSK transmission system each transmitted symbol conveys 2 information bits. This signal format may use phase conditions of 0°, 90°, 180° and 270° to represent the 11,01,00 and 10 logic states respectively. This is shown in Fig. 2.3.1. Substituting four modulation levels in equation (2.2.5), that is M = 4, we get:

$$S_{PSK}(t)_{[M=4]} = S_{4\phi\text{-}PSK}(t) = A \left[\sin \left(\frac{i\pi}{2} d_k\right) \cdot \cos \left(\omega_c t + \frac{\pi}{4}\right) + \cos \left(\frac{i\pi}{2} d_k\right) \cdot \sin \left(\omega_c t + \frac{\pi}{4}\right) \right] \qquad (2.3.1)$$

$$kT \leq t \leq (k+1)T \text{ and } i = 0,1,2,3$$

The information, d_k, is conveyed in the angle of both carrier components on a fifty-fifty basis. Thus, both parallel quadrature channels have the same symbol rate, which means that their bandwidths are equal. As a result, the QPSK efficiency is twice that of BPSK. The quadrature relation between its two components allows for detecting them separately, using two correlator receivers as shown in Fig. 2.3.2.

Assuming that an ideal Nyquist channel is available, the receiver will detect the 11 phase state correctly if the received carrier plus noise in the sampling instant is within the $\theta-\frac{\pi}{4}$ to $\theta+\frac{\pi}{4}$ region (Fig. 2.3.1). Otherwise, the transmitted phase state would be erroneously

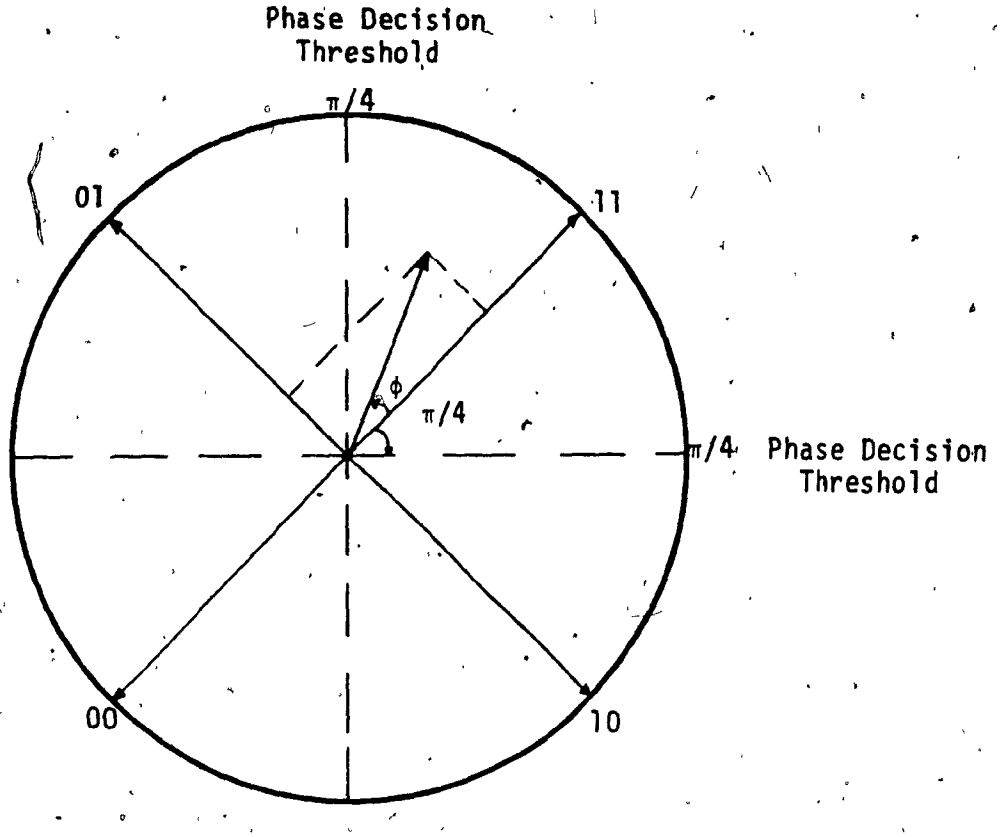

(a) Phasor Diagram

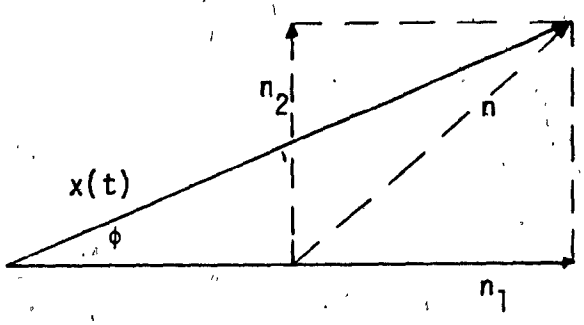

(b) Vector Diagram

Fig. 2.3.1 Phasor and Carrier Vector Diagrams of a Four-Phase PSK Demodulator

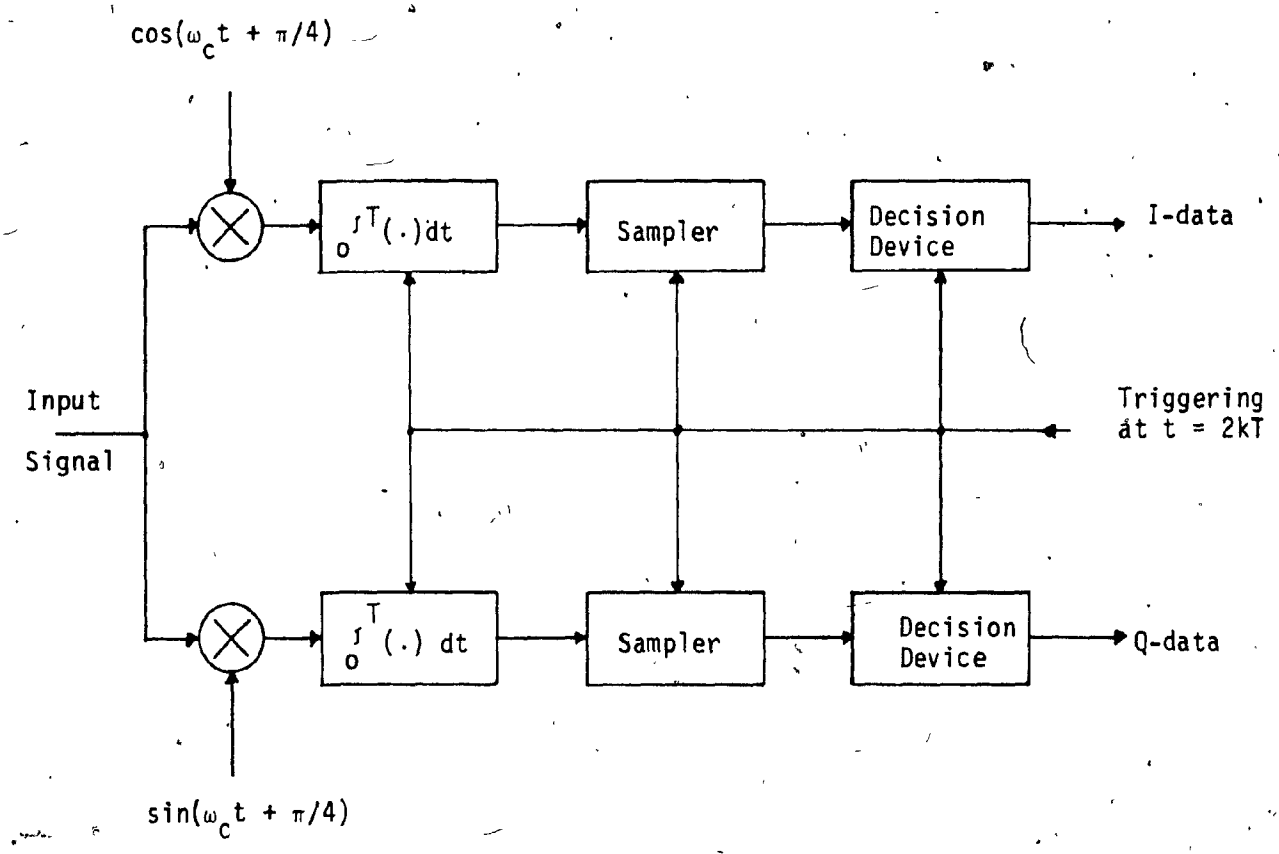

Fig. 2.3.2 Four-Phase PSK Coherent Detector

detected.

The received QPSK signal at the receiver is given by

$$x(t) = A \cos [\omega_c t + \theta(t)] + n(t) \tag{2.3.2}$$

where n(t) is the narrowband additive white Gaussian noise which may be written as:

$$n(t) = n_1(t) \cos(\omega_c t + \theta) + n_2(t) \sin (\omega_c t + \theta) \tag{2.3.3}$$

while $n_1(t)$ and $n_2(t)$ are statistically independent zero-mean Gaussian random variables having the joint function

$$p(n_1,n_2) = \frac{1}{2\pi\sigma^2} \exp \left[- \frac{n_1^2 + n_2^2}{2\sigma^2} \right] \tag{2.3.4}$$

Hence,

$$E\{n^2(t)\} = E\{n_1^2(t)\} = E\{n_2^2(t)\} = N_o \tag{2.3.5}$$

$$E\{n_1(t)\, n_2(t)\} = 0 \tag{2.3.6}$$

The received signal may then be rewritten as:

$$x(t) = A \cos (\omega_c t + \theta) + n_1(t) \cos (\omega_c t + \theta) + n_2(t) \cdot \sin (\omega_c t + \theta) \tag{2.3.7}$$

In Fig. 2.3.1, the vector diagram of the composite carrier plus noise wave is also depicted. It is evident that at the receiver an error takes place outside the region

$$\theta - \frac{\pi}{4} \leq \phi \leq \theta + \frac{\pi}{4} \tag{2.3.8}$$

where ϕ is the phase of the received signal plus noise and is given

by:

$$\phi = \theta + \tan^{-1} \frac{n_2 t}{A + n_1(t)} \tag{2.3.9}$$

The bit error probability of a QPSK signal, because of the circular symmetry, is then given by:

$$P(e) = \int_{\theta+\frac{\pi}{4}}^{\theta+\pi} p(\phi)d\phi + \int_{\theta-\pi}^{\theta-\frac{\pi}{4}} p(\phi)d\phi = 2\int_{\pi/4}^{\pi} p(\phi)d\phi \tag{2.3.10}$$

where $p(\phi)$ is the probability density function of the phase in equation (2.3.2) and is given by [7].

$$p(\phi) = \frac{1}{2\pi} e^{-\rho}[1 + \sqrt{4\pi\rho} \cdot \cos\phi \cdot e^{\rho\cdot\cos^2\phi} \cdot Q(\sqrt{2\rho}\cos\phi)] \tag{2.3.11}$$

$$-\pi \leq \phi \leq \pi$$

where

$$\rho = \text{signal to noise ratio} = \frac{A^2}{2\sigma^2} \tag{2.3.12}$$

and

$$Q(u) = \frac{1}{\sqrt{2\pi}} \int_u^{\infty} e^{-t^2/2}\, dt \tag{2.3.13}$$

From equation (2.3.10) it is difficult to evaluate the bit error rate of a system. However, a useful estimation of this formula is used for high S/N ratios. This is,

$$P(e) = \exp\left[-\rho \cdot \sin^2 \frac{\pi}{4}\right] \tag{2.3.14}$$

The bit error rate of a coherent QPSK system is also approximately given by:

$$P(e) = \text{erfc}\sqrt{\frac{E_S}{2N_0}} = \text{erfc}\sqrt{\frac{E}{2N_0}} \tag{2.3.15}$$

Comparing BPSK and QPSK on the basis of both systems transmitting equal numbers of symbols per second, it is concluded that the E/N_o ratio requirements for both systems are identical. However, comparing QPSK and BPSK on the basis of average energy per character to noise spectral density ratio, an increase of 3 dB in S/N ratio is required for QPSK to maintain the same bit error as the binary system.

2.4 BANDLIMITING REQUIREMENTS - NYQUIST

The power spectra of PSK signals, as shown by equation (2.2.9) contain sidelobes that may interfere with other adjacent channels. To suppress this out-of-band interference, in most applications, it is required to bandlimit the theoretically infinite bandwidth $(\sin x/x)^2$ of the PSK spectrum. The sidelobes can be removed by post-modulating band-pass filtering at the transmitter. However, it is known that narrow band-pass filtering rounds and widens each individual pulse of a digital waveform. As a result, it might cause more intersymbol-interference and degrade more the performance of the system. Based on the interchangeability of low-pass and band-pass filters and the Nyquist's theorem, the minimum bandwidth of a PSK system can be specified.

Nyquist proved that it is possible to transmit f_s independent symbols in a low-pass filter channel having a bandwidth of only $B = f_s/2$, without distortion in the sampling instant, that is without intersymbol interference [8]. In binary transmission systems, one symbol contains only one information bit. Hence, as discussed previously, the bit rate f_b is equal to the symbol rate f_s. In QPSK, $f_s = f_b/2$. Thus, a minimum bandwidth of $f_b/2$ is required in order to have distortionless transmission in QPSK systems.

To design the ideal Nyquist minimum bandwidth filter, with the required amplitude and phase characteristics, as shown in Fig. 2.4.1, would require an infinite number of sections, which practically is not possible. However, the same theorem continues, alleviating this problem by stating that, if a real valued transmittance function which has symmetrical skew about the cut-off frequency is added to the transmittance of an ideal low-pass filter, the same axis crossings of the impulse response persists.

To manufacture filters which approximate the raised-cosine characteristics of the Nyquist channel and have the smallest possible bandwidth (dashed line in Fig. 2.4.1), today is feasible. Filters with an approximation of a = 0.15 requiring only a 15% excess of Nyquist bandwidth are realizable. Hence, the practical efficiency of a QPSK system can be 2/1.15 = 1.74 b/s/Hz.

Figure 2.4.2 illustrates the time domain response of a minimum bandwidth Nyquist LPF. If the input to the filter is a random binary Non-Return to Zero (NRZ) sequence, then the output signal at the sampling instants will attain its maximum value for each transmitted bit. Thus, the filter does not introduce ISI. However, if the LPF does not have the required amplitude and phase characteristics, such as shown in Fig. 2.4.1, then the output signal $V_o(t)$, shown by the dashed line in Fig. 2.4.2, depending on the value of the previous bit, does not always attain its maximum value, and ISI is introduced.

The channel imperfections are usually evaluated by means of the "eye pattern" obtained by an oscilloscope. The signal to noise degradation, then, contributed by ISI is given by:

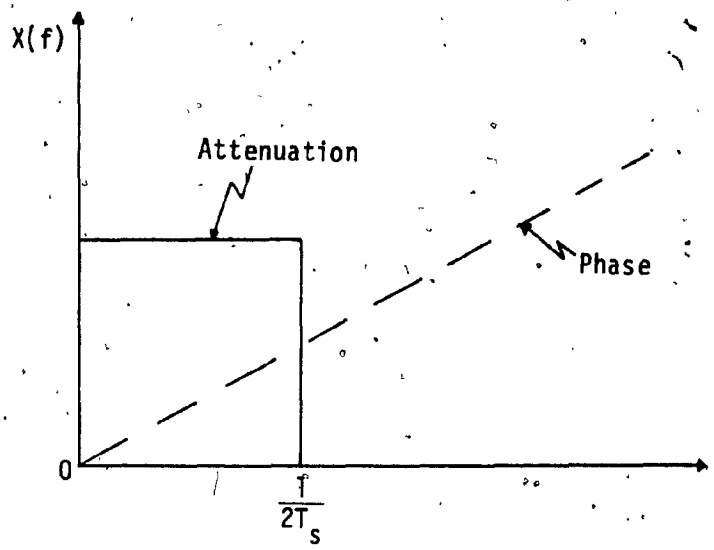

(a) Minimum Nyquist Bandwidth

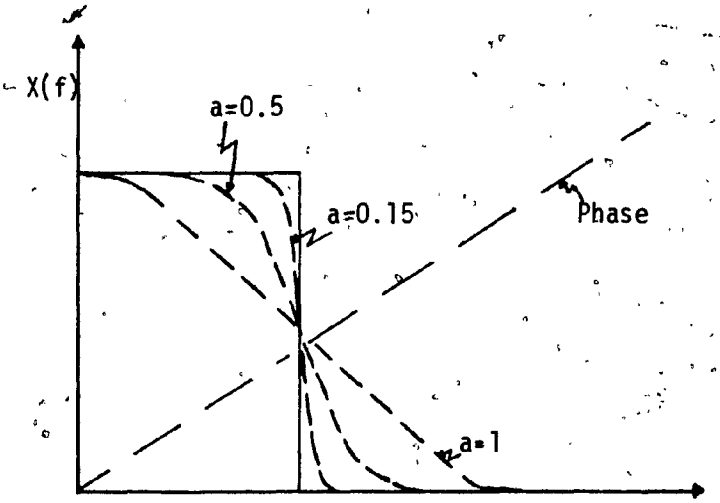

(b) Raised Cosine Transfer Function

Fig. 2.4.1 Nyquist and Raised Cosine Channels [34]

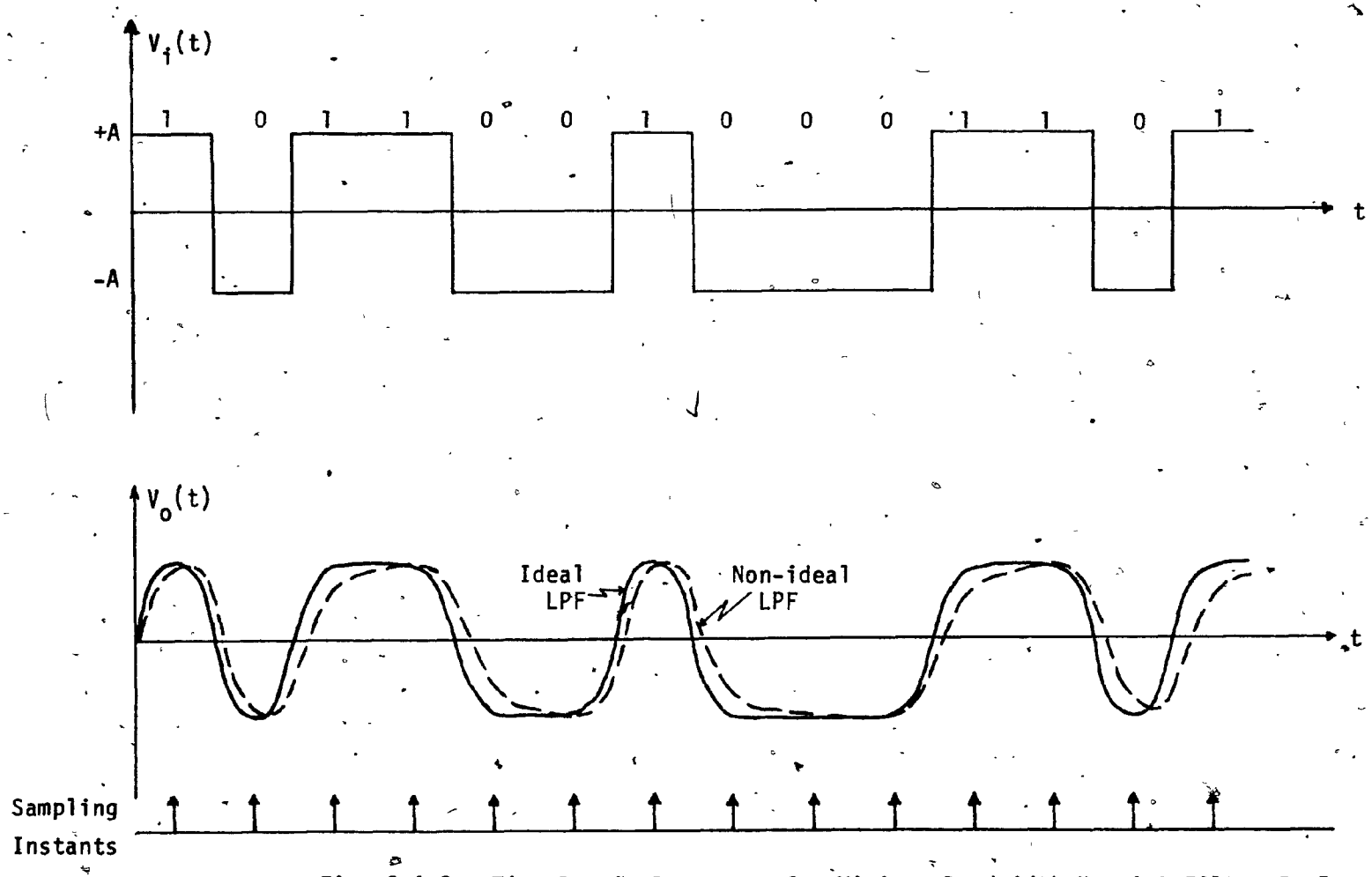

Fig. 2.4.2 Time Domain Response of a Minimum Bandwidth Nyquist Filter [34]

$$(S/N)_{degradation} = 20 \log \left[\frac{(existing\ eye\ opening)\%}{100\%}\right] [dB] \qquad (2.4.1)$$

Thus; if a given binary system, has to maintain a specified bit error rate, then its S/N ratio must be increased by an equivalent amount taken from equation (2.4.1).

2.5 REDUCTION OF AM MODULATION ON THE QPSK WAVEFORM - O-QPSK

The QPSK signal has a time invariant constant envelope when it is not filtered. But, since its power spectrum consists of sidelobes that cause out-of-band interference, the signal is bandlimited. As a result of such filtering an AM (amplitude modulation) component arises and the QPSK signal envelope becomes time variable. Especially, in some applications where tight filtering is required, the envelope variation might go through zero and its maximum steady state value, during one symbol interval. This large envelope fluctuation is produced in QPSK, due to the synchronous alignment of both binary sequences. When both data stream channels change state simultaneously an instantaneous transition of 180° occurs and the envelope passes through zero amplitude. The envelope fluctuations does not cause any problem in linear systems. However, when this type of signal passes through nonlinear devices, such as limiters, up-converters, TWTA, etc., which operate for economic reasons close to saturation, the envelope fluctuations are reduced but the bandlimited spectrum spreads. Today, a large number of communications systems employ non-linear devices. Thus, the QPSK signal at the output of a nonlinear device "regains" the spectrum that it had before filtering, and consequently an undesired amount of out-of-band interference is again introduced into adjacent channels.

Offset QPSK (O-QPSK) is a format of the conventional QPSK that alleviates this problem. In O-QPSK the two binary modulation sequences are shifted in the relative alignment of an amount equal to one-half of a symbol duration, thus avoiding 180° phase shifts. While the minimum of the envelope in a QPSK signal is zero, in the O-QPSK the signal is 1/2 of the steady state value. Therefore, with respect to QPSK system, O-QPSK has a lower AM component.

If an O-QPSK format modified to avoid phase transitions all together, then further suppression of out-of-band interference can be obtained in bandlimiting-hardlimiting applications. Such a modulation scheme is MSK (sometimes called Fast Frequency Shift-Keying - FFSK) which has continuous phase.

A comparative performance of QPSK and O-QPSK with MSK is presented in Chapter Five.

CHAPTER THREE

3. QPSK & O-QPSK SIGNALLING

3.1 MATHEMATICAL PRESENTATION AND ANALYSIS

3.1.1 QPSK & O-QPSK Signal

The quadrature PSK signal was derived in section 2.3, and given by:

$$S_{4\phi\text{-PSK}}(t) = A \sin\left(\frac{i\pi}{2} d_k\right) \cdot \cos\left(\omega_c t + \frac{\pi}{4}\right) + A \cos\left(\frac{i\pi}{2} d_k\right) \cdot \sin\left(\omega_c t + \frac{\pi}{4}\right) \qquad (3.1.1)$$

$$kT \leq t \leq (k+1)T, \quad i = 0,1,2,3$$

This presentation of the quaternary PSK signal can be viewed as being composed of two quadrature data channels. Since $\sin\left(\frac{i\pi}{2} d_k\right)$ and $\cos\left(\frac{i\pi}{2} d_k\right)$ are orthogonal and take on only the values ± 1, it implies that the data are conveyed at a rate of one bit per 2T seconds in each quadrature channel. Thus, in order to simplify the four-phase PSK signal expression let $\sin\left(\frac{i\pi}{2} d_k\right)$ and $\cos\left(\frac{i\pi}{2} d_k\right)$ be replaced by two streams $d_I(t)$ and $d_Q(t + \tau)$, consisting of even and odd bits respectively, that the input binary bit stream d_k is separated into.

Assuming that the symbol weighting shape of the two quadrature data channels has a function

$$p(t) = \begin{cases} 1/\sqrt{2} & |t| \leq T \\ 0 & \text{elsewhere} \end{cases} \qquad (3.1.2)$$

The last equation becomes:

$$S_{4\phi\text{-PSK}}(t) = \frac{A}{\sqrt{2}}\, d_I(t) \cdot \cos\left(\omega_c t + \frac{\pi}{4}\right) + \frac{A}{\sqrt{2}}\, d_Q(t+\tau) \cdot \sin\left(\omega_c t + \frac{\pi}{4}\right) \qquad (3.1.3)$$

where

$$d_I(t) = \pm 1\,, \quad 2kT \le t \le 2(k+1)T$$

$$d_Q(t) = \pm 1\,, \quad 2kT + \tau \le t \le 2(k+1)T + \tau$$

and

$$0 \le \tau \le 2T$$

Thus, a four phase PSK signal is viewed as two orthogonal binary channels, where antipodal symbols of 2T seconds are used in each channel, as shown in Fig. 3.1.1. The first term of (3.1.3) represents the in-phase channel, or I channel, where $\cos\left(\omega_c t + \frac{\pi}{4}\right)$ is the in-phase carrier term. The second term of (3.1.3) represents the quadrature channel, or Q channel, where $\sin\left(\omega_c t + \frac{\pi}{4}\right)$ is the quadrature carrier term. Due to orthogonality of $\cos\left(\omega_c t + \frac{\pi}{4}\right)$ and $\sin\left(\omega_c t + \frac{\pi}{4}\right)$ the two binary channels can be detected independently.

Setting $\tau = 0$ and $\tau = T$ in the last equation we get the expressions for standard quadrature PSK (QPSK) and offset quadrature PSK (O-QPSK) signalling. Thus,

$$S_{QPSK}(t) = \frac{A}{\sqrt{2}}\, d_I(t) \cdot \cos\left(\omega_c t + \frac{\pi}{4}\right) + \frac{A}{\sqrt{2}}\, d_Q(t) \cdot \sin\left(\omega_c t + \frac{\pi}{4}\right) \qquad (3.1.4)$$

for $2kT \le t \le 2(k+1)T$

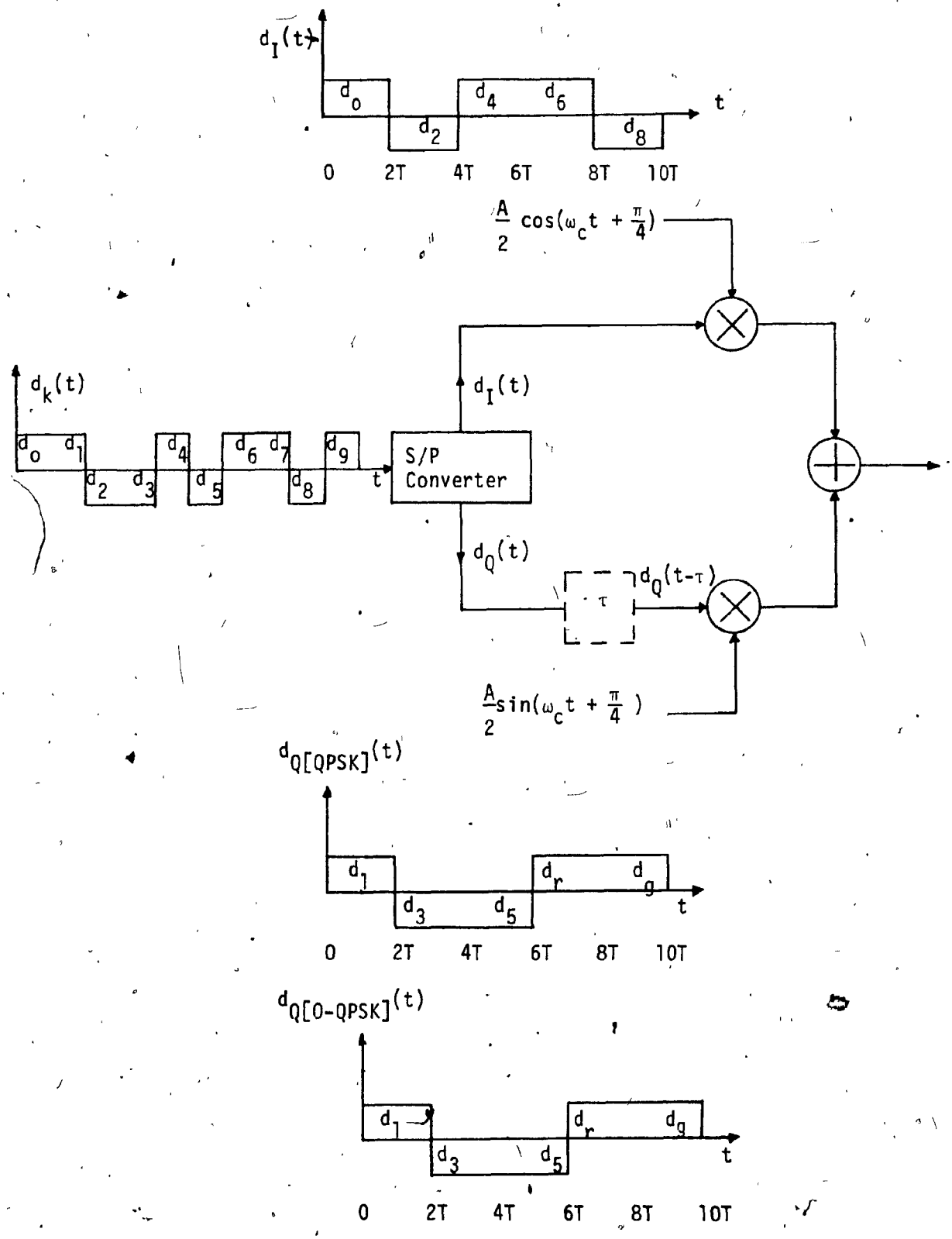

Fig. 3.1.1 Mechanization of a Quadriphase Modulator

and

$$S_{O\text{-}QPSK}(t) = \frac{A}{\sqrt{2}} d_I(t) \cdot \cos\left(\omega_c t + \frac{\pi}{4}\right) + \frac{A}{\sqrt{2}} d_Q(t+T) \cdot \sin\left(\omega_c t + \frac{\pi}{4}\right) \quad (3.1.5)$$

where

$$d_I(t) = \pm 1, \quad 2kT \le t \le 2(k+1)T$$

$$d_Q(t+T) = \pm 1, \quad (2k+1)T \le t \le (2k+3)T$$

From (3.1.4) and (3.1.5) it is seen that the distinction between the two modulation techniques is only in the alignment of the two binary streams. The odd and even bit streams, transmitted at a rate of 1/2T baud, are synchronously aligned in conventional QPSK modulation so that their transitions coincide. Offset QPSK modulation is obtained by a shift or offset in the relative alignment of $d_I(t)$ and $d_Q(t)$ binary waveforms of an amount equal to T (or equal to one-half of a symbol duration, Ts/2). The relative alignment of the binary waveforms $d_I(t)$ and $d_Q(t)$ for both modulation techniques is shown in Fig. 3.1.1. Due to the shift of T seconds in the quadrature binary stream the offset QPSK is sometimes called staggerred QPSK.

3.1.2 Carrier Phase Changes

Since the only difference between conventional and offset QPSK signalling is the alignment of $d_I(t)$ and $d_Q(t)$ streams, their four carrier phases must be the same according to their mathematical presentation. Using well-known trigonometric identities equation (3.1.3) can be written as:

$$S(t) = \frac{A}{2} d_I(t) [\cos \omega_c t - \sin \omega_c t] + \frac{A}{2} d_Q(t)[\cos \omega_c t + \sin \omega_c t] \quad (3.1.6)$$

Substituting the four possible combinations of the two binary streams $d_I(t)$ and $d_Q(t)$, the four permitted phase values of a quaternary system are obtained at bit intervals:

$$\begin{aligned}
&\text{a) } d_I(t) = d_Q(t) = +1 \\
&\qquad S(t) = A \cos \omega_c t \\
&\text{b) } d_I(t) = +1,\ d_Q(t) = -1 \\
&\qquad S(t) = -A \sin \omega_c t = A \cos (\omega_c t + \tfrac{\pi}{2}) \\
&\text{c) } d_I(t) = d_Q(t) = -1 \\
&\qquad S(t) = -A \cos \omega_c t = A \cos (\omega_c t + \pi) \\
&\text{d) } d_I(t) = -1,\ dQ(t) = +1 \\
&\qquad S(t) = A \sin \omega_c t = A \cos (\omega_c t - \tfrac{\pi}{2})
\end{aligned} \quad (3.1.7)$$

The carrier phase depends on the values of $\{d_I(t), d_Q(t)\}$ and is any one of the four phases shown in Fig. 3.1.2. In conventional QPSK, due to the time coincidence of the two data streams the carrier phase changes occur every 2T seconds. If neither binary component changes sign in the next 2T interval, the carrier phase remains the same (phase transition of 0°). If one component changes sign (state), then a phase shift of +90° occurs in the modulated signal. A switch in the states of both components results in a phase shift of 180°. The state diagram of conventional QPSK signalling is shown in Fig. 3.1.3 (a), while the QPSK waveform for a specific input data stream is illustrated in Fig. 3.1.4.

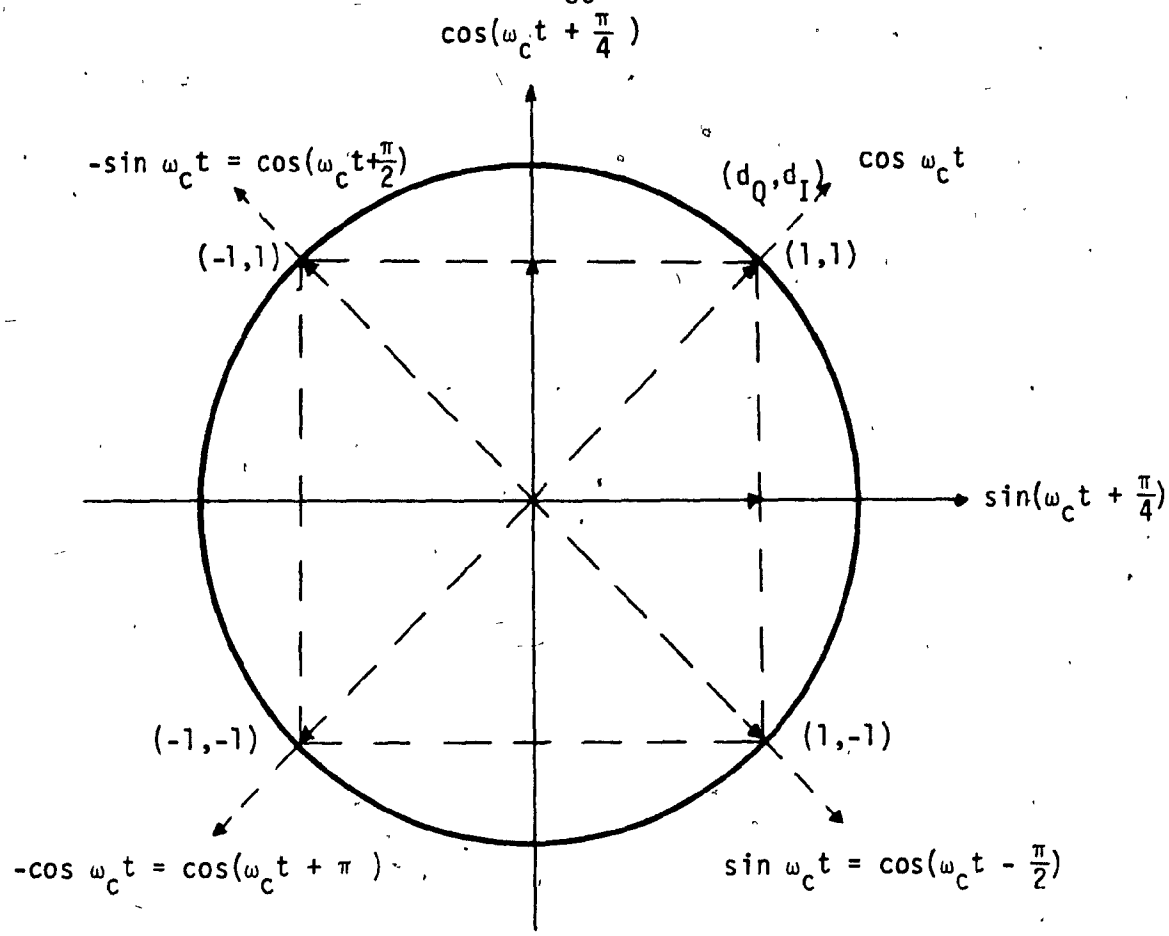

Fig. 3.1.2 Signal Space Diagram for QPSK and O-QPSK

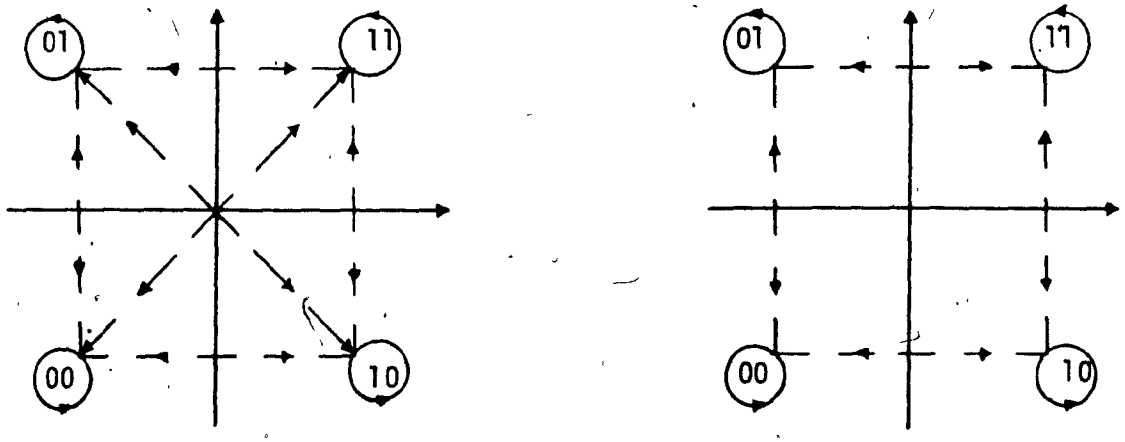

(a) QPSK (b) O-QPSK

Fig. 3.1.3 State Changes in QPSK and O-QPSK Signals

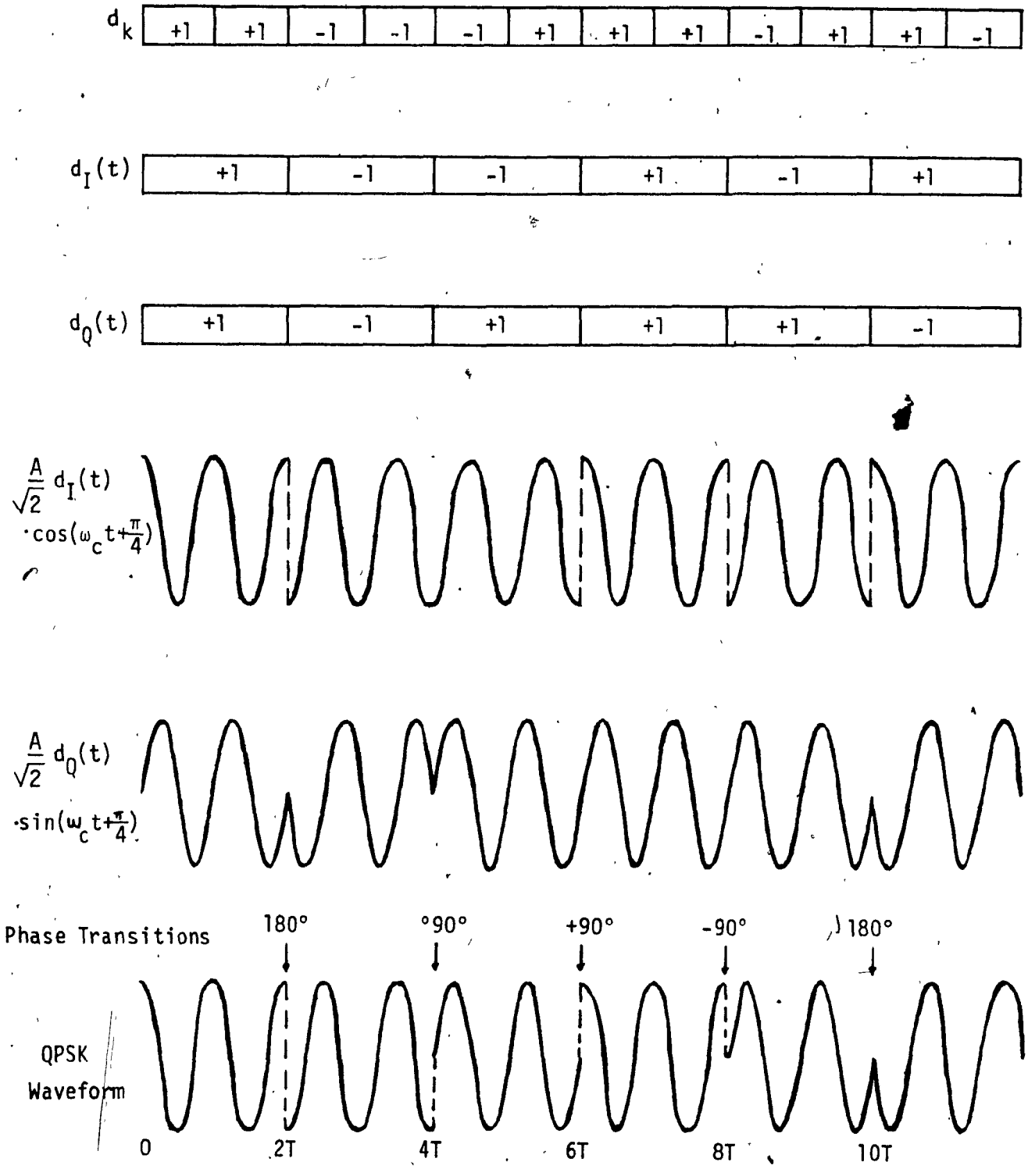

Fig. 3.1.4 QPSK Waveform

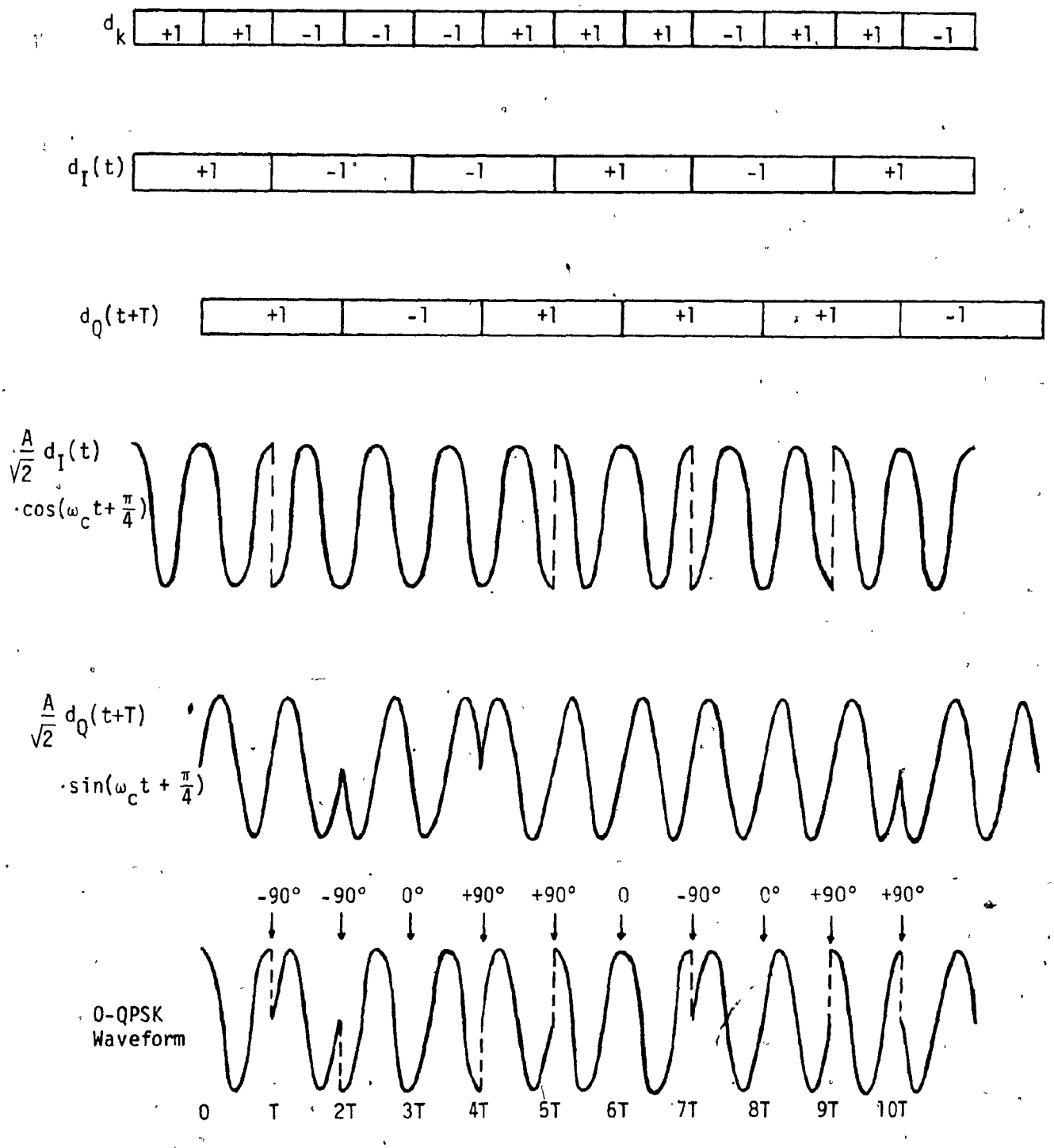

Fig. 3.1.5 O-QPSK Waveform

In O-QPSK, the two binary components cannot change state simultaneously because a delay of Ts/2 (half symbol period) is applied to one of the two binary streams. Thus, one component has transitions in the middle of the other symbol and hence only one component can change states. With this method, only ±90° transitions are allowed and 180° phase reversals are made in two steps at ±90° each. This is illustrated in Fig. 3.1.5 where a typical O-QPSK waveform is displayed with phase transitions occuring every T seconds. The state diagram of O-QPSK signalling is shown in Fig. 3.1.3 (b).

3.2 POWER SPECTRAL DENSITY AND AUTOCORRELATION

The general way of obtaining the power spectrum of any signal, is to find the Fourier transform of a sample of the signal on a finite time interval T. Then, the magnitude square of this Fourier transform is divided by T and averaged over all possible values of the signal. The power spectrum is finally obtained by taking the limit of the previous result as T tends to infinity.

The difference in time alignment in the two component streams does not alter the power spectral density and hence both QPSK and O-QPSK spectra are the same. Thus, the power spectra (shifted to baseband) of both modulation techniques are obtained by evaluating the Fourier transform X(f) of the "square-pulse" symbol shaping function x(t), given by (3.1.3), over a symbol interval and the magnitude squared of this Fourier transform is then divided by 2T (symbol interval). Evidently from (3.1.4) and/or (3.1.5) the quaternary PSK spectrum is the sum of two BPSK spectra centered at the carrier frequency f_c. The Fourier transform $X(f,kT)$ of the two binary components can be separated in two

parts which correspond to the positive and negative frequencies respectively.

$$X(f_+, kT) = \frac{1}{2} \int_0^{kT} x(t) \exp(-j2\pi ft)dt \qquad (3.2.1)$$

$$X(f_-, kT) = \frac{1}{2} \int_0^{kT} x(t) \exp(j2\pi ft)dt \qquad (3.2.2)$$

Note that $X(f_-,kT) = X^*(-f_+,kT)$ [* indicates that -j is made +j in (3.2.2)].

The Fourier transforms relative to positive frequencies of the in-phase and quadrature modulating signals, whose rates are $f_b/2$ and modulate the carriers $\cos(\omega_c t + \frac{\pi}{4})$ and $\sin(\omega_c t + \frac{\pi}{4})$, are given by:

$$X_I(f_+,2T) = \frac{1}{2} \int_0^{2T} \frac{A}{\sqrt{2}} \exp(-j2\pi ft)dt$$

$$= \frac{AT}{\sqrt{2}} \left[\frac{\sin 2\pi f T}{2\pi f T} \right] \exp(-j2\pi fT) \qquad (3.2.3)$$

$$X_Q(f_+,2T) = \int_0^{2T} \frac{A}{\sqrt{2}} \exp(-j2\pi ft)\, dt = \int_{-T}^{T} \frac{A}{\sqrt{2}} \exp(-j2\pi ft)dt$$

$$= \frac{AT}{\sqrt{2}} \left[\frac{\sin 2\pi f T}{2\pi f T} \right] \exp(-j2\pi fT) = X_I(f_+,2T) \qquad (3.2.4)$$

Also,

$$X_I(f-f_c) = X_Q(f-f_c) = \frac{AT}{\sqrt{2}} \left[\frac{\sin 2\pi(f-f_c)T}{2\pi(f-f_c)T} \right] \exp[-j2\pi(f-f_c)T] \qquad (3.2.5)$$

Thus the Fourier transform of the QPSK or O-QPSK signalling relative to the positive frequencies, is:

$$X(f_+,2T) = \frac{2\,AT}{\sqrt{2}} \left[\frac{\sin 2\pi(f-f_c)T}{2\pi(f-f_c)T} \right] \exp[-j2\pi(f-f_c)T] \qquad (3.2.6)$$

Taking the square magnitude of the last expression and divide it by the symbol interval, the one sided QPSK or O-QPSK spectrum is obtained:

$$G(f) = \frac{1}{2T}\left[\left|\frac{2\,AT}{\sqrt{2}}\left[\frac{\sin 2\pi(f-f_c)T}{2\pi(f-f_c)\,T}\right]\right|^2\right]$$

$$= A^2T\left[\frac{\sin 2\pi(f-f_c)T}{2\pi(f-f_c)\,T}\right]^2 \qquad (3.2.7)$$

Since the averaged value of the modulated signal is:

$$V_{rms}(t) = \left[\frac{1}{T}\int_0^T u^2(t)\,dt\right]^{1/2} = \left[\frac{1}{T}\int_0^T A^2\cos^2\omega_c t\,dt\right]^{1/2}$$

$$= \left[\frac{A^2 t}{2T}\Big|_0^T\right]^{1/2} = \sqrt{\frac{A^2}{2}} \qquad (3.2.8)$$

and the normalized (one ohm resistance) mean power of this signal is:

$$P_c = \left[\sqrt{\frac{A^2}{2}}\right]^2 = \frac{A^2}{2} \qquad (3.2.9)$$

the spectral density G(f) for QPSK and O-QPSK is given by

$$G(f) = 2P_cT\left[\frac{\sin 2\pi(f-f_c)T}{2\pi(f-f_c)\,T}\right]^2 \qquad (3.2.10)$$

where,

f = frequency offset from the carrier

T = unit bit duration

P_c = Power in modulated waveform

The autocorrelation function is the inverse Fourier transform of the power spectral density G(f) and is given by [8]:

$$R(\tau) = \begin{cases} A^2\left[1 - \frac{|\tau|}{2T}\right], & |\tau| \le 2T \\ 0, & |\tau| > 2T \end{cases} \qquad (3.2.11)$$

The power spectral density and autocorrelation function of Minimum Shift Keying (MSK) are given by [9]:

$$G_{MSK}(f) = \frac{8P_c\, T\{1 + \cos[4\pi(f-f_c)T]\}}{\pi^2\{1-16(f-f_c)^2\, T^2\}^2} \qquad (3.2.12)$$

$$R_{MSK}(\tau) = \begin{cases} \frac{A^2}{\pi}\{\pi\ [1- \frac{|\tau|}{2T}] \cos\ [\frac{\pi|\tau|}{2T}] + \sin [\frac{\pi|\tau|}{2T}]\}, & |\tau| \le 2T \\ 0 & |\tau| > 2T \end{cases}$$

(3.2.13)

Equation (3.2.10) shows that the QPSK or O-QPSK spectrum has its nulls at multiples of the symbol rate, namely,at :

$$f-f_c = \pm k\frac{f_b}{2}$$

with $k=1,2,3,4,\ldots$(i.e. $k \neq 0$). For $k = 0$, that is at $f = f_c$ the numerator and denominator of (3.2.10) become both equal to zero, and G(f) takes the value of 2 or 3 dB using l'Hopital rule. In a similar manner, from equation (3.2.12) it is observed that the MSK spectrum has its nulls at

$$f-f_c = (2k \pm 1)\frac{f_b}{4} \qquad k = 1,2,3,\ldots(k \neq 0)$$

and for $k = 0$ the main lobe becomes equal to $\frac{16}{\pi^2}$ or 2.09 dB. The spectra of 3.2.10 and (3.2.12) are plotted in Fig. 3.2.1 as a function of $(f-f_c)$ normalized to the data bit rate $R = 1/T$. The rates of fall-off of these spectra are different owing to the difference in the pulse shapes of the modulating signals. The QPSK or O-QPSK spectrum falls off at a rate proportional to $[(f-f_c)/f_b]^{-2}$ whereas the MSK spectrum falls off at a

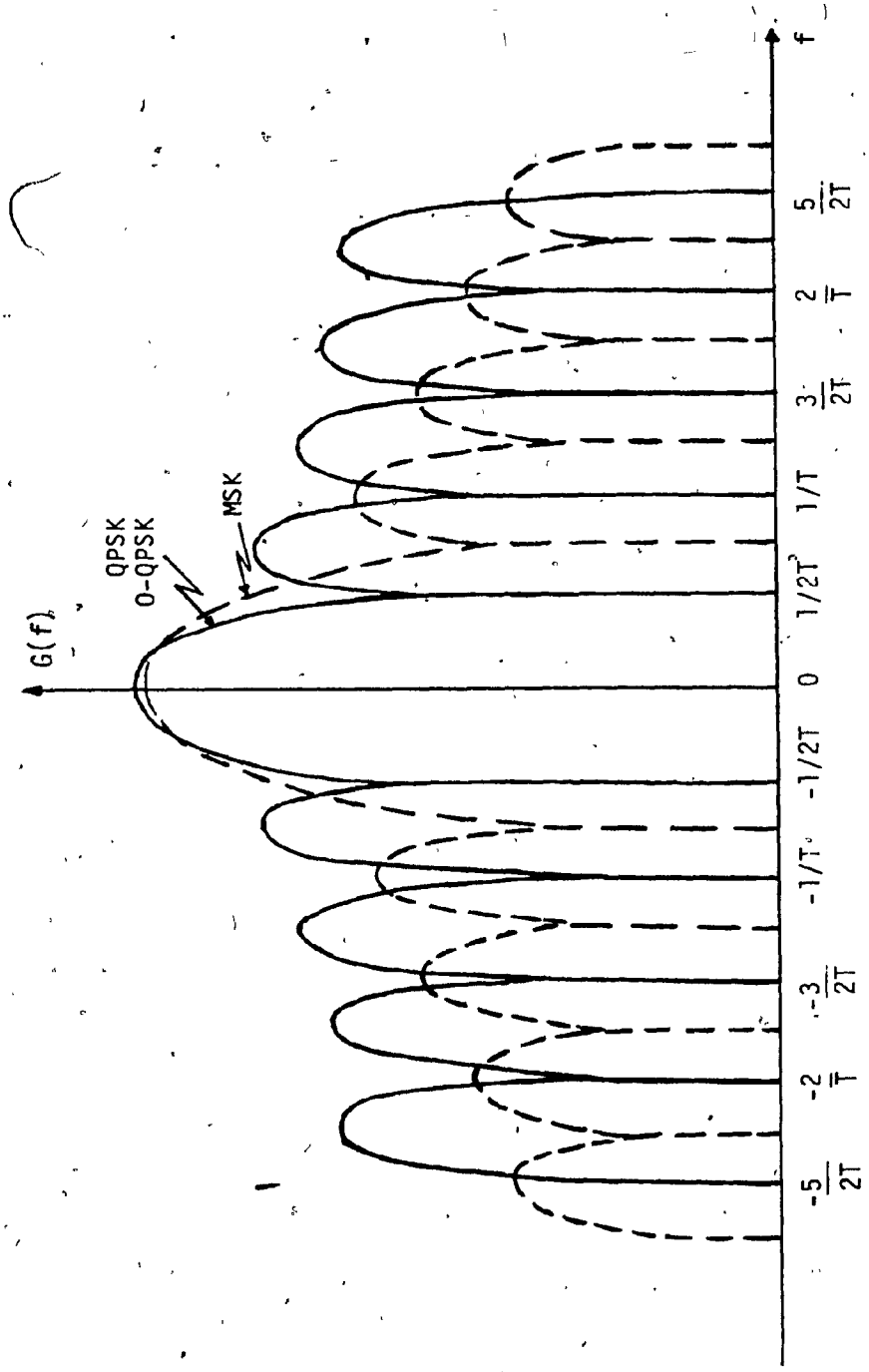

Fig. 3.2.1 Spectral Density of QPSK, O-QPSK, and MSK

rate proportional to $[(f-f_c)/f_b]^{-4}$. This can be explained on the basis that the smoother the pulse shape, the faster is the drop of the spectral sidelobes to zero. Thus, since MSK has sinusoidal modulating pulses, it also has lower sidelobes than QPSK and O-QPSK. However, the main spectral lobe single-sided bandwidth of a MSK signal is 50% wider than that of a conventional QPSK or an O-QPSK signal.

A measure of the compactness of a modulation waveform's spectrum is the bandwidth B which contains 99 percent of the total power. From Fig. 3.2.1 it is observed that the 99% radiated bandwidth for QPSK or O-QPSK is at $f \tilde{=}$ (4 to 5) times 2/T [9]. The bandwidth B which contains 99 percent of the total power for a MSK singal is $B \tilde{=} 1.2/T$. This and the fact that the mainlobe single stated bandwidth of a MSK signal is 50% wider than that of a QPSK or O-QPSK, indicate that in narrow-band satellite links conventional QPSK and O-QPSK are more preferred methods than that of MSK.

Figure 3.2.2 [9] shows E_b/N_o (energy per bit to additive noise spectral density ratio) performance degradation versus B_nT with respect to ideal antipodal PSK as a function of cascaded filter noise bandwidth, with error probability as a parameter for O-QPSK and MSK systems. The performance curves show a crossover point, such that for channel bandwidths $B < 1.1/T$ the performance of QPSK is superior to that of MSK and for $B > 1.1/T$ the bit error rate performance of MSK is superior to that of O-QPSK. Both modulation techniques begin to severely degrade when the channel bandwidth becomes of the order of their spectral mainlobes. However, as channel bandwidth decreases, the MSK signal degrades sooner than the O-QPSK since its mainlobe is wider than that of O-QPSK.

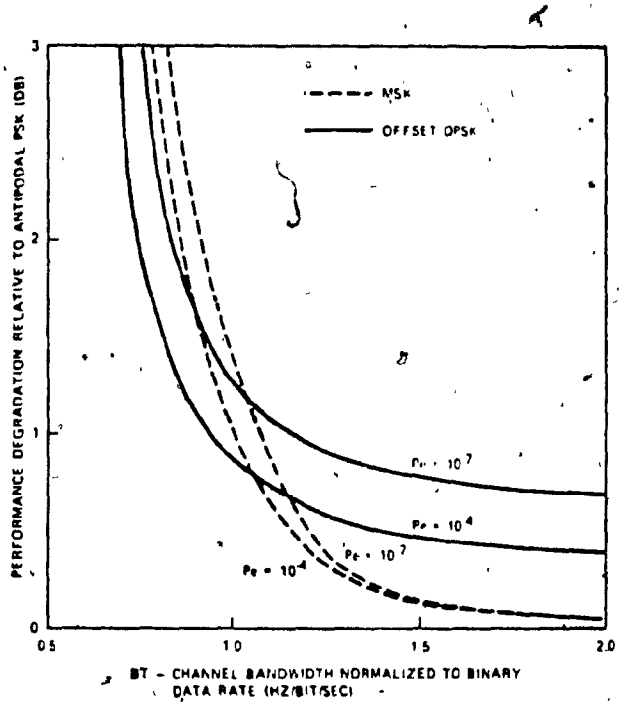

Fig. 3.2.2 Performance Degradation of O-QPSK and MSK with respect to Filter Noise Bandwidth

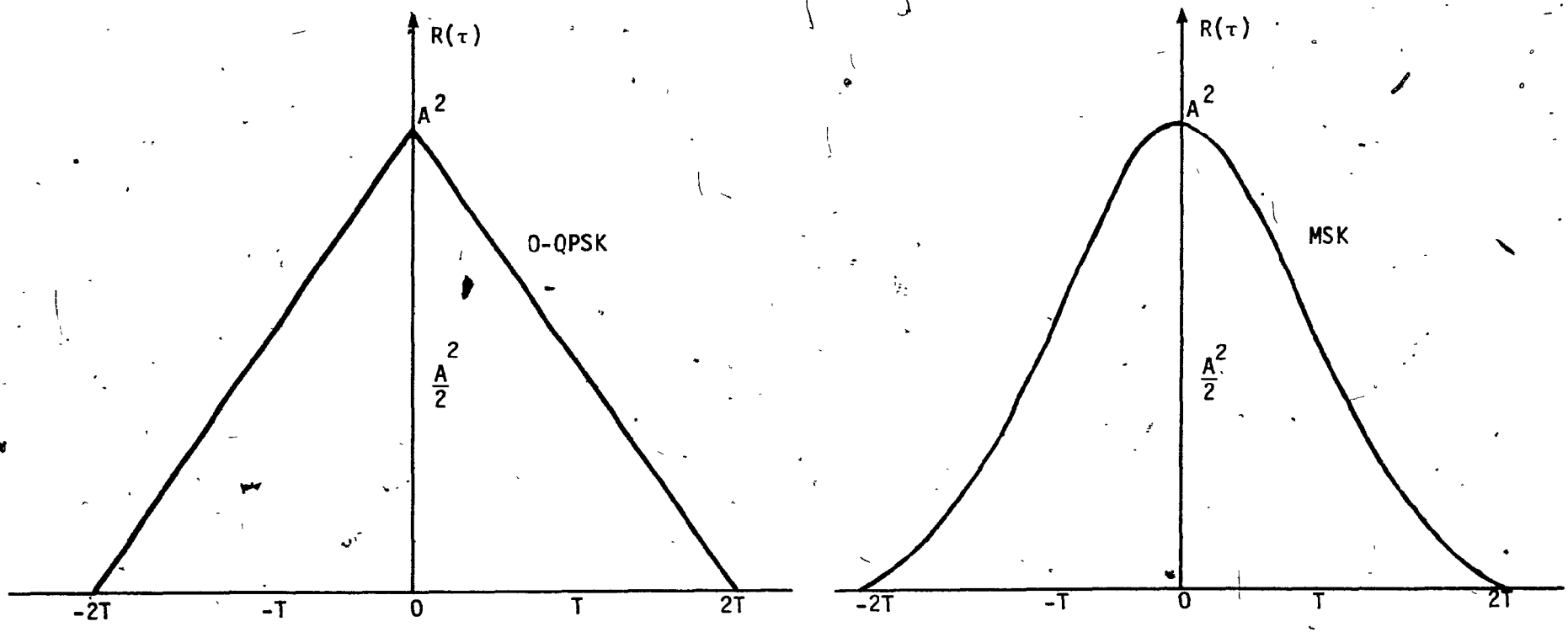

Fig. 3.2.3 Normalized Autocorrelation for O-QPSK and MSK

Equations (3.2.11) and (3.2.13) are plotted in Fig. 3.2.3 for comparison. It is easily seen that both autocorrelation functions are zero for time exceeding the symbol duration. This can be explained as for independent binary data bits, the signs of quadrature components in each in-phase and quadrature channel are independent from one symbol interval (2T) to the next. Owing to their similarity and their equal zero crossing time-length autocorrelation functions, the O-QPSK and MSK have equivalent bit error rate performance.

3.3 BANDLIMITING AND NON-LINEARITY EFFECTS

3.3.1 Envelope Fluctuations

In Figures 3.1.4 and 3.1.5 the envelope of the modulated signal is constant because bandlimiting was not considered. As described in the previous section, however, the power spectra of PSK signals are composed of sidelobes that may interfere with other communication systems. Hence, bandlimiting is applied at the transmitter to remove the sidelobes and suppress the out-of-band interference.

The effect of such filtering is the introduction of envelope variations, near bit transitions, which go through zero amplitude whenever the carrier changes phase by 180° [10]. In general, bandlimiting of a digital waveform causes rounding and widening of every pulse. Thus, in a QPSK signal, when both the in-phase channel data and the quadrature channel data change state, which results in a carrier phase change of 180°, the binary symbols can be taken as having the same phase but opposite amplitude polarities. Consequently, due to the opposite polarity overlap of the binary symbols, the envelope of the composite signal vanishes where its phase changes rapidly.

Rapid phase transitions of 180° produce high frequency power

components that result in large amounts of out-of-band interference. However, as shown in Fig. 3.3.1, because of the envelope droop of a filtered QPSK signal, very little power is associated with the high frequency content at the region of 180° phase transitions. At the ± 90° phase transitions, which occur when one channel data changes phase at the keying instant, the phase transition does not produce high frequencies since the slope of the phase is small in the transition region. The envelope fluctuation in this case is of the order of 3dB.

In O-QPSK signals, as discussed in section 3.1, because of the one bit period delay between the two data channels, there is no 180° phase transitions. Such transitions are made in two steps of 90°. As a result, the envelope fluctuations of the modualted signal arise only due to ±90° phase transitions. Evidently, the overall envelope variations of a O-QPSK signal are smaller than those of a QPSK signal.

From equations (3.1.4) and (3.1.5) the QPSK and O-QPSK signals can be written as:

$$S_{QPSK}(t) = \frac{A}{\sqrt{2}}\left[\sum_{k=-\infty}^{\infty} d_I(t)\, p(t-2kT)\cos\left(\omega_c t + \frac{\pi}{4}\right)\right.$$

$$\left. + \sum_{k=-\infty}^{\infty} d_Q(t)\, p\,(t-2kT)\sin\left(\omega_c t + \frac{\pi}{4}\right)\right] \qquad (3.3.1)$$

$$S_{O\text{-}QPSK}(t) = \frac{A}{\sqrt{2}}\left[\sum_{k=-\infty}^{\infty} d_I(t)\, p(t-2kT)\cos\left(\omega_c t + \frac{\pi}{4}\right)\right.$$

$$\left. + \sum_{k=-\infty}^{\infty} d_Q(t)\, p\{t-(2k+1)T\}\cdot \sin\left(\omega_c t + \frac{\pi}{4}\right)\right] \qquad (3.3.2)$$

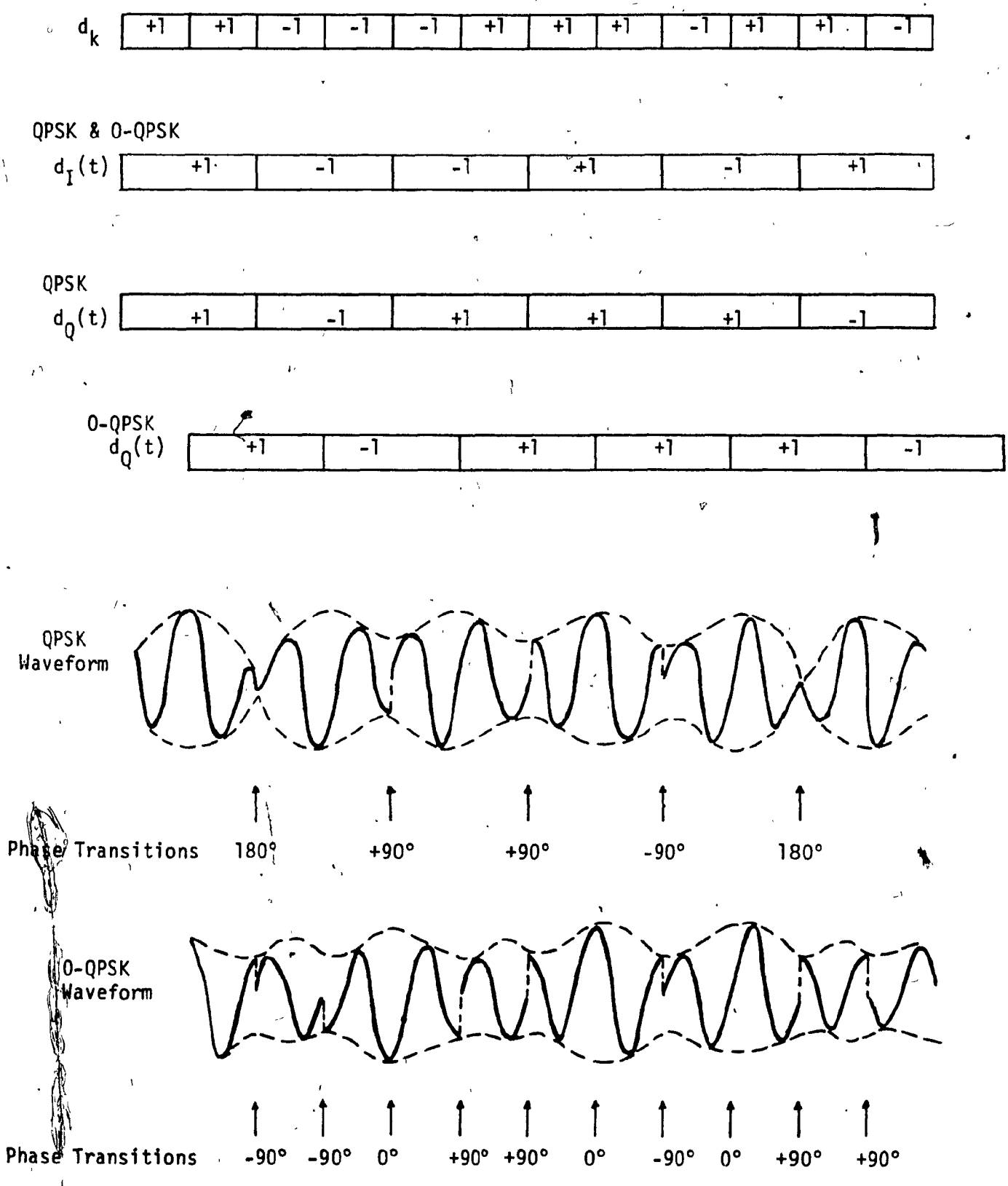

Fig. 3.3.1 Bandlimited QPSK and O-QPSK Waveforms

where,

$$p(t) = \begin{cases} \text{rectangular pulse} & \text{for } |t| \le T \\ 0 & \text{elsewhere} \end{cases}$$

If the above signals pass through a bandlimiting device whose impulse response is h(t), then, the filtered quadrature modulated signal is given by:

$$U_{QPSK}(t) = \frac{A}{\sqrt{2}}\left[\frac{1}{2}\sum_k [d_I(t)\, R_e\{p(t-2kT)*h(t)\} - d_Q(t)\, I_m\{p(t-2kT)*h(t)\}]\right] \cdot \cos(\omega_c t + \frac{\pi}{4}) - \frac{A}{\sqrt{2}}\left[\frac{1}{2}\sum_k [d_I(t)\, I_m\{p(t-2kT)*h(t)\} + d_Q(t)\cdot R_e\{p(t-2kT)*h(t)\}]\right] \cdot \sin(\omega_c t + \frac{\pi}{4}) \qquad (3.3.3)$$

$$U_{O\text{-}QPSK}(t) = \frac{A}{\sqrt{2}}\left[\frac{1}{2}\sum_k [d_I(t)\, R_e\{p(t-2kT)*h(t)\} - d_Q(t)\cdot I_m\{p[t-(2k+1)T*h(t)\}]\right] \cos(\omega_c t + \frac{\pi}{4}) - \frac{A}{\sqrt{2}}\left[\frac{1}{2}\sum_k [d_I(t)\, I_m\{p(t-2kt)*h(t)\} + d_Q(t)\cdot R_e\{[t-(2k+1)T*h(t)\}]\right] \sin(\omega_c t + \frac{\pi}{4}) \qquad (3.3.4)$$

The amplitudes of the filtered quaternary signals are given by:

$$V_{QPSK}(t) = \frac{A}{2}\left[\sum_k [R_e^2\{p(t-2kT)*h(t)\} + I_m^2\{p(t-2kT)*h(t)\}]\right]^{1/2} \qquad (3.3.5)$$

$$V_{O\text{-}QPSK}(t) = \frac{A}{2\sqrt{2}}\left[\sum_k [R_e^2\ \{p(t-2kT)*h(t)\} + I_m^2\ \{p[t-(2k+1)T]*h(t)\}\right.$$
$$\left. + I_m^2\ \{p(t-2kT)*h(t)\} + R_e^2\ \{p[t-(2k+1)T]*h(t)\}\right]^{1/2} \qquad (3.3.6)$$

Letting $e^2(t) = R_e^2\ \{p(t)*h(t)\} + I_m^2\ \{p(t)*h(t)\}$ where $e(t)$ is the envelope of the filtered signal, equations (3.3.5) and (3.3.6) can be written as:

$$V_{QPSK}(t) = \frac{A}{2}\left[\sum_k e^2(t-2kT)\right]^{1/2} \qquad (3.3.7)$$

$$V_{O\text{-}QPSK}(t) = \frac{A}{2\sqrt{2}}\left[\sum_k [e^2(t-2kT) + e^2(t-T-2kT)]\right]^{1/2} \qquad (3.3.8)$$

From the last two expressions it becomes evident that the QPSK envelope goes through zero amplitude when both data streams change state simultaneously, whereas the O-QPSK envelope does not have any zero crossings because of the time delay between $e(t-2kT)$ and $e(t-T-2kT)$. Thus, as shown in Fig. 3.3.2, the overall envelope variations of an O-QPSK signal are smaller than those of a QPSK signal.

3.3.2 Nonlinearity Effects on the Quaternary PSK Spectrum

In satellite communications because of the limited available power in the transponder, the TWT amplifiers are usually operated at its maximum peak output power. In this operating mode, as was mentioned in chapter one, the TWTA exhibits AM/AM and AM/PM conversion effects. A quadrature model of a general nonlinearity which takes into account these conversion effects has been developed [11] and shown in Fig. 3.3.3.

If the input signal to a nonlinear power amplifier is given by:

$$V_i(t) = r(t)\cdot\cos[\omega_c t + \Theta(t)]$$
$$= R_e\{[x(t) + j\,y(t)]\,e^{j\omega_c t}\} \qquad (3.3.9)$$

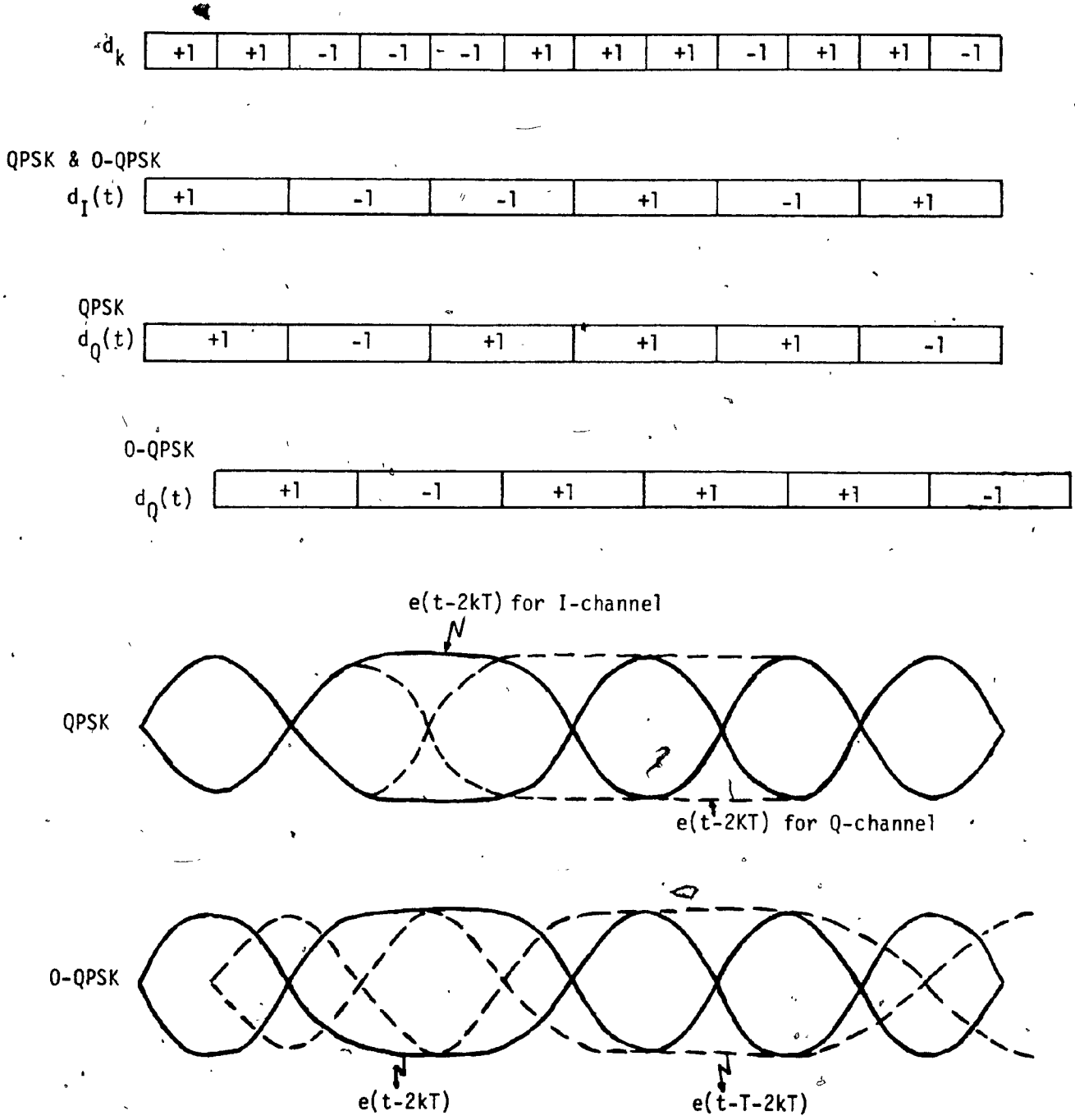

Fig. 3.3.2 Overall Amplitude Fluctuations of QPSK & O-QPSK

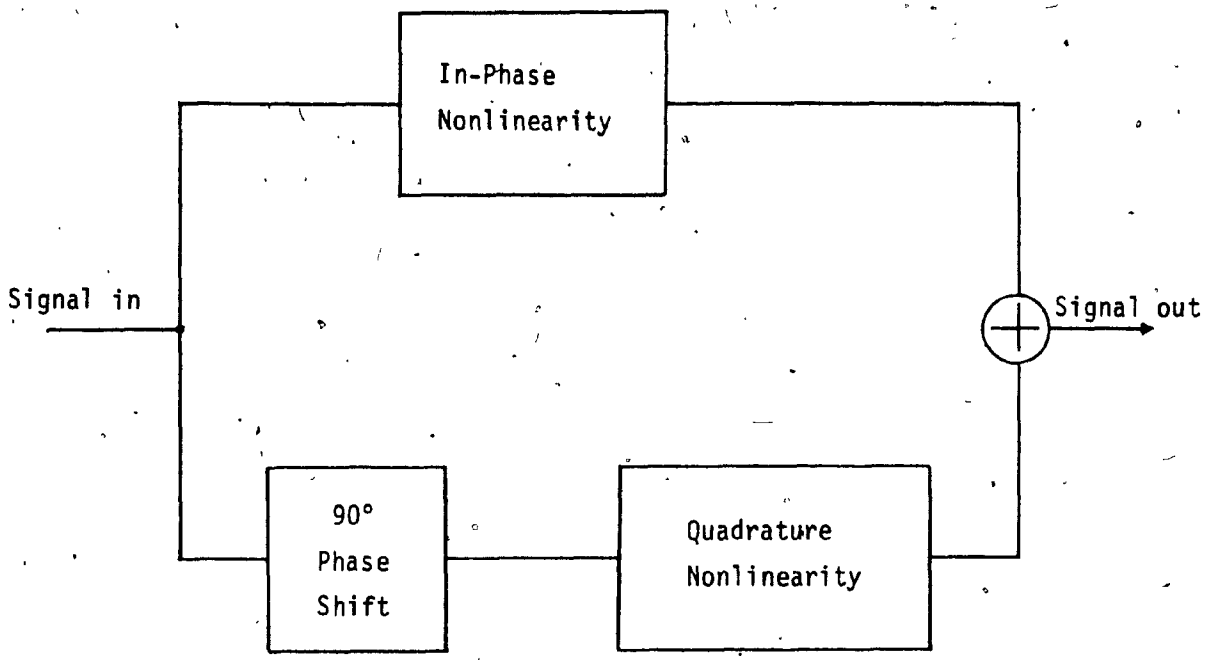

Fig. 3.3.3 Quadrature Model of a Nonlinear Power Amplifier [11]

where $r(t)$ and $\theta(t)$ are the envelope and phase function respectively, and $x(t)$ and $y(t)$ are the real and imaginary parts of the complex baseband signal.

Then, the output of the nonlinear power amplifier is given by

$$V_o(t) = R\{r(t)\}\cos\,[\omega_c t + \theta(t) + \phi\{r(t)\}\,] \qquad (3.3.10)$$

where $R\{r(t)\}$ is the amplitude distortion and $\phi\{r(t)\}$ is the phase distortion introduced by the TWTA. Equation (3.3.10) can be readily rewritten as:

$$V_o(t) = R\{r(t)\} \cdot \cos\phi\{r(t)\} \cdot \cos\,[\omega_c t + \theta(t)] - R\{r(t)\} \cdot \sin\phi\{r(t)\} \cdot \sin\,[\omega_c t + \theta(t)] \qquad (3.3.11)$$

The terms $\cos\phi\{r(t)\}$ and $\sin\phi\{r(t)\}$ represent the nonlinear input amplitude to output phase conversion effect (AM/PM) while the term $R\{r(t)\}$ represents the nonlinear input amplitude to output amplitude conversion effect (AM/AM). The in-phase and quadrature nonlinearities of Fig. 3.3.3 are described by the envelope nonlinearities: $R\{r(t)\} \cdot \cos\phi\{r(t)\}$ and $R\{r(t)\} \cdot \sin\phi\{r(t)\}$.

From equation (3.1.8) the quaternary PSK signal can take the form:

$$S_{QPSK}(t) = A \sum_{k=-\infty}^{\infty} p(t-2kT)\cos\,[\omega_c t + \theta_k] \qquad (3.3.12)$$

where,

θ_K = equiprobable transmitted symbol selected from the set

$$\{\frac{\pi}{4} + \frac{2\pi i}{M}\}, i = 0,1,\ldots,M-1.$$

Equation (3.3.12) can be expanded as:

$$S_{QPSK}(t) = A \left[\sum_{k=-\infty}^{\infty} p(t-2kT) \cos \theta_k \cdot \cos \omega_c t \right.$$

$$\left. - \sum_{k=-\infty}^{\infty} p(t-2kT) \sin \theta_k \cdot \sin \omega_c t \right] \qquad (3.3.13)$$

or

$$S_{QPSK}(t) = R_e \{ e^{j\omega_c t} \sum_{k=-\infty}^{\infty} A(\cos \theta_k + j \sin \theta_k) \, p(t-2kT) \} \qquad (3.3.14)$$

Assuming, as before, that h(t) is the low-pass equivalent of the impulse response of the filtering between the modulator and the TWTA, the filtered equivalent signal at the input of the TWTA is:

$$U_{QPSK}(t) = \frac{1}{2} R_e \{ e^{j\omega_c t} \sum_{k=-\infty}^{\infty} A(\cos \theta_k + j \sin \theta_k) \, [p(t-2kT) * h(t)] \} \qquad (3.3.15)$$

Putting, the respective in-phase and quadrature components of the pulse response of the filter as:

$$R(t-2kT) = \frac{1}{2} R_e \{ p(t-2kT) * h(t) \} \qquad (3.3.16a)$$

and

$$I(t-2kT) = \frac{1}{2} I_m \{ p(t-2kT) * h(t) \} \qquad (3.3.16b)$$

then,

$$U_{QPSK}(t) = \sum_{-\infty}^{\infty} A[\cos \theta_k \cdot R(t-2kT) - \sin \theta_k \cdot I(t-2kT)] \cos \omega_c t$$

$$- \sum_{-\infty}^{\infty} A[\cos \theta_k \cdot I(t-2kT) + \sin \theta_k \, R(t-2kT)] \sin \omega_c t \qquad (3.3.17)$$

Equation (3.3.17) can be rewritten as:

$$U_{QPSK}(t) = x(t) \cos \omega_c t - y(t) \sin \omega_c t \qquad (3.3.18a)$$

or

$$U_{QPSK}(t) = \sqrt{x^2(t) + y^2(t)} \cdot \cos\left[\omega_c t + \text{arc} \cdot \tan \frac{y(t)}{x(t)}\right] \quad (3.3.18b)$$

where,

$$x(t) = \sum_{k=-\infty}^{\infty} A\left[\cos \theta_k \cdot R(t-2kT) - \sin \theta_k \cdot I(t-2kT)\right] \quad (3.3.19a)$$

$$y(t) = \sum_{k=-\infty}^{\infty} A\left[\cos \theta_k \cdot I(t-2kT) + \sin \theta_k \cdot R(t-2kT)\right] \quad (3.3.19b)$$

If the amplitude distortion (AM/AM) and the phase distortion (AM/PM) functions are assumed to be $g(\cdot)$ and $f(\cdot)$, respectively, then according to equation (3.3.10) the output of the TWTA is given by

$$V_o(t) = g\{A(t)\} \cdot \cos\left[\omega_c t + \text{arc} \cdot \tan \frac{y(t)}{x(t)} + f\{A(t)\}\right] \quad (3.3.20)$$

where,

$$A = \sqrt{x^2(t) + y^2(t)}$$

From the last expression it becomes evident that, due to the nonlinearity effect of the TWTA, large envelope fluctuations at the input of the TWTA are translated to more signal distortion at the output. The power spectrum at the output of the TWTA is given by [12].

$$W_o(f) = \int_{-\infty}^{\infty} e^{j\omega\tau}\, d\tau \frac{1}{2T} \int_{-T}^{T} \frac{1}{2} \{R_e[H\{x(t), y(t)\} H^*\{x(t+\tau), y(t+\tau)\} e^{-j\omega_c t}\}\, dF\,[x(t), y(t), x(t+\tau), y(t+\tau)]\, dt \quad (3.3.21)$$

where $F[x(t), y(t), x(t+\tau), y(t+\tau)]$ represents the probability distribution function of $x(t)$, $y(t)$, $x(t+\tau)$ and $y(t+\tau)$.

Figures 3.3.4 a,b and c show the power spectrum of quaternary PSK signals at the output of the TWTA for various symbol rates and input back-offs. It is seen that for a given symbol rate, the spread of the power spectrum which is primarily caused by the amplitude nonlinearity rather than the phase nonlinearity of the TWTA, decreases as the satellite input back-off increases.

The AM/AM conversion effect, in other words, produces new generated sidelobes which are superimposed on the low-level sidelobes of the bandlimited spectrum which results in adjacent channel interference. Tighter filtering is therefore required at the satellite output and/or at the earth station input in order to reduce this undesired interference or at least to keep it within acceptance levels. However, tighter filters will produce large amounts of intersymbol interference (ISI). Thus, trade-off is required to provide reduced adjacent channel interference while at the same time maintaining manageable ISI so that optimum system performance can be achieved. The AM/PM conversion effect is the cause for excessive phase errors at the receiver causing the performance of the system to degrade, as shown in Fig. 3.3.5 [13]. Both conversion effects are proportional to the envelope fluctuations r(t), as illustrated by equation (3.3.20) and modulated signals with small envelope variations are required for use in nonlinear channels. This is obtained by hard-limiting the signal prior to the TWTA. However, in QPSK, while hard-limiting restores the constant envelope to the modulated signal, at the same time restores essentially all the frequency sidelobes back to their original level prior to bandlimiting. This is shown in Fig. 3.3.6(a). On the other hand, hardlimiting does not produce the aforementioned

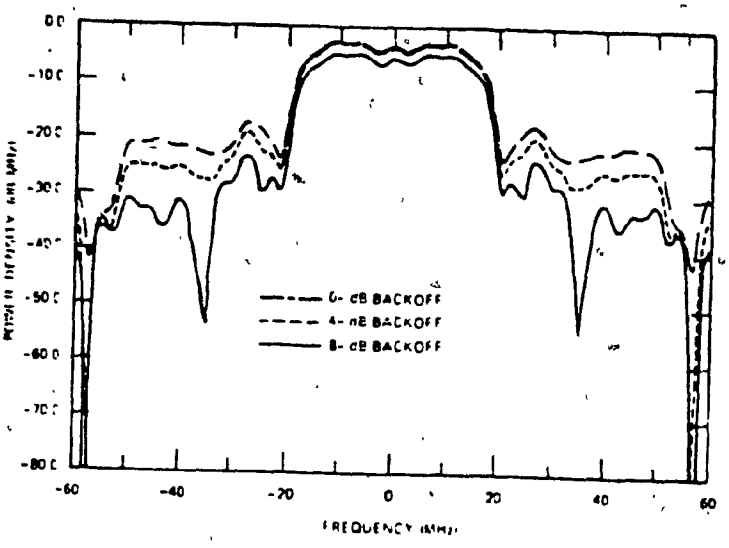

a SYMBOL RATE = 25 Mbaud (PEAKS OF 0-, 4- AND 8-dB INPUT BACKOFF CURVES CORRESPOND TO -14.5, -15.0 AND -18.5 dB RESPECTIVELY)

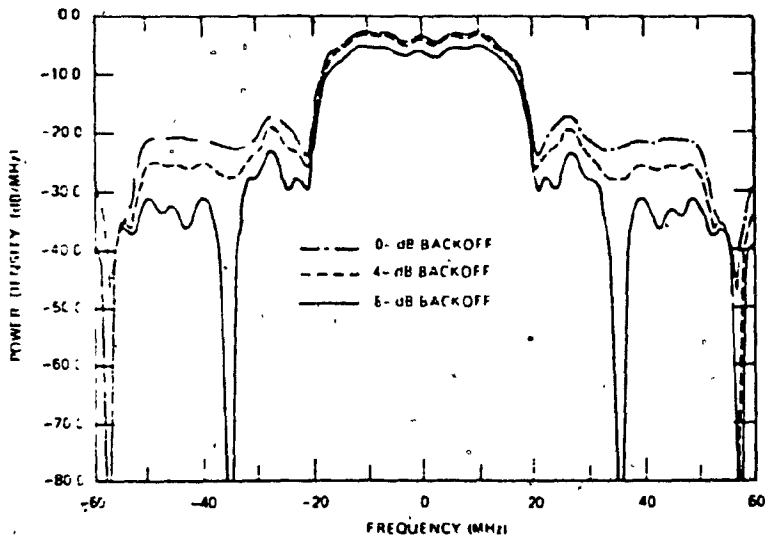

b SYMBOL RATE = 32 Mbaud (PEAKS OF 0-, 4- AND 8- dB INPUT BACKOFF CURVES CORRESPOND TO -15.5, -16.0 AND -17.5 dB RESPECTIVELY)

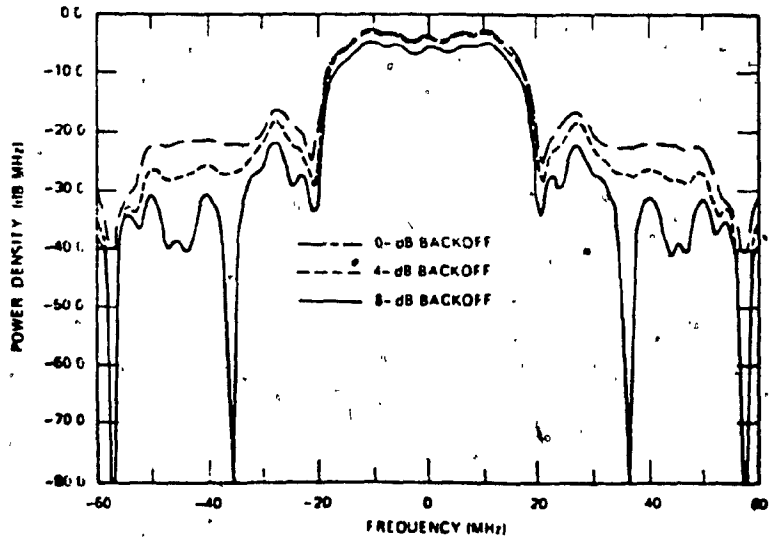

c SYMBOL RATE = 40 Mbaud (PEAKS OF 0-, 4-, AND 8- dB INPUT BACKOFF CURVES CORRESPOND TO -16.5, -17.0, AND -18.5 dB, RESPECTIVELY)

Fig. 3.3.4 Power Spectra of Quaternary PSK Signals at the Output of TWTA for Various Symbol Rates and Input Backoffs [12]

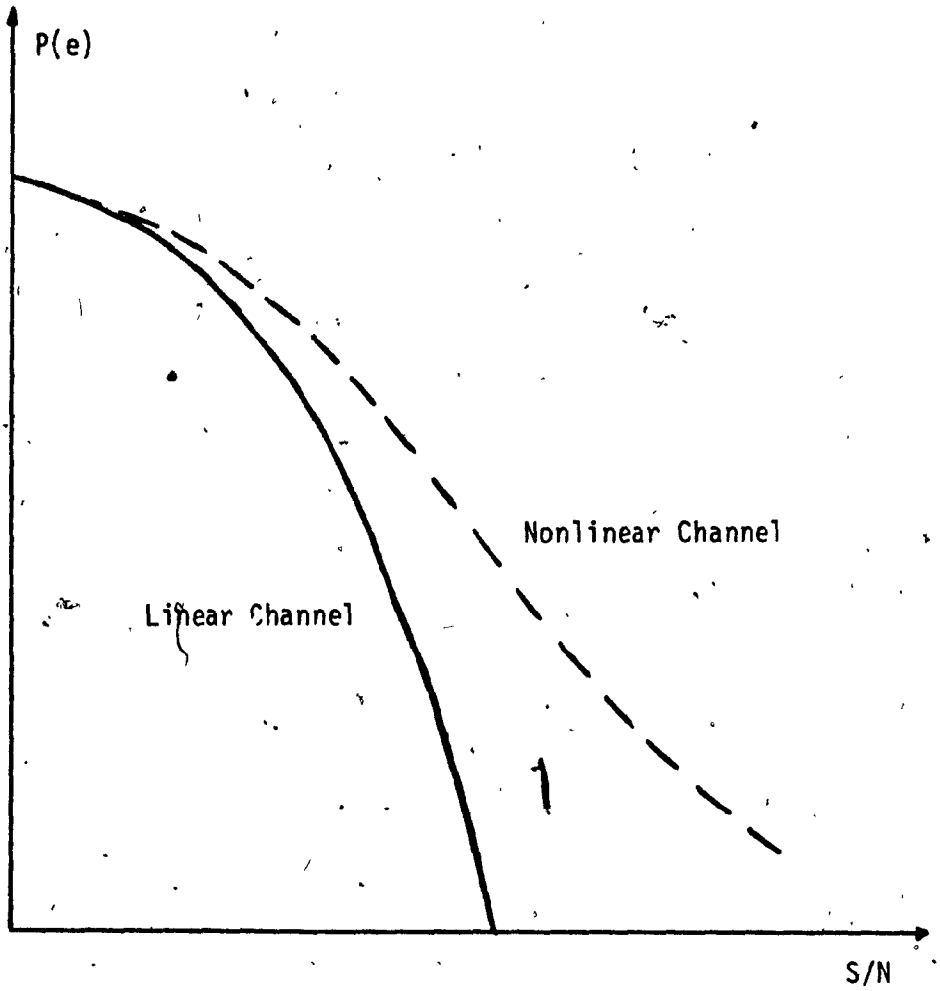

Fig. 3.3.5 Performance Degradation in Linear and Nonlinear Channels with small S/N, due to AM/PM Conversion effect

deleterious effects on an O-QPSK signal. When the bandlimited O-QPSK signal passes through a hardlimiter, the 3 dB envelope droop is removed without affecting the phase. Consequently, the absence of rapid phase shifts (and hence high frequency content) in the region of a 90° phase change means that hardlimiting will not generate the frequency sidelobes that the spectrum had prior to bandlimiting. Thus, with O-QPSK signal out-of-band interference is suppressed when the signal passes through a hardlimiter.

Tests [10] indicate that, as discussed previously, the power spectra of conventional and offset QPSK signals are identical up to the output of the filter. However, after limiting, unlike QPSK, the spectrum of O-QPSK remains essentially unchanged and seems to retain approximately its filtered value in the high frequency region. Thus, it becomes evident that O-QPSK signalling is more advantageous than QPSK in nonlinear channels. Fig. 3.3.6 illustrates the spectral spreading of QPSK and O-QPSK signals. As can be seen, at the output of the TWTA, the bandlimited and hardlimited QPSK retains its filtered spectrum. A lowpass BT_s product of 1 was used for the tests in Fig. 3.3.6, while BT_s products of 0.75, 0.625 and 0.5 were also used by Rhodes [10]. In all cases the results showed that the spectrum of the O-QPSK signal after hardlimiting remains essentially at its filtered nature. Therefore, the out-of-band suppression by O-QPSK signalling seems to be achieved for any practical bandwidth restriction. Fig. 3.3.7 illustrates the filtered as well as filtered and limited spectra of O-QPSK with BT_s equals to 0.5. Fig. 3.3.8 shows that the power spectrum of MSK signal after filtering and hardlimiting is approximately the same as that after filtering alone. This is because the MSK signal has a smoother phase transition than O-QPSK. MSK, therefore, is more immune to out-of-band interference.

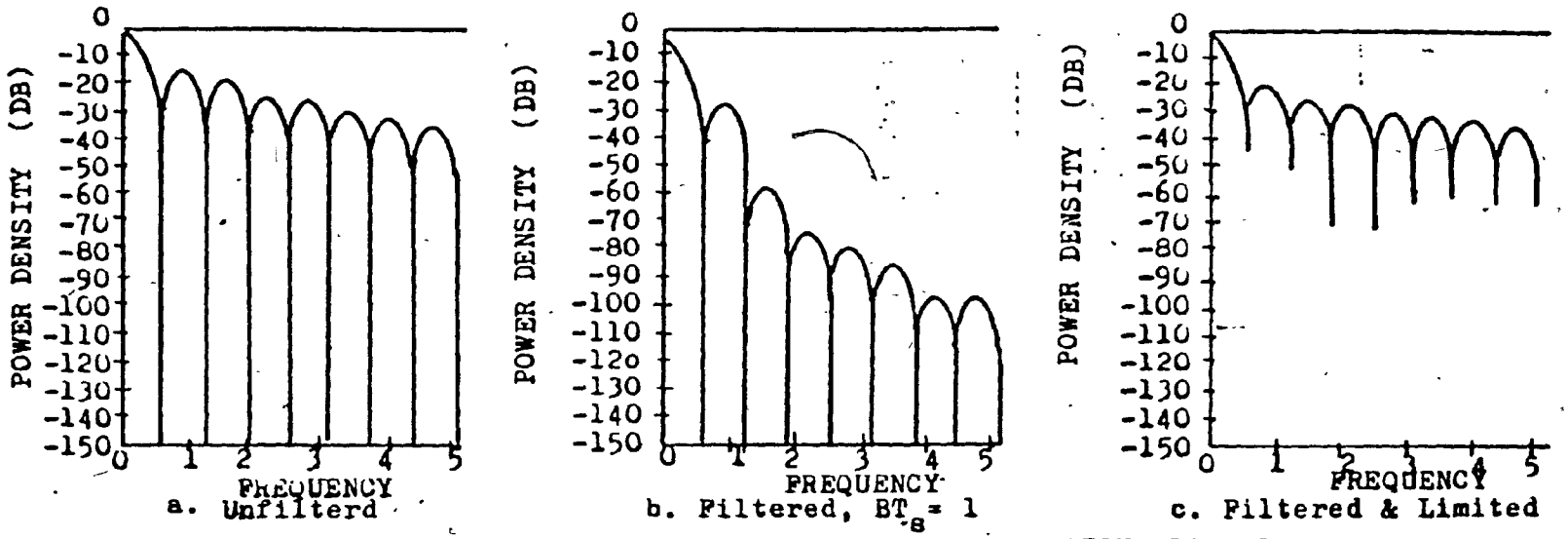

a. Unfilterd b. Filtered, $BT_s = 1$ c. Piltered & Limited

Power Spectra Obtained From Simulation of Conventional QPSK Signals

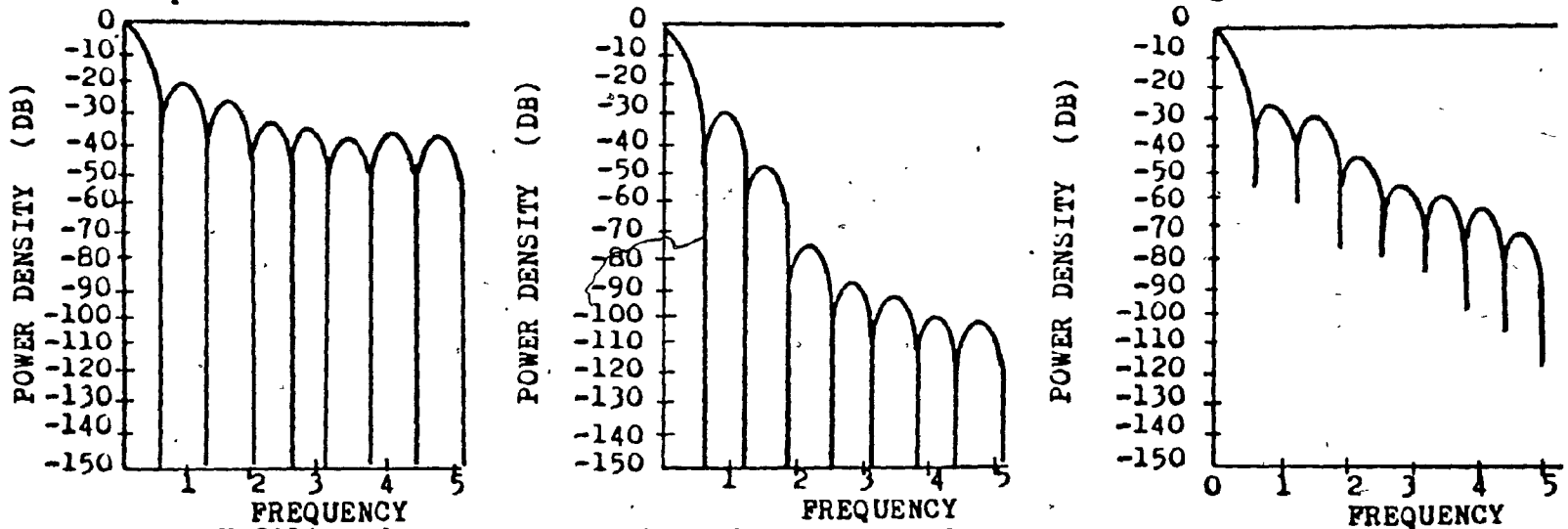

a. Unfiltered b. Filtered, $BT_s = 1$ c. Piltered & Limited

Power Spectra Obtained From Simulation of Offset QPSK Signals

B= low-pass equivalent bandwidth

T_s=Symbol duration

Fig. 3.3.6 Spectral Spreading of QPSK and O-QPSK Signals [34]

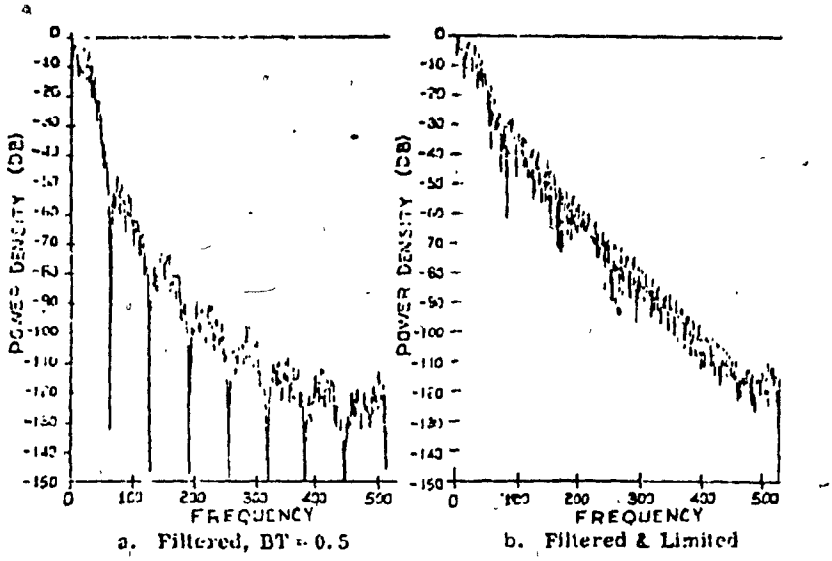

Fig. 3.3.7 Spectra for O-QPSK with Reduced Filter Bandwidth [10]

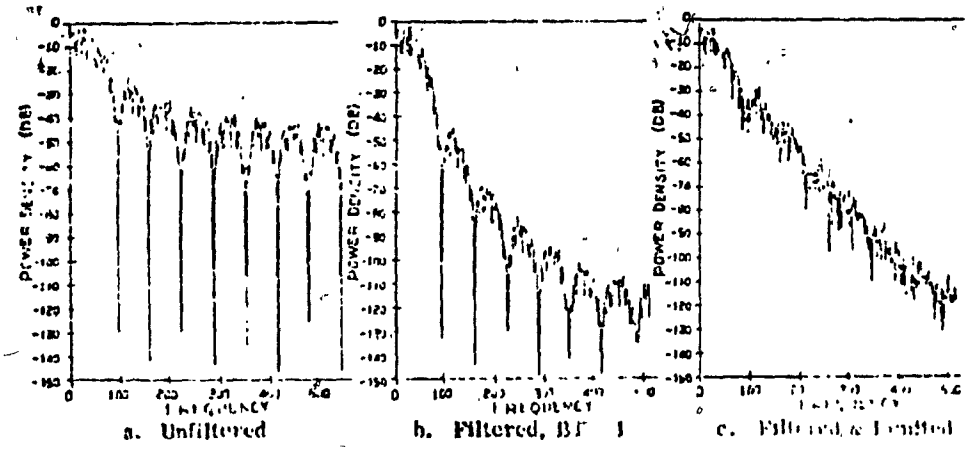

Fig. 3.3.8 Power Spectra Spreading of MSK Signals [10]

CHAPTER FOUR

4. THE QPSK AND O-QPSK MODEM

4.1 MODULATOR

Since, as discussed in section 3.1, the only difference between QPSK and O-QPSK is the time delay of half the symbol period ($T_s/2$) applied to one of the data streams in the latter system, the block diagrams of both are the same. Such a functional diagram is depicted in Fig. 4.1.1.

4.1.1 Scrambler

Most of today's digital transmission systems employ scrambling-descrambling circuits in order to ensure that the transmitted PSK spectrum is continuous and void of discrete frequency components, even though the NRZ data input may consist of repetitive patterns.

The principle of scrambling is illustrated in Fig. 4.1.2 [14] where a 5-stage self-synchronizing scrambler is shown. The output data is given by:

$$b_k = a_k \oplus b_{k-3} \oplus b_{k-5} \qquad (4.1.1)$$

where the symbol $\oplus$ denotes mod-2 addition.

The scrambling process adds a pseudo-random pattern to the input binary sequence by converting the binary pulses into a long term recurring sequence. The scrambler is basically a pseudo-random binary sequence (P.R.B.S) generator against which the data is exclusive-NORed to scramble it. Figure 4.1.3 shows a data scrambler. The P.R.B.S. generator consists of a binary linear feedback M stage shift-register.

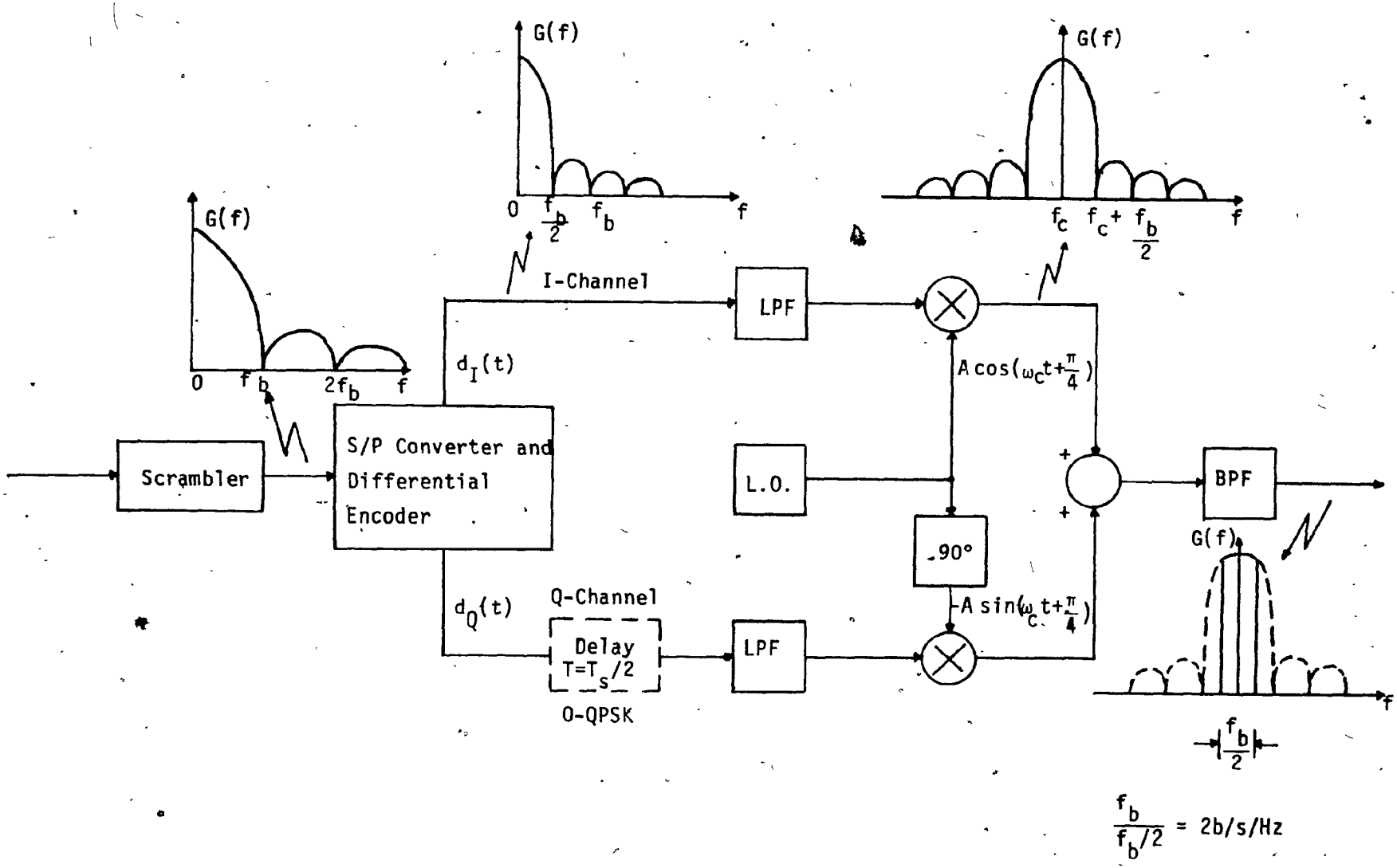

Fig. 4.1.1 Block Diagram of a Four-Phase PSK Modulator

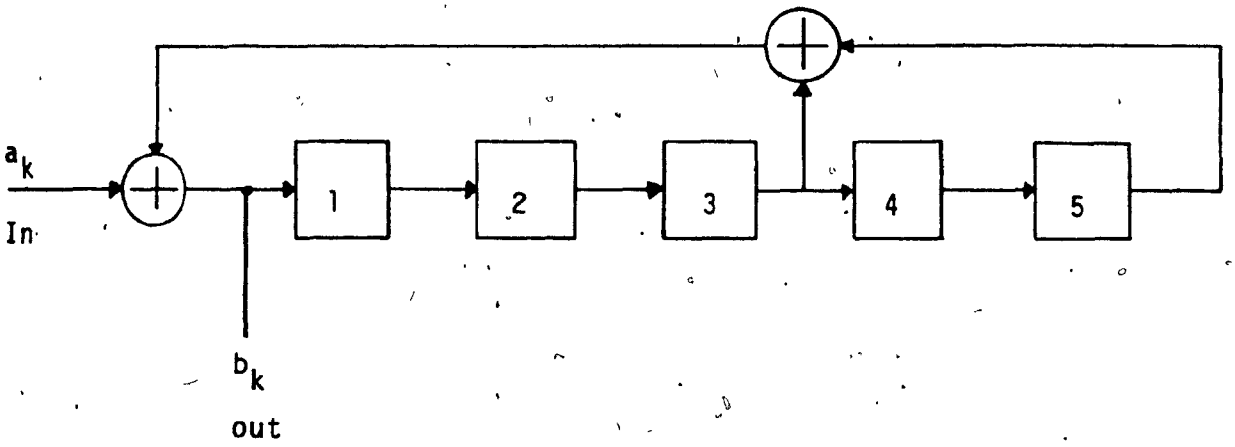

Fig. 4.1.2 Scrambler Principle

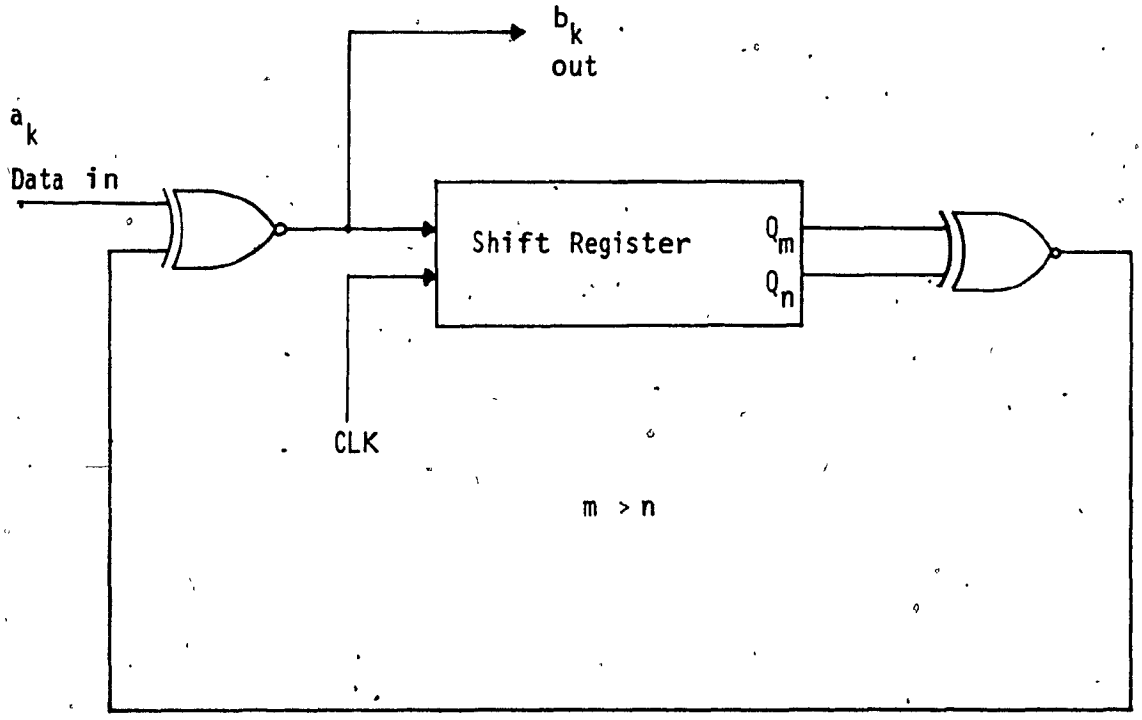

Fig. 4.1.3 Data Scrambler

Certain output stages of the shift register are modulo-2 added in an exclusive-NOR gate. The output from the adder is fed back into the input of the shift register. The so generated pulse sequence is well-known as maximal length sequence (m-sequence). The maximum period of the m-sequence is 2^{M-1} bits, M being the number of stages in the shift-register. The higher the number of stages used in the shift-register the higher would be the "randomness" in the scrambled signal. During normal operation, the scrambler produces an equiprobable output, that is, an average p(o)= p(1) = 0.5.

4.1.2 S/P Converter

The serial to parallel converter transforms the incoming data binary stream whose bit rate is f_b into two parallel symbol streams, I and Q, with rates $f_s = f_b/2$, as shown in Fig. 3.1.1. The converter alternates between its two outputs, the even bits of the binary input stream being present at the in-phase output while the odd bits being present at the quadrature phase output. The baseband spectrum of the individual I and Q channels has the same shape as that of the incoming data stream but since the symbol rate of both channels is half the bit rate, the nulls of the spectrum become multiples of half the bit rate. This is illustrated in Fig. 4.1.1.

4.1.3 Differential Encoding

Differential encoding is employed to coherent QPSK and O-QPSK systems to resolve the phase ambiguity of the recovered data at the receiver. Ambiguity as to the exact phase orientation of the received signal is caused because of the carrier recovery network. Differential

encoding is discussed extensively in section 4.5.

4.1.4 Oscillator and Phase Shift Network

The two encoded data streams $\{d_I\}$ and $\{d_Q\}$ are filtered respectively by low-pass filters and are applied to balanced mixers. The oscillator in conjunction with a 90° phase shift network generates two carriers of the same frequency but 90° out of phase, the in-phase carrier and the quadrature phase carrier. The two carriers are applied to two mixers, one carrier to each mixer. These carriers can be expressed by:

$$C_I = A \cos (\omega_c t + \frac{\pi}{4})$$

$$C_Q = A \sin (\omega_c t + \frac{\pi}{4}) \qquad (4.1.2)$$

4.1.5 Balanced Mixers and Summer

The encoded data stream $\{d_I\}$ modulates the in-phase carrier in a balanced mixer while the encoded data stream $\{d_Q\}$ modulates the quadrature phase carrier in the second balanced mixer. Multiplication of a carrier by a logic state "1" which corresponds to a positive rectangular pulse whose value is expressed by equation (3.1.2) does not change the phase of the unmodulated carrier

$$U_{m_I}^{+}(t) = \frac{A}{\sqrt{2}} \cos (\omega_c t + \frac{\pi}{4}) \qquad (4.1.3)$$

However, multiplication of the carrier by a logic state "0" which corresponds to a negative rectangular pulse of the same value, produces a 180° change in the phase of the unmodulated carrier.

$$U_{m_I}(t) = \pm\frac{A}{\sqrt{2}} \cos\left(\omega_c t + \frac{\pi}{4}\right) = \frac{A}{\sqrt{2}} \cos\left(\omega_c t + \frac{\pi}{4} + \pi\right) \quad (4.1.4)$$

Thus, an alternate encoded logic sequence of ones and zeros shifts the carrier instantaneously from 0° to 180° and vice versa. The power spectrum of the modulated signal at the output of the mixer is shown in Fig. 4.1.1.

The quadrature phase carrier, which is in 90° phase difference with the in-phase carrier is modulated with the second encoded data stream in the second balanced mixer. Its phase changes from 90° to 270° and vice versa, by the alternate second encoded logic sequence of ones and zeros. Both mixers outputs are BPSK modulated signals and are said to be orthogonal because there is 90° shift in the I and Q modulated signals.

The modulated carriers are linearly combined in the summing network to produce a four-phase PSK signal. The QPSK signal consists of two signals in quadrature, which occupy the same spectrum, but independently recoverable at the receiver.

Finally, the four-phase PSK signal is bandlimited by the transmit band-pass filter (BPF) to suppress the out-of-band interference.

In the O-QPSK modulator, a time delay equal to one half the symbol duration, $T_s/2$, is inserted into the Q data channel as shown in Fig. 4.1.1. Because of this delay, the phase transitions in the O-QPSK waveform occur every T seconds (Fig. 3.1.5), whereas the QPSK waveform has transitions only every 2T seconds (Fig. 3.1.4) since both data channels are synchronously aligned.

4.2 DEMODULATOR

4.2.1 Optimum Detection of QPSK and O-QPSK

As discussed in section 2.2 for optimum PSK detection, sampling

must occur at the symbol rate, because at this rate the signal has its maximum value for each specified symbol interval. Therefore, since a quaternary PSK signal consists of two binary data channels where components are antipodal, optimum detection can be obtained by taking samples at times t = 2kT for both quadrature channels of a QPSK system, or at times t = 2kT (I-channel) and t = (2k+1)T (Q-channel) for an O-QPSK system.

From Fig. 2.1.2 it becomes evident that the reference signal which is required at an optimum correlator receiver must be

$$S(t) = S_2(t) - S_1(t) \qquad (4.2.1)$$

Since both components of the quaternary PSK signal are orthogonal, the use of a correlator receiver for detection will produce one component of the quaternary signal depending on the reference signal that is used. This is explained by the fact that the orthogonal to the reference signal component is cancelled at the output of the integrator, as the integral of the product of two orthogonal signals is zero. Omitting, the amplitude value A of the carrier (no loss of generality), the reference signal required for the in-phase and quadrature phase channels are:

$$S_I(t) = S_{I_2}(t) - S_{I_1}(t) = \sqrt{2} \cos\left(\omega_c t + \frac{\pi}{4}\right) \qquad (4.2.2)$$

$$S_Q(t) = S_{Q_2}(t) - S_{Q_1}(t) = \sqrt{2} \sin\left(\omega_c t + \frac{\pi}{4}\right) \qquad (4.2.3)$$

In QPSK reception, the integration periods of both correlator receivers must be from 2kT to (2k + 2)T, while in O-QPSK reception the periods of integration must be from 2kT to (2k+2)T for the I-channel and (2k+1)T to (2k+3)T for the Q-channel. Thus, at the outputs of the

integrators the signals are:

$$I_I(t) = \int_{2kT}^{(2k+2)T} \{\frac{1}{\sqrt{2}} d_I(t) \cos(\omega_c t + \frac{\pi}{4}),$$

$$+ \frac{1}{\sqrt{2}} d_Q(t) \sin(\omega_c t + \frac{\pi}{4})\}\sqrt{2} \cos(\omega_c t + \frac{\pi}{4}) dt$$

$$= d_I(t)\, T, \text{ for the I channel} \qquad (4.2.4)$$

$$I_{Q(QPSK)}(t) = \int_{2kT}^{(2k+2)T} \{\frac{1}{\sqrt{2}} d_I(t) \cos(\omega_c t + \frac{\pi}{4})$$

$$+ \frac{1}{\sqrt{2}} d_Q(t) \sin(\omega_c t + \frac{\pi}{4})\}\sqrt{2} \sin(\omega_c t + \frac{\pi}{4}) dt$$

and,

$$I_{Q(O\text{-}QPSK)}(t) = \int_{(2k+1)T}^{(2k+3)T} \{\frac{1}{\sqrt{2}} d_I(t) \cos(\omega_c t + \frac{\pi}{4})$$

$$+ \frac{1}{\sqrt{2}} d_Q(t) \sin(\omega_c t + \frac{\pi}{4})\}\sqrt{2} \sin(\omega_c t + \frac{\pi}{4}) dt$$

$$= d_Q(t)\, T, \text{ for the Q-channel} \qquad (4.2.5)$$

In order to regenerate the I and Q channel symbols, the samples obtained at the output of the integrators should be held for 2T sec. Such an optimum four-phase PSK receiver is shown in Fig. 4.2.1.

In practical applications, however, low-pass filters are employed instead of integrators, because when the data rate is high then the integrators do not have enough time to reset, before the next symbol proceeds too far. In such case the products at the mixers outputs are:

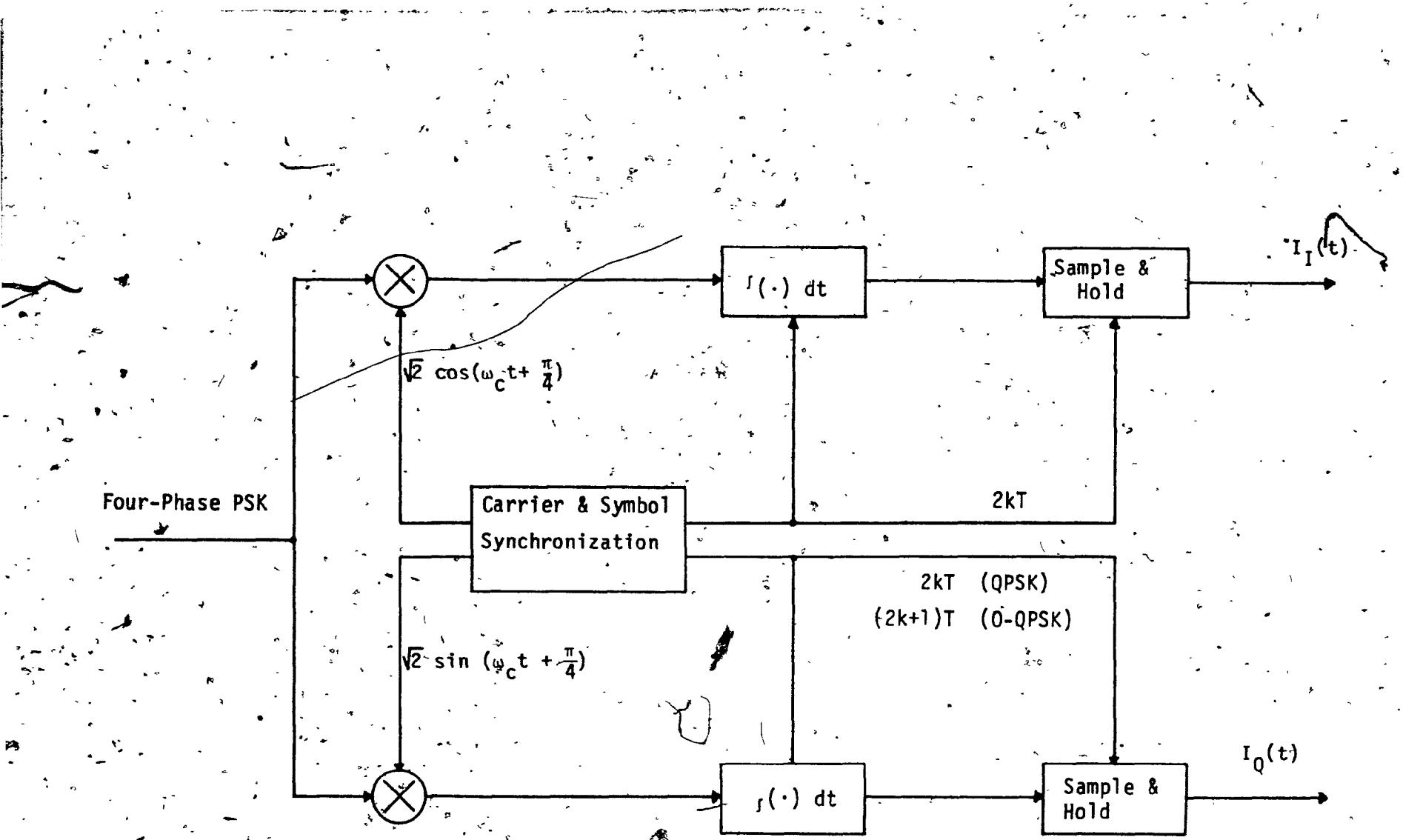

Fig. 4.2.1 Four-Phase PSK Optimum Receiver

$$m_I(t) = \{\frac{1}{\sqrt{2}}\ d_I(t)\cdot\cos\ (\omega_c t + \frac{\pi}{4})$$

$$+ \frac{1}{\sqrt{2}}\ d_Q(t)\ \sin\ (\omega_c t + \frac{\pi}{4})\}\sqrt{2}\ \cos\ (\omega_c t + \frac{\pi}{4})$$

$$= \frac{d_I(t)}{2} - \frac{d_I(t)}{2}\ \sin\ 2\omega_c t + \frac{d_Q(t)}{2}\ \cos\ 2\omega_c t \quad (4.2.6)$$

and

$$m_Q(t) = \{\frac{1}{\sqrt{2}}\ d_I(t)\ \cos\ (\omega_c t + \frac{\pi}{4})$$

$$+ \frac{1}{\sqrt{2}}\ d_Q(t)\ \sin\ (\omega_c t + \frac{\pi}{4})\}\sqrt{2}\ (\omega_c t + \frac{\pi}{4})$$

$$= \frac{d_Q(t)}{2} - \frac{d_Q(t)}{2}\ \sin\ 2\omega_c t + \frac{d_I(t)}{2}\ \cos\ 2\omega_c t \quad (4.2.7)$$

At the outputs of the low-pass filters the I- and Q-data are recovered as:

$$m_{FI}(t) = \frac{d_I(t)}{2}$$

and (4.2.8)

$$m_{FQ}(t) = \frac{d_Q(t)}{2}$$

The detected symbols are then sampled at their midpoints, where the symbol maximum values are present due to bandlimiting, and the recovered data are next decoded in order to obtain the initial data stream.

4.2.2 Practical Receiver

A block diagram of a coherent QPSK or O-QPSK receiver is

shown in Fig. 4.2.2. The incoming four-phase signal is applied to carrier recovery circuit and to power splitter which provides the I and Q channels with identical characteristics of the incoming signal but half its rate. The carrier recovery circuit provides an accurate and stable carrier reference for coherent detection of the I- and Q-data in the two balanced mixers. The timing recovery circuit produces the proper clocking for the threshold detectors which generate the data pulses, and also for the parallel-to-serial converter, the differential decoder and the descrambler. The data descrambler performs the inverse operation of that of the scrambler and can be realized with a binary linear feed forward (M stages) shift register. The feed forward connection is exactly the same on the feedback connection in the scrambler and is made by a modulo-2 adder as shown in Fig. 4.2.3 for the case of M equal 6.

If b_k and c_k are the descrambler input and output respectively, then

$$c_k = b_k \oplus b_{k-3} \oplus b_{k-5}$$

$$= a_k \oplus b_{k-3} \oplus b_{k-5} \oplus b_{k-3} \oplus b_{k-5} = a_k \qquad (4.2.9)$$

The output of the descrambler is the original data sequence at the input of the scrambler at the transmittter.

A descrambler which corresponds to the scrambler of Fig. is shown in Fig. 4.2.4.

The carrier timing recovery and bit timing recovery circuits are described analytically in the following two sections.

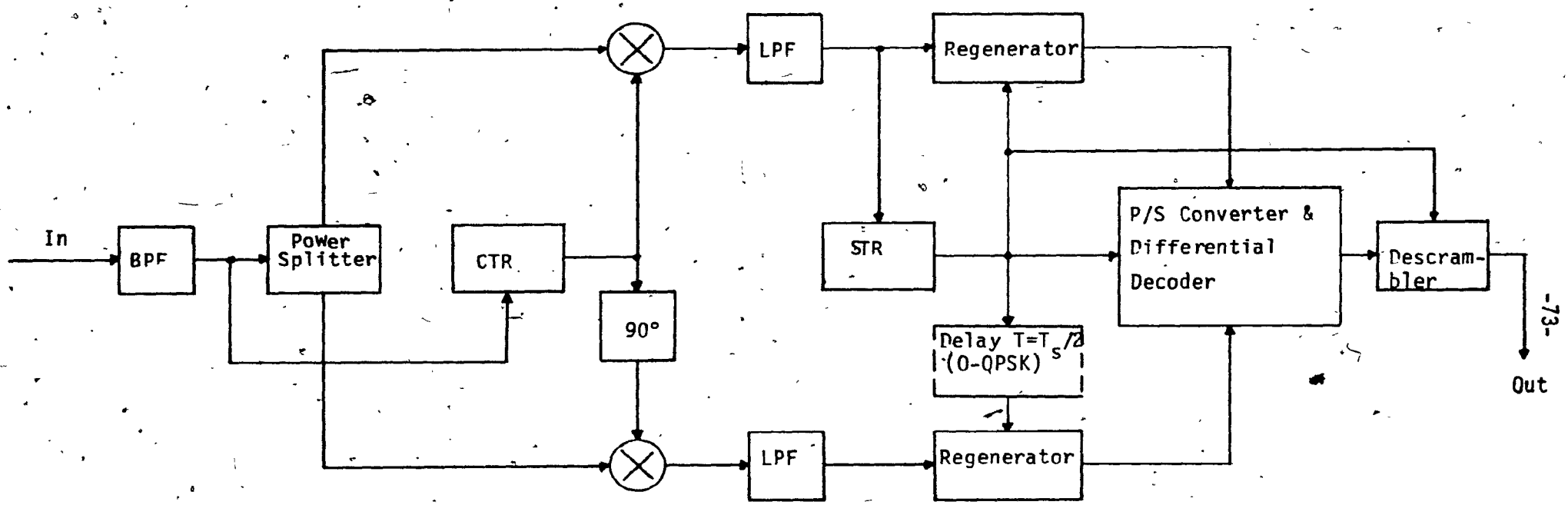

Fig. 4.2.2 Four-Phase PSK Coherent Demodulator.

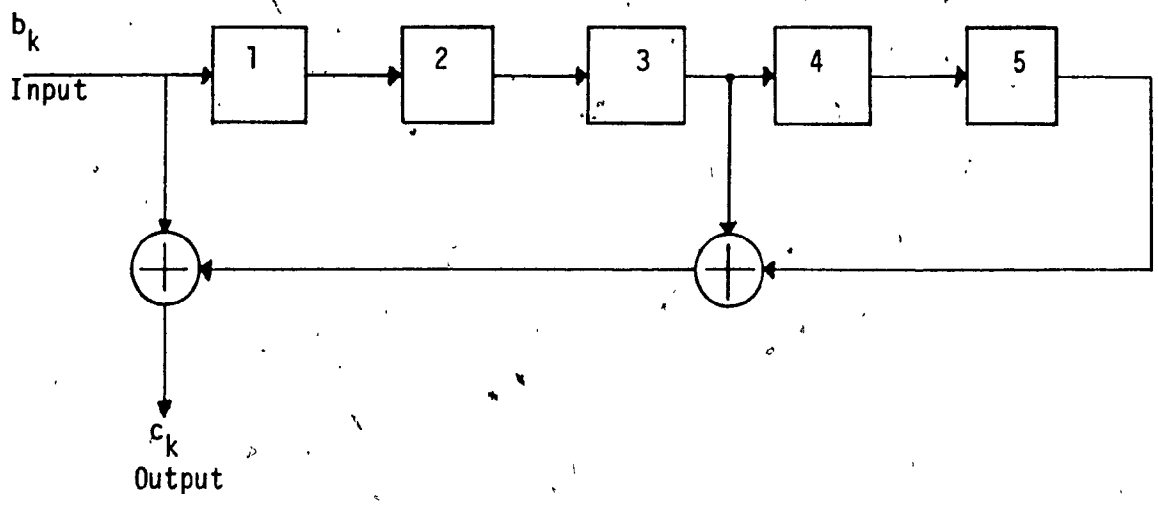

Fig. 4.2.3 Descrambler Principle

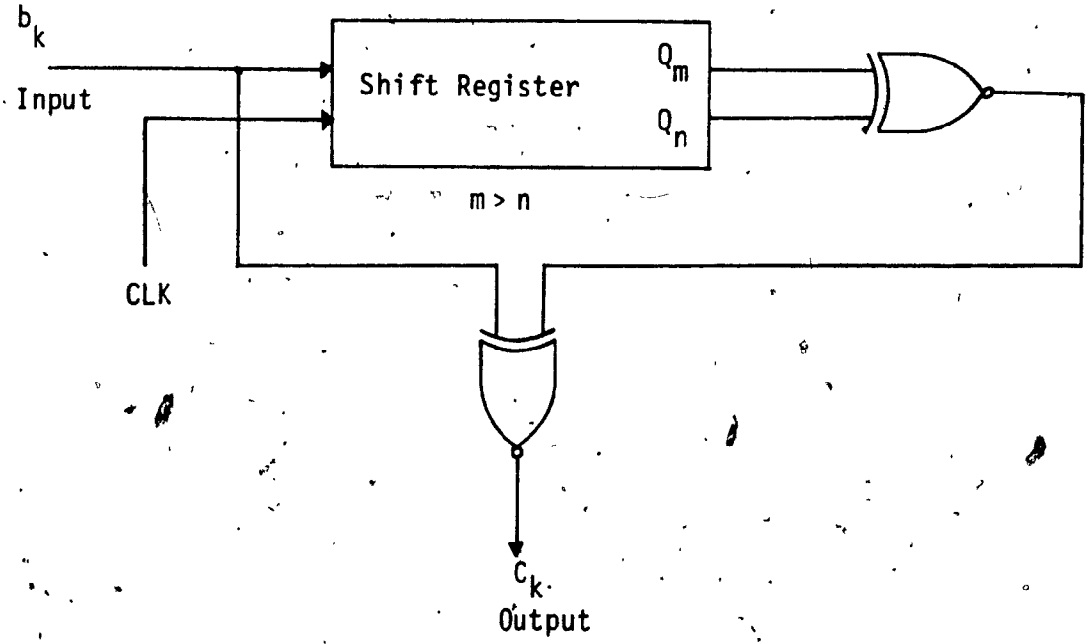

Fig. 4.2.4 Data Descrambler

4.3 CARRIER RECOVERY CIRCUIT (CTR)

In digital modulation systems with four-phase PSK and coherent detection, it is very important to realize an accurate and stable synchronizer which will provide the carrier reference necessary for the coherent demodulation of the I- and Q-data. The most popular methods of recovering the carrier reference use nonlinear signal processing and are described below.

4.3.1 Quadrupler

The four-phase PSK signal

$$S(t) = A \cos(\omega_c t + \theta) \tag{4.3.1}$$

passes through a X4 multiplier, as shown in Fig. 4.3.1 (a) and (b), and the output is

$$S^4(t) = A^4 \cos^4(\omega_c t + \theta)$$

$$= \frac{3}{8} A^4 + \frac{1}{2} A^4 \cos(2\omega_c t + 2\theta) + \frac{1}{8} A^4 \cos(4\omega_c t + 4\theta) \tag{4.3.2}$$

It follows that a narrow BPF may be employed to separate the $\cos(4\omega_c t + 4\theta)$ signal which is the fourth harmonic of the desired coherent reference. Finally, a frequence divider (Fig. 4.3.1 a) is employed to yield the required signal reference $\cos(\omega_c t + \theta)$ where $\theta = \frac{2\pi i}{M} = \pi i/2$, $i = 0,1,2,3$. However, since the BPF must be very narrow which is difficult to realize and also since the X4 multiplier inevidably degrades the signal-to-noise ratio, a phase-lock-loop (PLL) is usually employed as shown in Fig. 4.3.1(b). As one can see the carrier recovery circuit can lock-on to anyone of the four transmitted phases represented by θ.

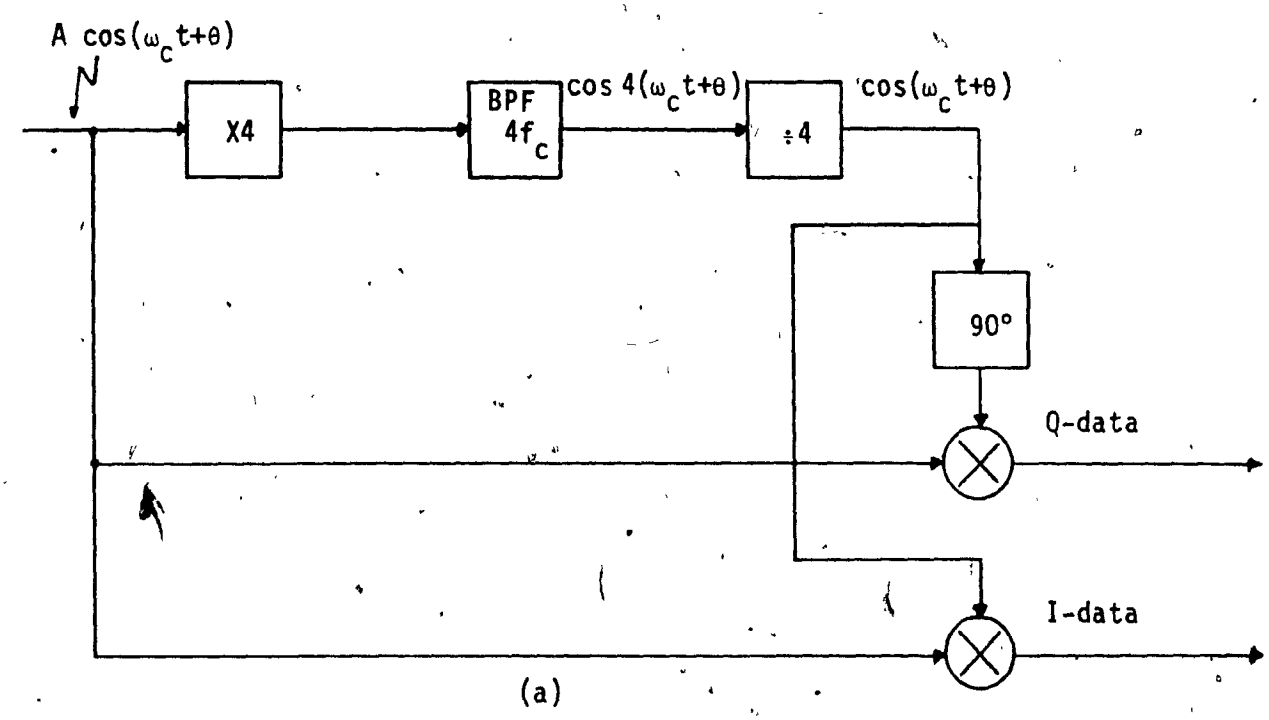

(a)

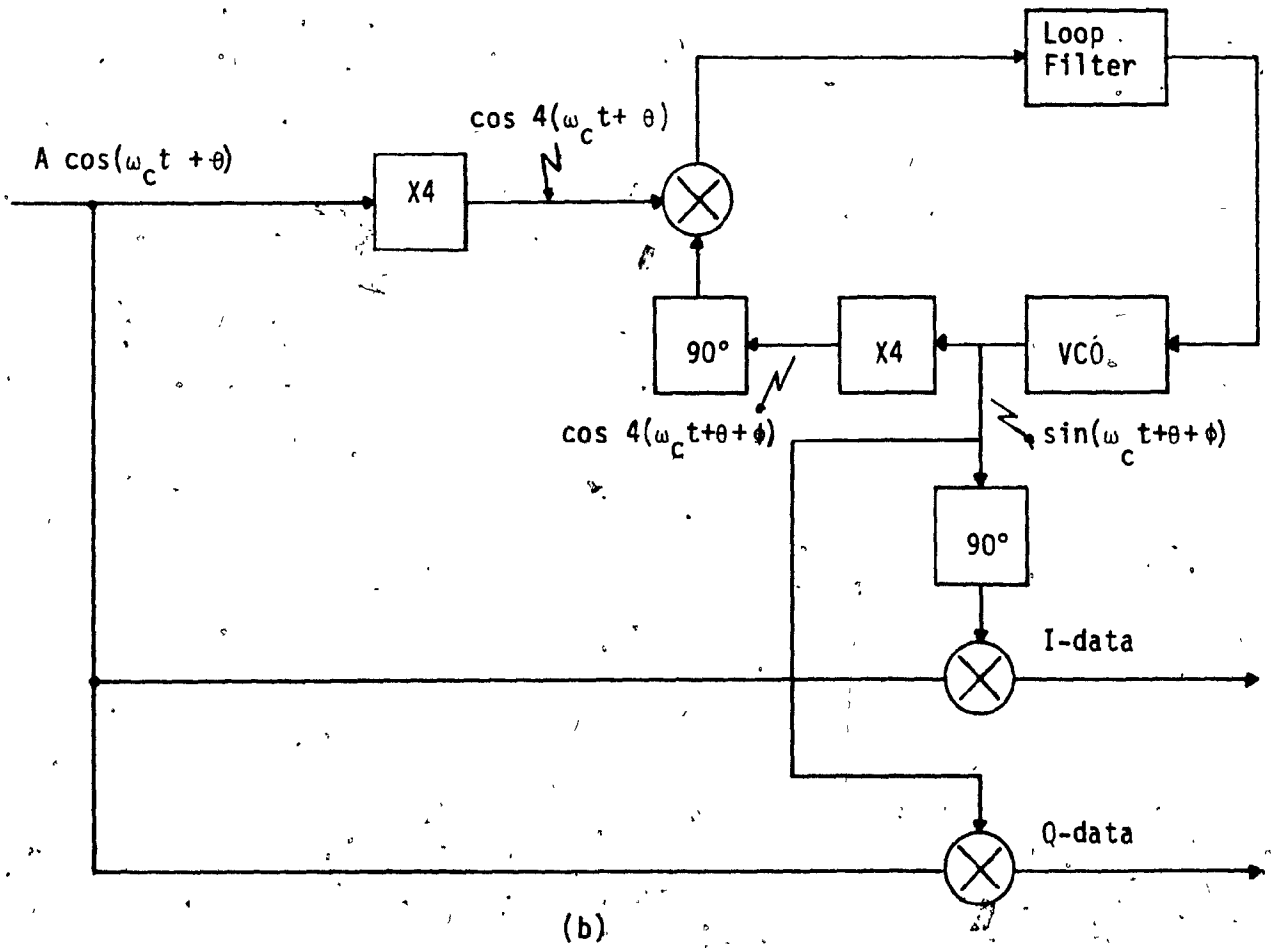

(b)

Fig. 4.3.1 Quadrupler Method [20]

Namely, θ =0°, 90°, 180°, 270°. This four-fold ambiguity is resolved by differential encoding as discussed in section 4.5.

4.3.2 Remodulation Method

Four-phase PSK carrier recovery using the remodulation method (sometimes called Phase-reverse modulation) is shown in Fig. 4.3.2 [15]. In this method, the demodulated I- and Q-data streams are used to remodulate the received four-phase signal producing two-phase signals at the output of the second mixers. The two signals are then combined using an adder and the resultant signal is the desired coherent reference. Setting the delays of each channel $T_1 = T_I = T_Q = T$, the products on the first pair of mixers are:

$$m_{I_1}(t) = [d_I(t) \cos \omega_c t + d_Q(t) \sin \omega_c t] \times 2\cos(\omega_c t + \phi) \tag{4.3.3}$$

$$m_{Q_1}(t) = [d_I(t) \cos \omega_c t + d_Q(t) \sin \omega_c t] \times 2\sin(\omega_c t + \phi) \tag{4.3.4}$$

These two signals at the output of the LPF's have the form:

$$m_{FI_1}(t) = d_I(t) \cdot \cos \phi - d_Q(t) \cdot \sin \phi \tag{4.3.5}$$

$$m_{FQ_1}(t) = d_Q(t) \cdot \cos \phi + d_I(t) \cdot \sin \phi \tag{4.3.6}$$

Thus, the products of the second pair of mixers are:

$$m_{I_2}(t-T) = [d_I(t-T) \cos \omega_c(t-T) + d_Q(t-T) \cdot \sin \omega_c(t-T)] \times [d_I(t-T) \cos \phi - d_Q(t-T) \cdot \sin \phi] \tag{4.3.7}$$

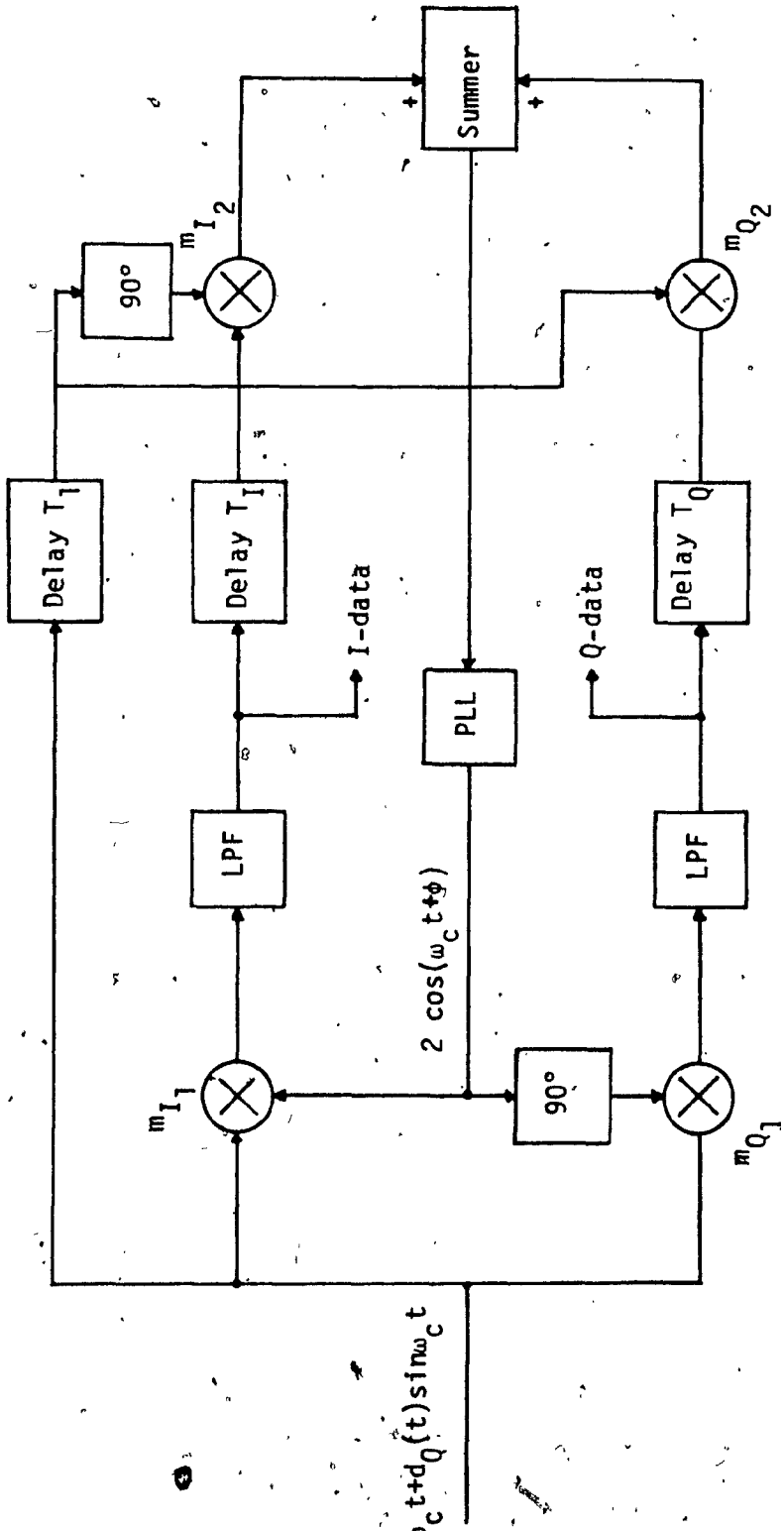

Fig. 4.3.2. Remodulation Method [15]

$$m_{Q_2}(t-T) = [d_I(t-T)\cos\omega_c(t-T) + d_Q(t-T)\cdot\sin\omega_c(t-T)]$$
$$\times [d_Q(t-T)\cos\phi + d_I(t-T)\cdot\sin\phi] \qquad (4.38)$$

Defining $\tau = t-T$, and since $d_I(t-T)\cdot d_Q(t-T) = \pm 1 = D(t)$, the last expressions can be rewritten as:

$$m_{I_2}(\tau) = [\cos\phi\cdot\cos\omega_c\tau - \sin\phi\cdot\sin\omega_c\tau]$$
$$+ D(t)[\cos\phi\cdot\sin\omega_c\tau - \sin\phi\cdot\cos\omega_c\tau] \qquad (4.3.9)$$

$$m_{Q_2}(\tau) = [\cos\phi\cdot\sin\omega_c\tau + \sin\phi\cdot\cos\omega_c\tau]$$
$$+ D(t)[\cos\phi\cdot\cos\omega_c\tau + \sin\phi\cdot\sin\omega_c\tau] \qquad (4.3.10)$$

Therefore, the sum of the products is:

$$\Sigma(\tau) = m_{I_2}(\tau) + m_{Q_2}(\tau)$$
$$= 2[\cos\phi\cdot\cos\omega_c\tau + \cos\phi\cdot\sin\omega_c\tau] \text{ when } D(t) = +1 \qquad (4.3.11)$$
$$= 2[\sin\phi\cdot\cos\omega_c\tau - \sin\phi\cdot\sin\omega_c\tau] \text{ when } D(t) = -1 \qquad (4.3.12)$$

As a result, the resultant signal at the output of the combiner can have the form:

$$\Sigma(\tau) = 2[\cos(\phi+45°)\cdot\sin\omega_c\tau + \cos(\phi-45°)\cdot\cos\omega_c\tau] \qquad (4.3.13)$$

Evidently, a clean tone is present at ω_c rather than $4\omega_c$, as in the case of the carrier recovery implementing the quadrupler. The combined single phase component is acquired by the PLL in order to generate the single phase carrier.

4.3.3 Costas Loop Method

This recovery carrier technique is very similar to the re-modulation method. The two demodulated quadrature signals are used to cross-modulate each other and then by substraction of the resultants a carrier reference is generated.

As shown in Fig. 4.3.3 the filtered product outputs of the first pair of mixers are:

$$m_{FI_1}(t) = \frac{A}{\sqrt{2}} [d_I(t) \cos \omega_c t + d_Q(t) \sin \omega_c t] \times 2 \cos (\omega_c t + \phi)$$

$$= \frac{A}{\sqrt{2}} [d_Q(t) \cdot \cos \phi + d_I(t) \sin \phi] \qquad (4.3.14)$$

$$m_{FQ_1}(t) = \frac{A}{\sqrt{2}} [d_I(t) \cdot \cos \omega_c t + d_Q(t) \cdot \sin \omega_c t] \times 2\sin(\omega_c t + \phi)$$

$$= \frac{A}{\sqrt{2}} [d_I(t) \cdot \cos \phi - d_Q(t) \cdot \sin \phi] \qquad (4.3.15)$$

The product outputs of the second pair of mixers are:

$$m_{I_2}(t) = \frac{A}{\sqrt{2}} [d_Q(t) \cdot \cos \phi + d_I(t) \cdot \sin \phi] \cdot d_I(t)$$

$$= \frac{A}{\sqrt{2}} [\cos \phi + \sin \phi] \qquad (4.3.16)$$

$$m_{Q_2}(t) = \frac{A}{\sqrt{2}} [d_I(t) \cos \phi - d_Q(t) \sin \phi] \cdot d_Q(t)$$

$$= \frac{A}{\sqrt{2}} [\cos \phi - \sin \phi] \qquad (4.3.17)$$

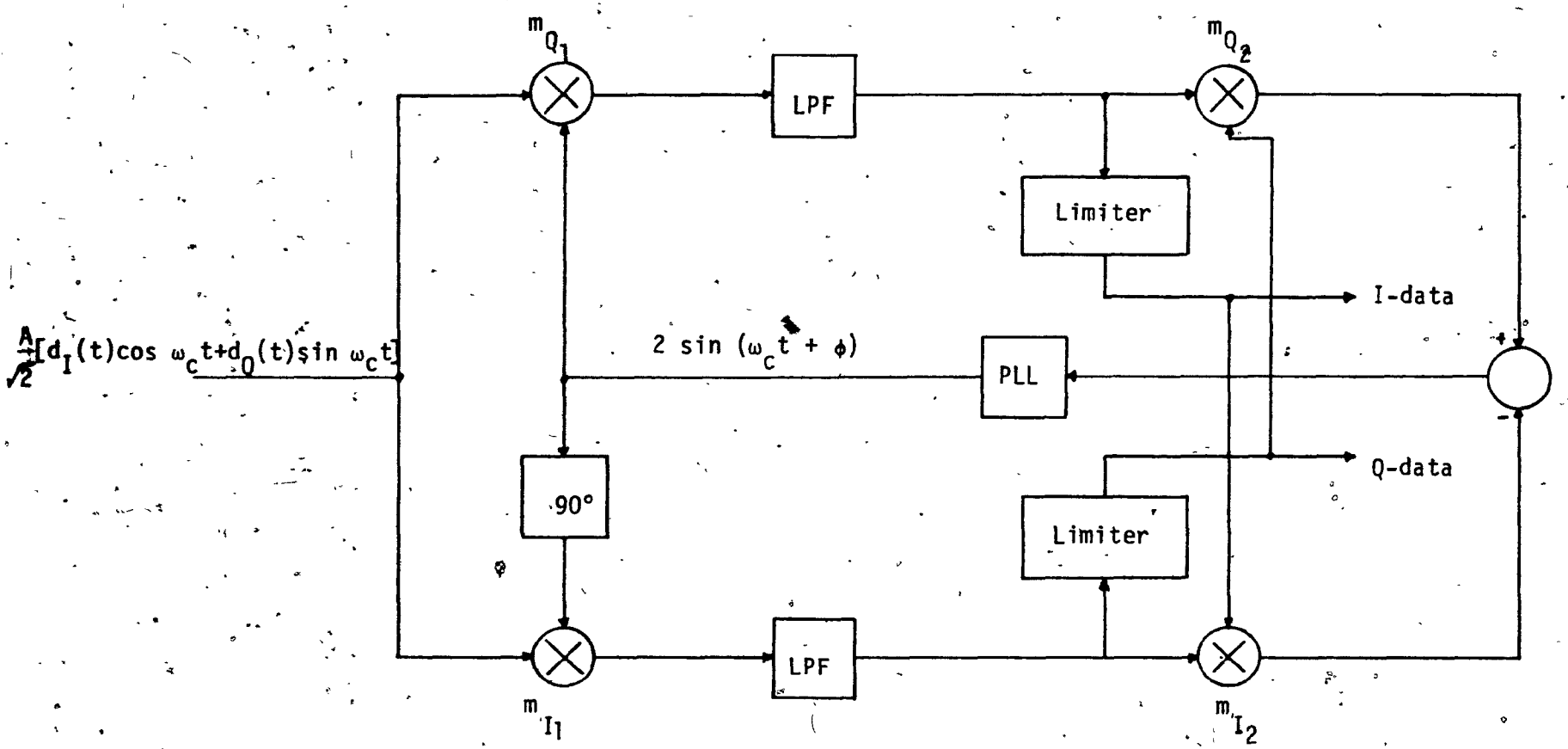

Fig. 4.3.3 Costas Loop Method [20]

The resultant signal of the subtractor is:

$$\Sigma_{dif}(t) = \sqrt{2}A \cdot \sin \phi \qquad (4.3.18)$$

The Costas loop carrier recovery technique, as the remodulation method, arises four-phase ambiguity which is resolved by coding as discussed in section 4.5.

4.4 BIT TIMING RECOVERY (BTR)

Timing recovery is one of the most important function performed by a coherent modem. The objective is to extract a tone located at the bit or symbol rate, depending upon the fed signal to the timing recovery network, which is required in the operation of the threshold detectors, the parallel-to-serial converter, the differential decoder and the descrambler.

The timing recovery circuit usually employs a nonlinear signal processing element which generates a discrete spectral component at the bit rate multiple. This can be achieved by the NRZ to RZ digital code conversion, shown in Fig. 4.4.1 along with the waveforms which show how the timing tone is extracted from the received data.

Another timing recovery technique is the pre-demodulation technique which is shown in Fig. 4.4.2. Let the received signal be

$$S(t) = d(t) \cos \omega_c t \qquad (4.4.1)$$

where d(t) is a NRZ waveform with period of T. For simplicity, assuming

$$d(t) = A \cos \omega_a t \qquad (4.4.2)$$

where,

$$\omega_a = \omega_b/2 = \frac{1}{2} \text{ clock rate}$$

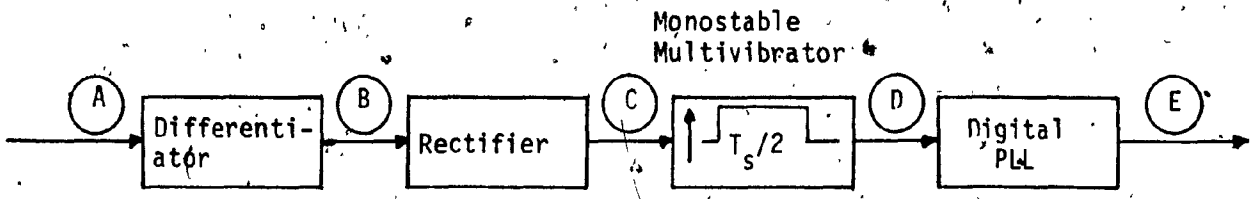

(a) Block Diagram of a Symbol Timing Recovery Circuit

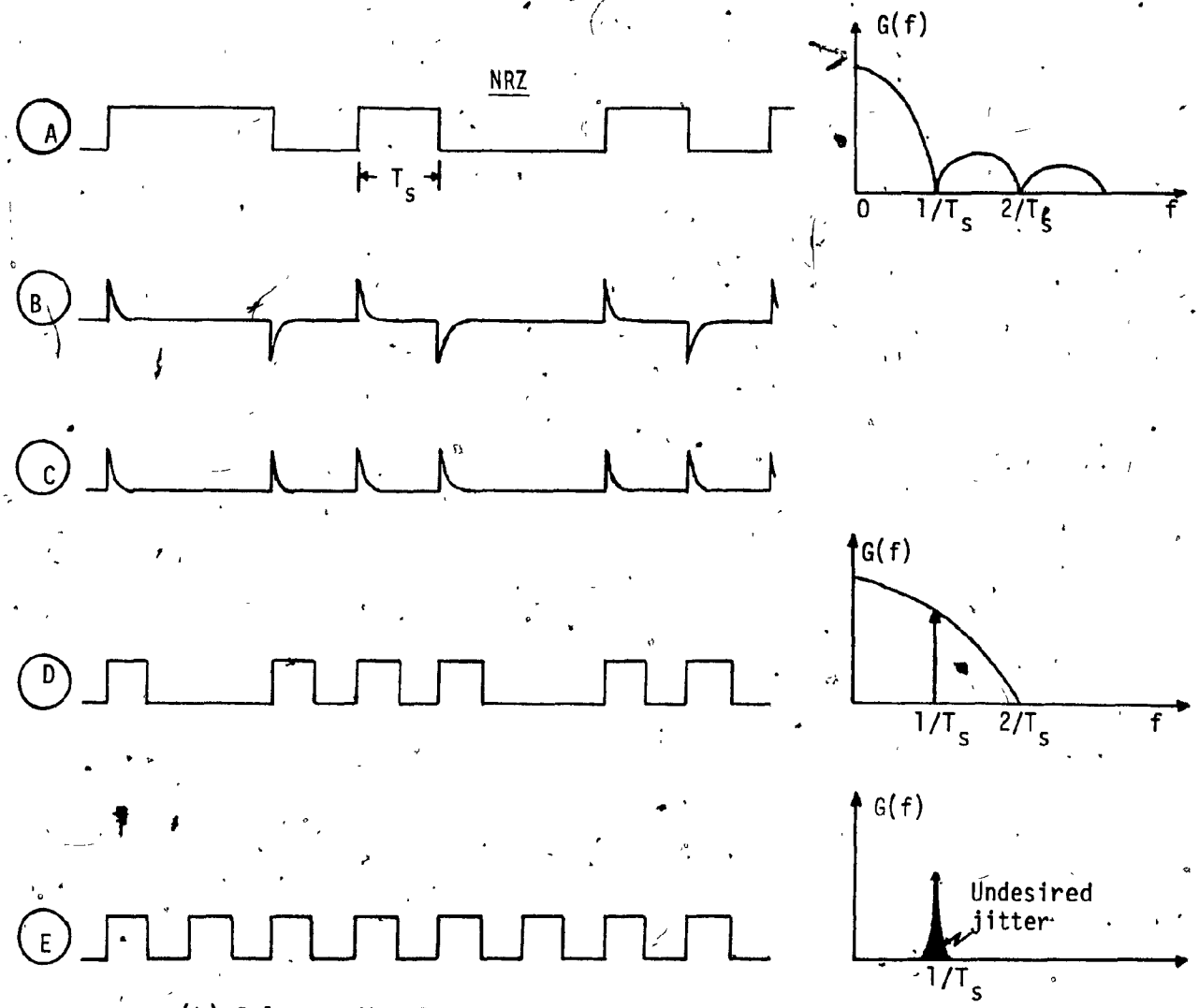

(b) Relevant Waveforms

Fig. 4.4.1 NRZ to RZ Digital Code Conversion

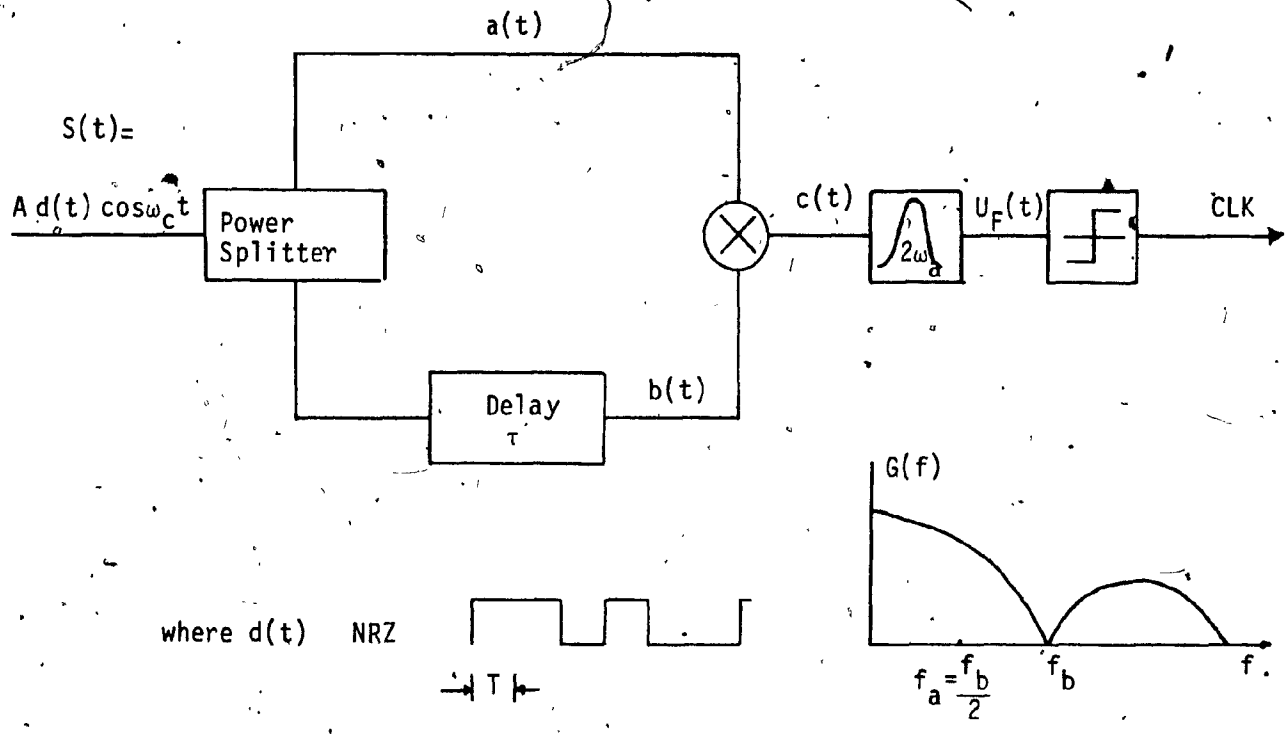

Fig. 4.4.2 , Pre-demodulation BTR Method

The product of the the two parallel sequences is:

$$c(t) = a(t)\cdot b(t) = [d(t)\cos\omega_c t]\cdot[d(t+\tau)\cos\omega_c(t+\tau)]$$

$$= d(t)\cdot d(t+\tau)\cdot\frac{1}{2}[\cos(2\omega_c t + \omega_c\tau) + \cos\omega_c\tau] \qquad (4.4.3)$$

where,

$$d(t)\cdot d(t+\tau) = A\cos\omega_a t \cdot A\cos(\omega_a t + \omega_a\tau)$$

$$= \frac{A^2}{2}[\cos(2\omega_a t + \omega_a\tau) + \cos\omega_a\tau] \qquad (4.4.4)$$

Therefore,

$$c(t) = \frac{A^2}{4}[\cos(2\omega_a t + \omega_a\tau) + \cos\omega_a\tau]\,[\cos(2\omega_c t + \omega_c\tau) + \cos\omega_c\tau]$$

$$= \frac{A^2}{8}[\cos[2(\omega_c+\omega_a)t + (\omega_c+\omega_a)\tau] + \cos[2(\omega_c-\omega_a)t + (\omega_c-\omega_a)\tau]$$

$$+ \frac{A^2}{8}\cos\omega_a\tau\cdot\cos(2\omega_c t+\omega_c\tau) + \frac{A^2}{8}\cos\omega_c\tau\cdot\cos(2\omega_a t + \omega_a\tau)$$

$$+ \frac{A^2}{8}\cos\omega_c\tau\cdot\cos\omega_a\tau] \qquad (4.4.5)$$

The output $U_F(t)$ of the filter does not contain the terms of frequencies $2\omega_c$, $2(\omega_c \pm \omega_a)$ nor the terms which are d.c. components.

Thus,

$$U_F(t) = \frac{A^2}{8}\cos\omega_c\tau\cdot\cos(2\omega_a t + \omega_a\tau) \qquad (4.4.6)$$

The frequency of this output $U_F(t)$ is:

$$2\omega_a = 2\frac{\omega_b}{2} = \omega_b = \text{clock rate}$$

It is clear that when the recovered tone is located at the symbol rate, then it is applied directly to the regenerator but it is

multiplied by 2 before being applied to the various circuits following the parallel to serial converter, as is the descrambler. However, if the recovered tone is located at the bit rate then it is divided by 2 before being applied to the regenator.

4.5. DIFFERENTIAL ENCODING AND DECODING

4.5.1 Phase Ambiguity Effects

When QPSK or O-QPSK receivers employ coherent carrier recovery circuits differential encoding becomes necessary. This is required because the carrier recovery network might introduce 180° or 90° phase ambiguity into the carrier. The phase ambiguity effects can be appreciated by considering θ_1, as the one of the four phases where the reference carrier resides and which is in phase with the original carrier reference. Referring to equation 3.1.7 and Fig. 3.1.2, one would observe that the other three phase references, which are $\theta_2 = \theta_1 + 90°$, $\theta_3 = \theta_1 + 180° = -\theta_1$ and $\theta_4 = \theta_1 + 270° = \theta_2 + 180° = -\theta_2$, can be derived but the I and Q channel outputs do not not have a one-to-one correspondence to the inputs. The possibilities that may arise for QPSK and O-QPSK are illustrated in Table 4.5.1. From this table it becomes evident that there might be a four-fold ambiguity in either QPSK or O-QPSK. In the latter scheme, there is an additional ambiguity, that is, which axis (I or Q) is the delayed axis.

To ensure the one-to-one correspondence between input and output, the demodulated data in both channels of the receiver must be coming out in correct time sequence and polarity irrespective of the recovered coherent phase reference. This can be resolved by employing differential encoding and decoding.

Table 4.5.1 QPSK and O-QPSK Phase Ambiguity Effects

CARRIER PHASE	OUTPUT CHANNEL	CONVENTIONAL QPSK	OFFSET QPSK	EXISTING POSSIBILITIES
θ_1 (original carrier reference)	I	I_{2k-1} I_{2k} I_{2k+1}	I_{2k-1} I_{2k} I_{2k+1}	Outputs of I and Q channels have a one-to-one correspondence to the inputs
	Q	Q_{2k-1} Q_{2k} Q_{2k+1}	Q_{2k-1} Q_{2k} (or Q_{2k}) (or Q_{2k+1})	
θ_2 = $\theta_1 + 90°$	I	Q_{2k-1} Q_{2k} Q_{2k+1}	Q_{2k-1} Q_{2k} Q_{2k+1}	Channels I and Q are interchanged, channel Q is inverted
	Q	$-I_{2k-1}$ $-I_{2k}$ $-I_{2k+1}$	$-I_{2k-1}$ $-I_{2k}$ (or $-I_{2k}$) (or $-I_{2k+1}$)	
$-\theta_1$ = $\theta_1 + 180°$	I	$-I_{2k-1}$ $-I_{2k}$ $-I_{2k+1}$	$-I_{2k-1}$ $-I_{2k}$ $-I_{2k+1}$	Both channels are inverted
	Q	$-Q_{2k-1}$ $-Q_{2k}$ $-Q_{2k+1}$	$-Q_{2k-1}$ $-Q_{2k}$ (or $-Q_{2k}$) (or Q_{2k+1})	
$-\theta_2$ = $\theta_1 + 270°$	I	$-Q_{2k-1}$ $-Q_{2k}$ $-Q_{2k+1}$	$-Q_{2k-1}$ $-Q_{2k}$ $-Q_{2k+1}$	Channel I and Q are interchanged, channel I is inverted
	Q	I_{2k-1} I_{2k} I_{2k+1}	I_{2k-1} I_{2k} (or I_{2k}) (or I_{2k+1})	

4.5.2 Coding for QPSK

Differential encoding is obtained by transmitting the change in the phase between successive states, instead of representing the data bits by the absolute phase of the carrier. The differential encoder encodes the incoming data in both data channels (I and Q) in such a way that phase shifts are caused at the output of the transmitter under predetermined conditions. These conditions are; the state of the incoming data streams and the previous state of the encoder, as shown in Fig. 4.5.1. Referring to Fig. 3.1.2 and representing the counterclockwise rotation from one state to another as positive change in phase and the clockwise rotation as the negative one, the encoding truth table is derived as shown in Table 4.5.2. Use of logic levels is made by assigning logic 1 for +1 and logic 0 for -1.

From Table 4.5.2 the encoding laws may be derived as

$$E = \bar{A}B\bar{C}\bar{D} + AB\bar{C}\bar{D} + \bar{A}\bar{B}\bar{C}D + A\bar{B}\bar{C}D + \bar{A}BC\bar{D} + ABC\bar{D} + \bar{A}\bar{B}CD + \bar{A}BCD \quad (4.5.1)$$

$$F = A\bar{B}\bar{C}\bar{D} + AB\bar{C}\bar{D} + \bar{A}\bar{B}\bar{C}D + A\bar{B}\bar{C}D + \bar{A}BC\bar{D} + ABC\bar{D} + \bar{A}\bar{B}CD + \bar{A}BCD \quad (4.5.2)$$

These expressions can be simplified and written as:

$$E = \bar{A}\bar{B}C + \bar{A}B\bar{D} + AB\bar{C} + A\bar{B}D \quad (4.5.3)$$

$$F = \bar{A}\bar{B}D + \bar{A}BC + AB\bar{D} + A\bar{B}\bar{C} \quad (4.5.4)$$

It is seen from Table 4.5.2 that a 0 output at both outputs of the encoder will not produce any change in the phase of the transmitted carrier. A 0 at the in-phase output channel and a 1 at the quadrature phase output channel will produce a + 90° change in the phase of the carrier. The inverse outputs at the encoder, that is a 1

Table 4.5.2 DIFFERENTIAL ENCODER TRUTH TABLE FOR QPSK

PRESENT INPUTS		PREVIOUS INPUTS		PHASE ADVANCE	ENCODED OUTPUTS	
CH.I (A)	CH.Q (B)	CH.I (C)	CH.Q (D)		CH.I (E)	CH.Q (F)
0	0	0	0	0°	0	0
0	1	0	0	-90°	1	0
1	0	0	0	+90°	0	1
1	1	0	0	180°	1	1
0	0	0	1	+90°	0	1
0	1	0	1	0°	0	0
1	0	0	1	180°	1	1
1	1	0	1	-90°	1	0
0	0	1	0	-90°	1	0
0	1	1	0	180°	1	1
1	0	1	0	0°	0	0
1	1	1	0	+90°	0	1
0	0	1	1	180°	1	1
0	1	1	1	+90°	0	1
1	0	1	1	-90°	1	0
1	1	1	1	0°	0	0

Table 4.5.3 DIFFERENTIAL DECODER TRUTH TABLE FOR QPSK

PRESENT INPUTS		PREVIOUS INPUTS		PHASE ADVANCE	DECODED OUTPUTS	
CH.I (E)	CH.Q (F)	CH.I (C)	CH.Q (D)		CH.I (A)	CH.Q (B)
0	0	0	0	0°	0	0
1	0	0	0	+90°	0	1
0	1	0	0	-90°	1	0
1	1	0	0	180°	1	1
0	1	0	1	0°	0	0
0	0	0	1	+90°	0	1
1	1	0	1	-90°	1	0
1	0	0	1	180°	1	1
1	0	1	0	0°	0	0
1	1	1	0	+90°	0	1
0	0	1	0	-90°	1	0
0	1	1	0	180°	1	1
1	1	1	1	0°	0	0
0	1	1	1	+90°	0	1
1	0	1	1	-90°	1	0
0	0	1	1	180°	1	1

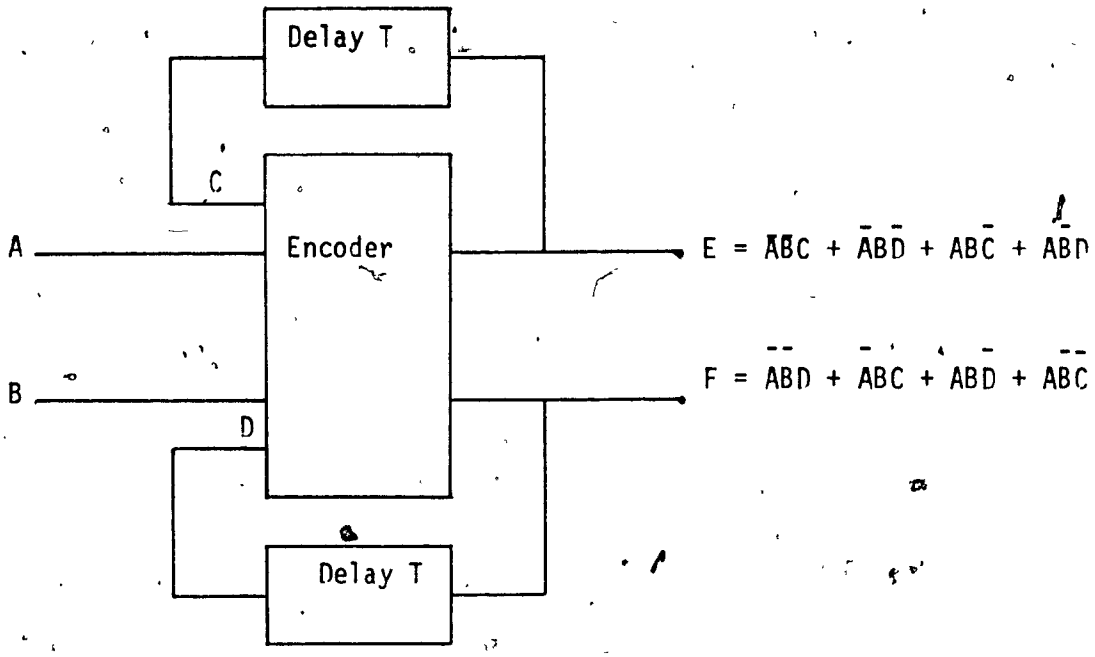

Fig. 4.5.1 Encoder for QPSK

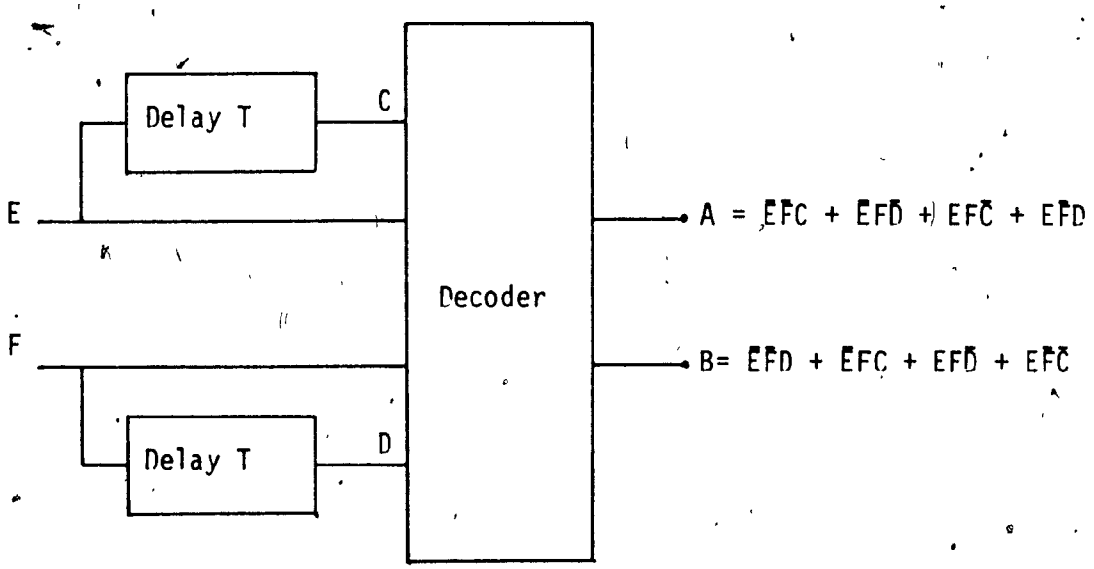

Fig. 4.5.2 Decoder for QPSK

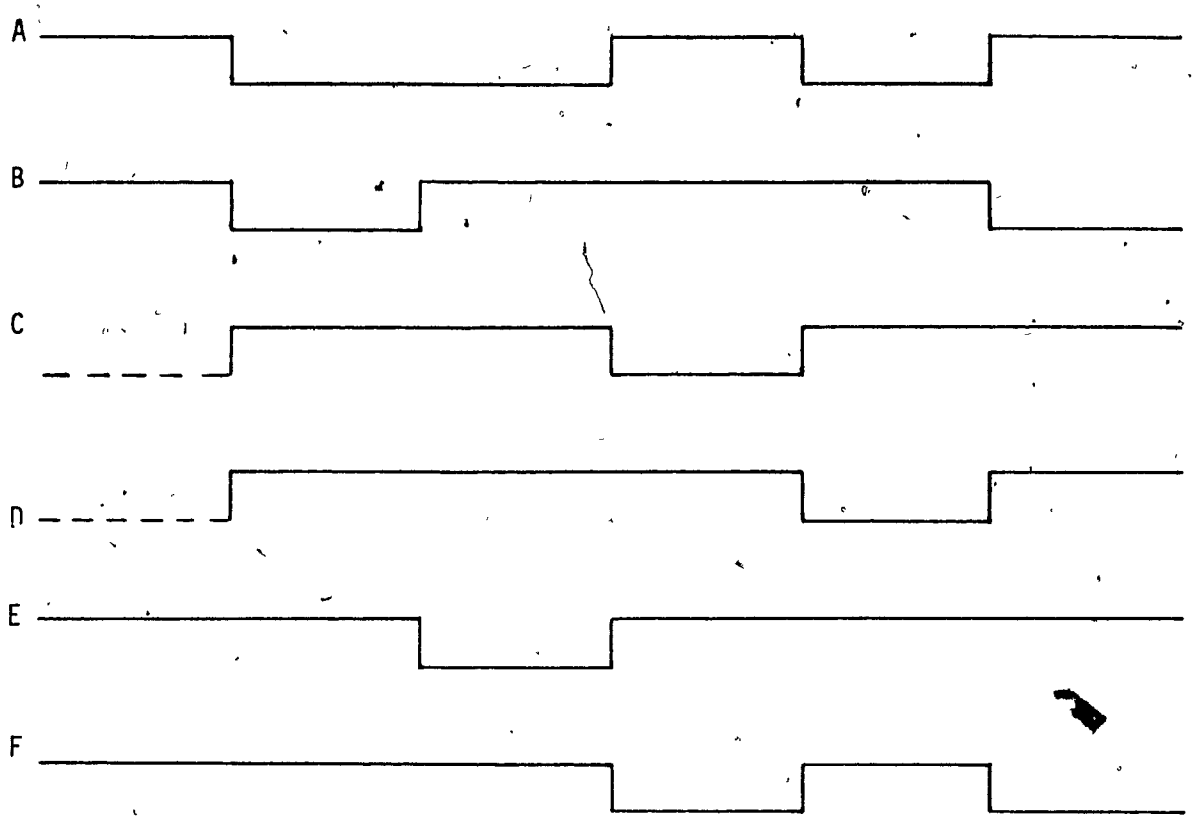

Fig. 4.5.3 QPSK Encoder Waveforms

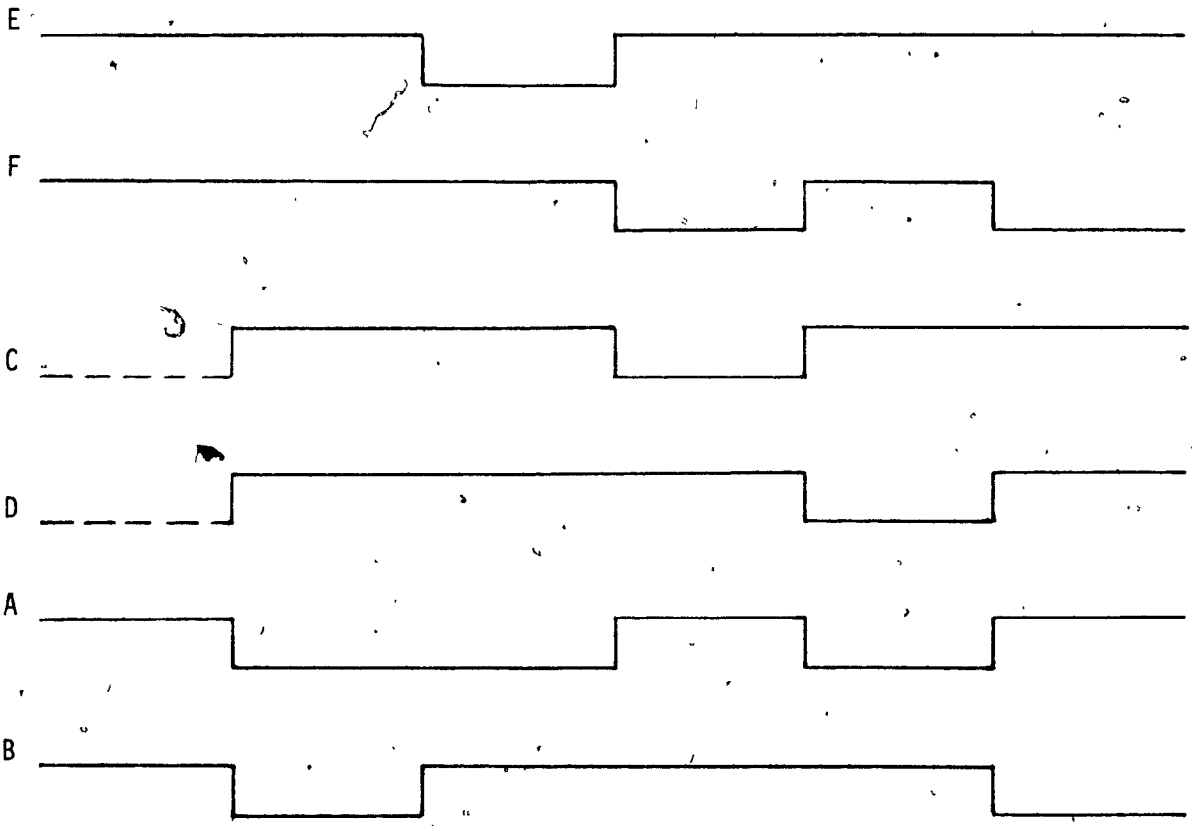

Fig. 4.5.4 QPSK Decoder Waveforms

at the in-phase channel and a zero at the quadrature phase channel will produce a -90° change in the phase of the transmitted carrier. Finally, a 1 at both outputs of the encoder will produce a 180° change.

In a similar fashion, with the assistance of Figs. 3.1.2 and 4.5.2 and Table 4.5.2 the decoder laws can be obtained:

$$A = \bar{E}\bar{F}CD + E\bar{F}\bar{C}D + E\bar{F}C\bar{D} + E\bar{F}CD + \bar{E}FCD + \bar{E}F\bar{C}D + \bar{E}FC\bar{D} + EFCD \quad (4.4.5)$$

$$B = \bar{E}\bar{F}\bar{C}D + E\bar{F}\bar{C}\bar{D} + \bar{E}\bar{F}CD + E\bar{F}C\bar{D} + EFC\bar{D} + \bar{E}FCD + \bar{E}FC\bar{D} + \bar{E}\bar{F}CD \quad (4.4.6)$$

These expressions can be simplified and rewritten as:

$$A = \bar{E}\bar{F}C + \bar{E}F\bar{D} + EF\bar{C} + E\bar{F}D \quad (4.4.7)$$

$$B = \bar{E}\bar{F}D + \bar{E}FC + EF\bar{D} + E\bar{F}\bar{C} \quad (4.4.8)$$

Figures 4.5.3 and 4.5.4 illustrate the encoder and decoder waveforms.

4.5.3 Coding for O-QPSK

From Table 4.5.1 it is realized that the O-QPSK signals might suffer a 4-fold ambiguity too. However, the O-QPSK receiver has an additional ambiguity to contend with, that is, which axis is the delay axis. It is conceivable that carrier phase ambiguity resolution by differential coding on pairs of bits, as in QPSK, cannot be implemented.

However, referring to Fig. 3.1.5 and Table 4.5.1, it is seen that an O-QPSK signal is possible to be differentially encoded. The differential encoder, shown in Fig. 4.5.5, performs two logic operations in a symbol interval. Namely, it encodes the I-bits by exclusive-ORing the present I-bit with the previous encoded bit of the Q-channel, and the Q-bits by exclusive-NORing the present Q-bit with the previous encoded bits of the I-channel. The reverse operation also holds. The

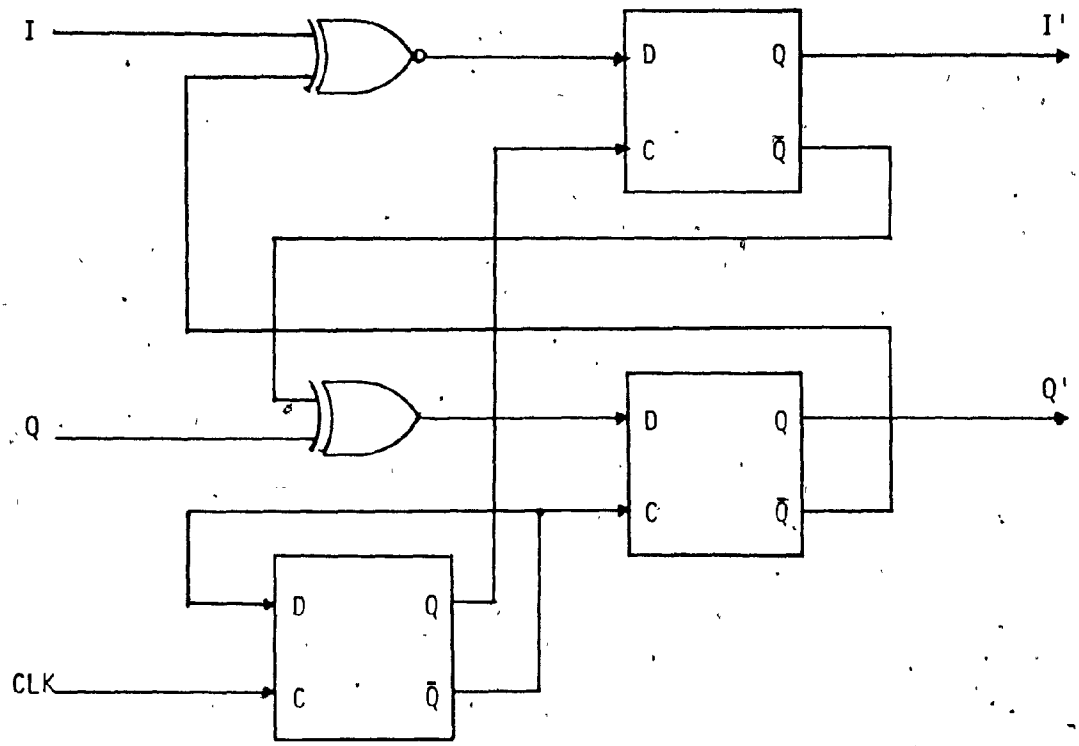

Fig. 4.5.5 Encoder for O-QPSK

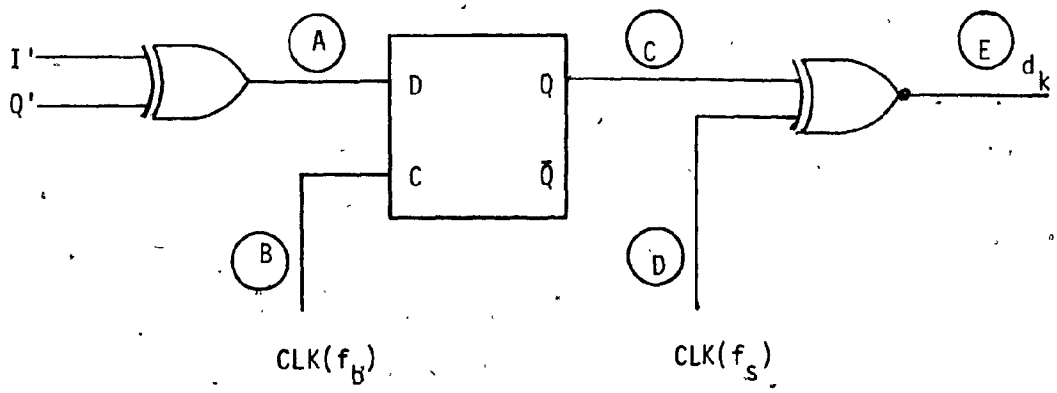

Fig. 4.5.6 Decoder for O-QPSK

differential encoder laws are given by:

$$I'_{2k} = I_{2k} \oplus Q'_{2k-1}$$

and (4.5.9)

$$Q'_{2k} = Q_{2k} \oplus \overline{I'_{2k-1}}$$

or

$$I'_{2k} = I_{2k} \oplus \overline{Q'_{2k-1}}$$

and (4.5.10)

$$Q'_{2k} = Q_{2k} \oplus I_{2k}$$

where I'_{ik} and Q'_{ik} are the outputs of the encoder.

Assuming the same data stream, as in Fig. 3.1.5, and assigning logic 1 for +1 and logic 0 for -1, the encoded I- and Q- waveforms are illustrated in Fig. 4.5.7.

The data decoding of a differential encoded coherent O-QPSK signal can be realized from Fig. 4.5.7. Alternate exclusive-OR and exclusive-NOR operations applied to the demodulated I- and Q- data streams result in the recovery of the transmitted I- and Q- data. In order, however, to resolve the additional ambiguity about the channel identification uncertainty, the circuit of Fig. 4.5.6 is implemented. Clearly, the exclusive-OR gate is not sensitive to which input is the I- and Q- data. Fig. 4.5.8 illustrates the relationship of the decoded waveform with the two parallel detected waveforms.

By this encoding-decoding process the 90° and 180° phase ambiguity introduced by the carrier recovery circuit is removed as well as the ambiguity of which channel is the delayed one.

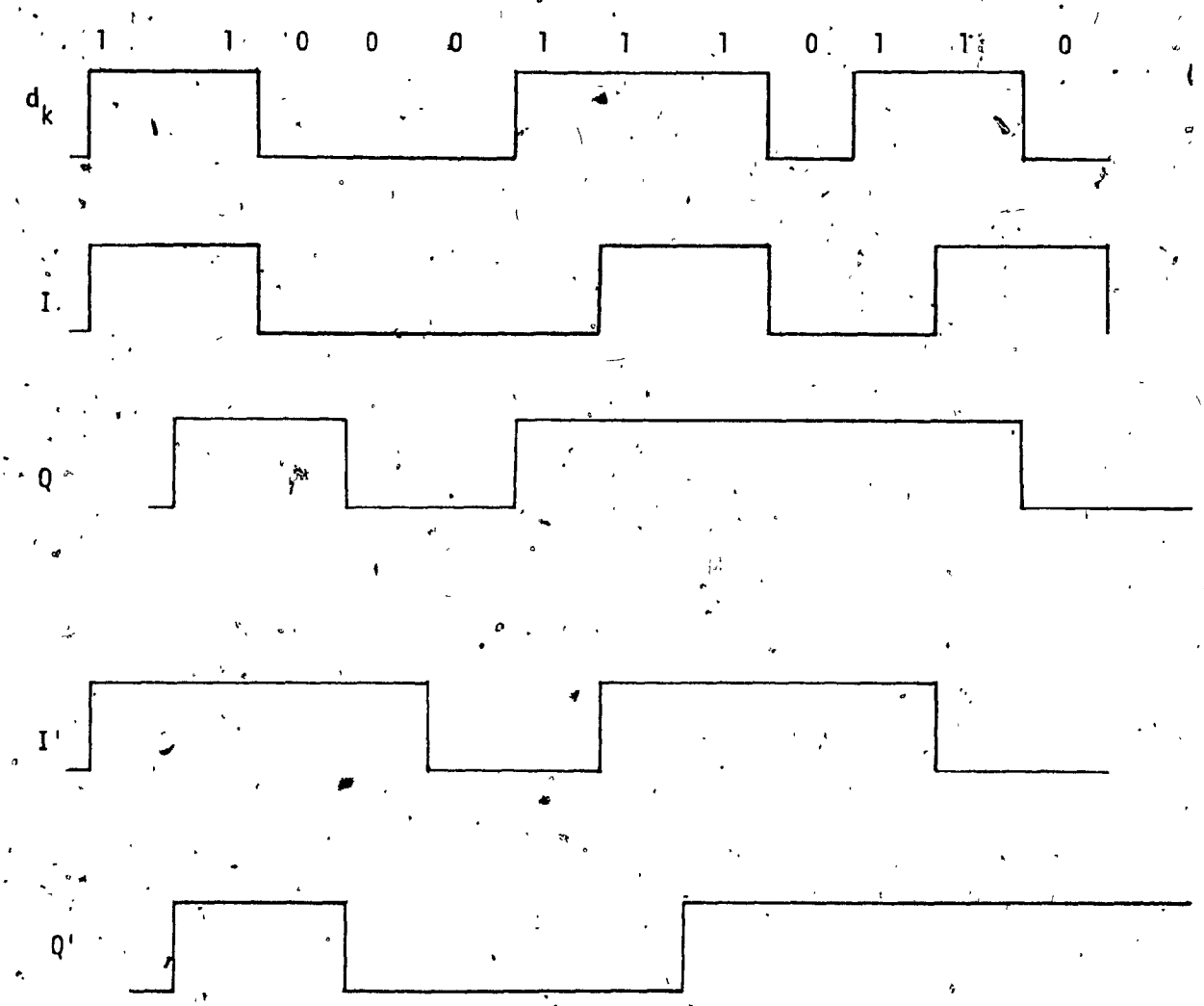

Fig. 4.5.7 O-QPSK Encoder Waveforms

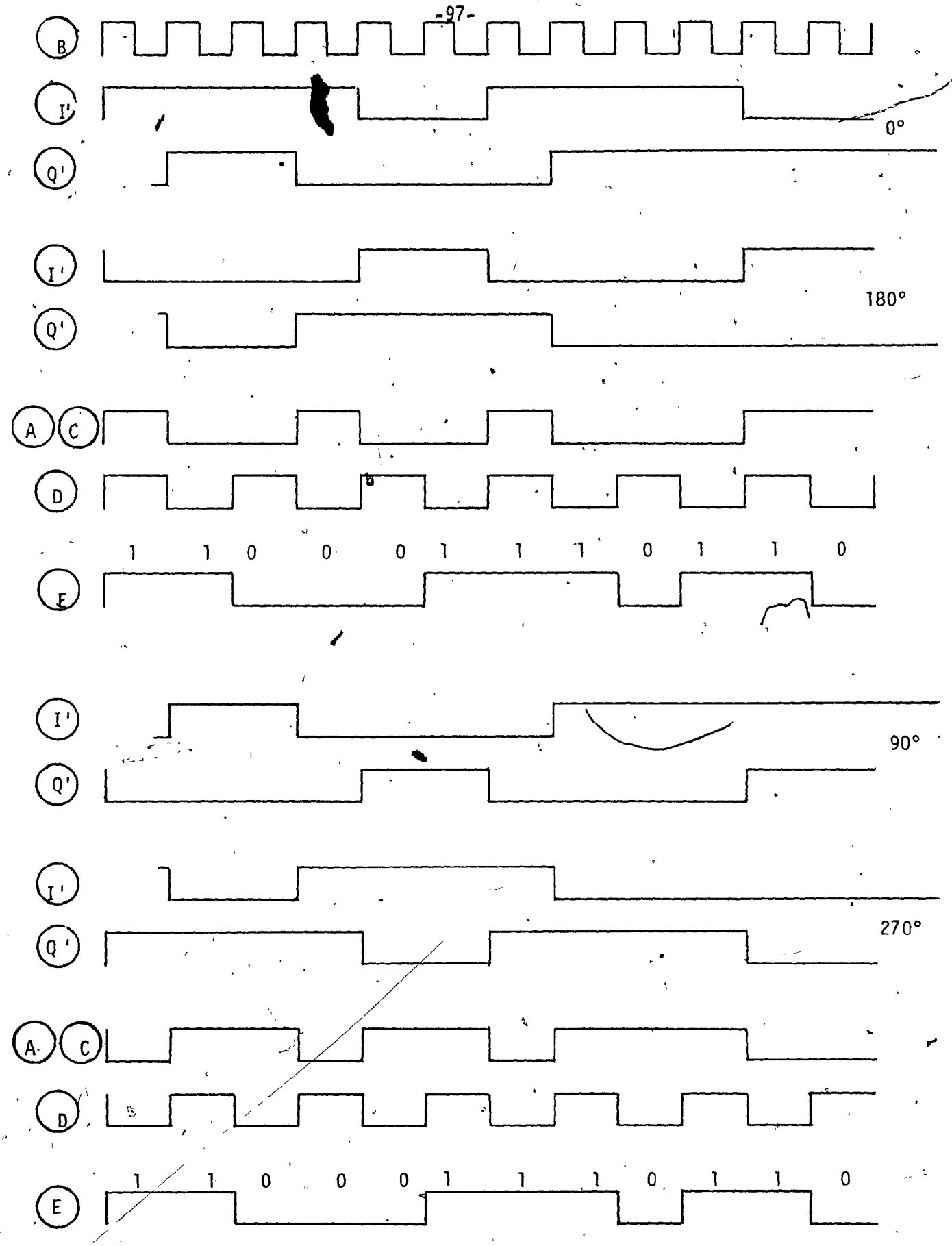

Fig. 4.5.8 O-QPSK Decoder Waveforms

CHAPTER FIVE

5. COMPARATIVE PERFORMANCE STUDY

5.1 BANDLIMITING AND NONLINEARITY EFFECTS AT SAMPLING INSTANTS

As discussed in section 3.3.1, the envelope of O-QPSK, because of the time delay between I and Q channels, does not have zero crossing and the overall envelope fluctuations are smaller than that of QPSK as shown in Figs. 3.3.1 and 3.3.2. However, at the critical sampling points O-QPSK has much larger amplitude fluctuations than QPSK, that results in greater sensitivity to degradation through nonlinear channels making more difficult the design of an optimum receiver [2]. As the above modulation techniques are four-phase modulation, at the receiver the carrier recovery network usually employs a multiply by four method as described in chapter four. Consequently, the large amplitude fluctuations of O-QPSK at the sampling instants imply much larger fluctuations of the carrier recovery fourth powered signal.

This nonlinear distortion and its effects can be readily conceived by studying the space diagrams of QPSK and O-QPSK signals. Figures 5.1.1 and 5.1.2 [16] show the behaviour of the two aforementioned signals with 100, 50 and 30% cosine roll-offs. As can be seen, with 100% cosine roll-off the signal moves directly from one state to the other in each channel. For QPSK signals, the I and Q channels are co-timed and when both change state simultaneously the amplitude of the modulated signal drops to zero as shown by the diagonal paths in Fig. 5.1.1 (a). Both channels are sampled at the same time and even assuming that the modulating signals consists of baseband impulses instead of rectangular pulses, there are always signals at the sampling times at both channels.

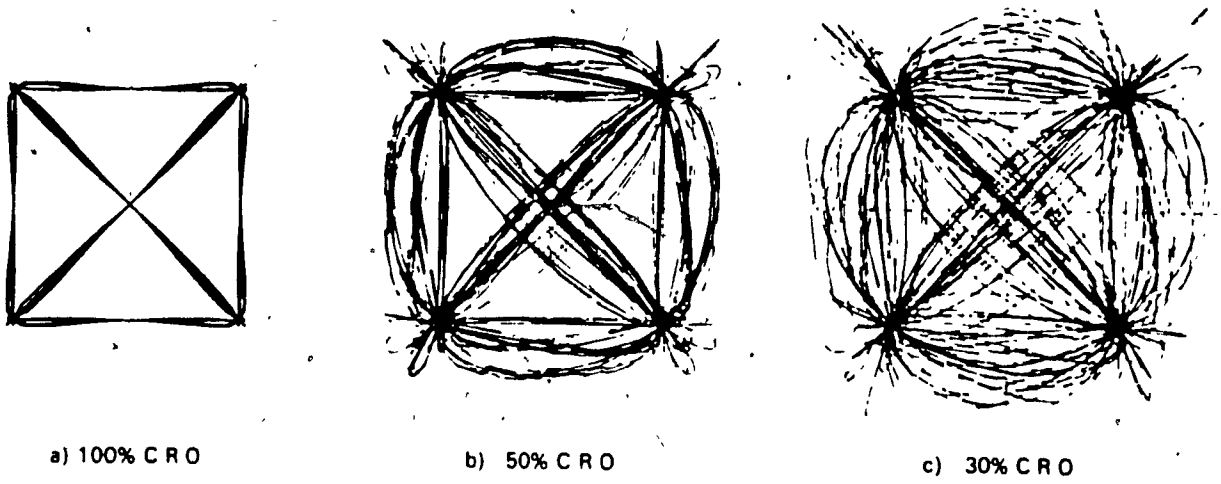

a) 100% C R O b) 50% C R O c) 30% C R O

Fig. 5.1.1 QPSK Signal Space Diagram
for Various Cosine Roll-offs [16]

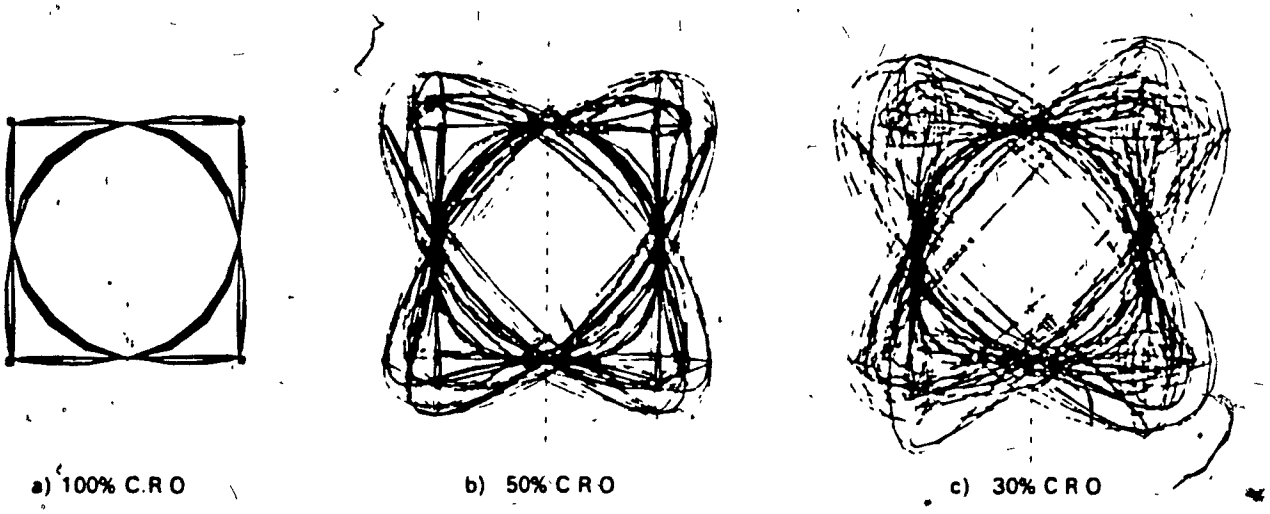

a) 100% C.R O b) 50% C R O c) 30% C R O

Fig. 5.1.2 O-QPSK Signal Space Diagram
for Various Cosine Roll-offs [16]

In O-QPSK signals, however, because of the half symbol period offsetting in the two quadrature channel streams, when for instance the I channel is sampled there is no signal in the Q channel and vice versa.

When both QPSK and O-QPSK signals are bandlimited the impulses become shaped pulses. In the case of QPSK, if no large intersymbol interference effect from the filter is assumed the sample signal points do not change but rather stay where they are, that is, I-axis = ± 1 and Q axis = ± 1, as illustrated in Fig. 5.1.3 (a). For O-QPSK, however, when both channels change state simultaneously the amplitude of the signal remains almost constant as shown by the inner circle of Fig.5.1.2(a), and when only one channel changes state, the signal moves along the sides of the square, as in the case of QPSK. Thus, the signal envelope at the sampling instants is no longer only a function of the sampled channel. This is illustrated in Fig. 5.1.3 (c), where if the I channel is sampled, Q channel may have the values ± 1 (transition from +1 to +1 or -1 to -1) and zero (transition from +1 to -1 or -1 to +1). Therefore, the samples lie not only at the corners of the square, as in QPSK, but also at the centres of the vertical sides. Similarly, when the Q channel is sampled I channel has its possible values in the horizontal sides. In other words, sample points in O-QPSK are located on four lines perpendicular to I and Q axis, because sampling points in I-channel are transitions in Q-channel and vice-versa.

Now, when the signal is fourth powered at the carrier recovery network the four signal points of QPSK converge to a point on negative real axis, as shown in Fig. 5.1.3(b), assuming absence of noise and intersymbol interference. This can be verified from the expression of the received signal:

$$S(t) = A \cos (\omega_c t + \theta) \qquad (5.1.1)$$

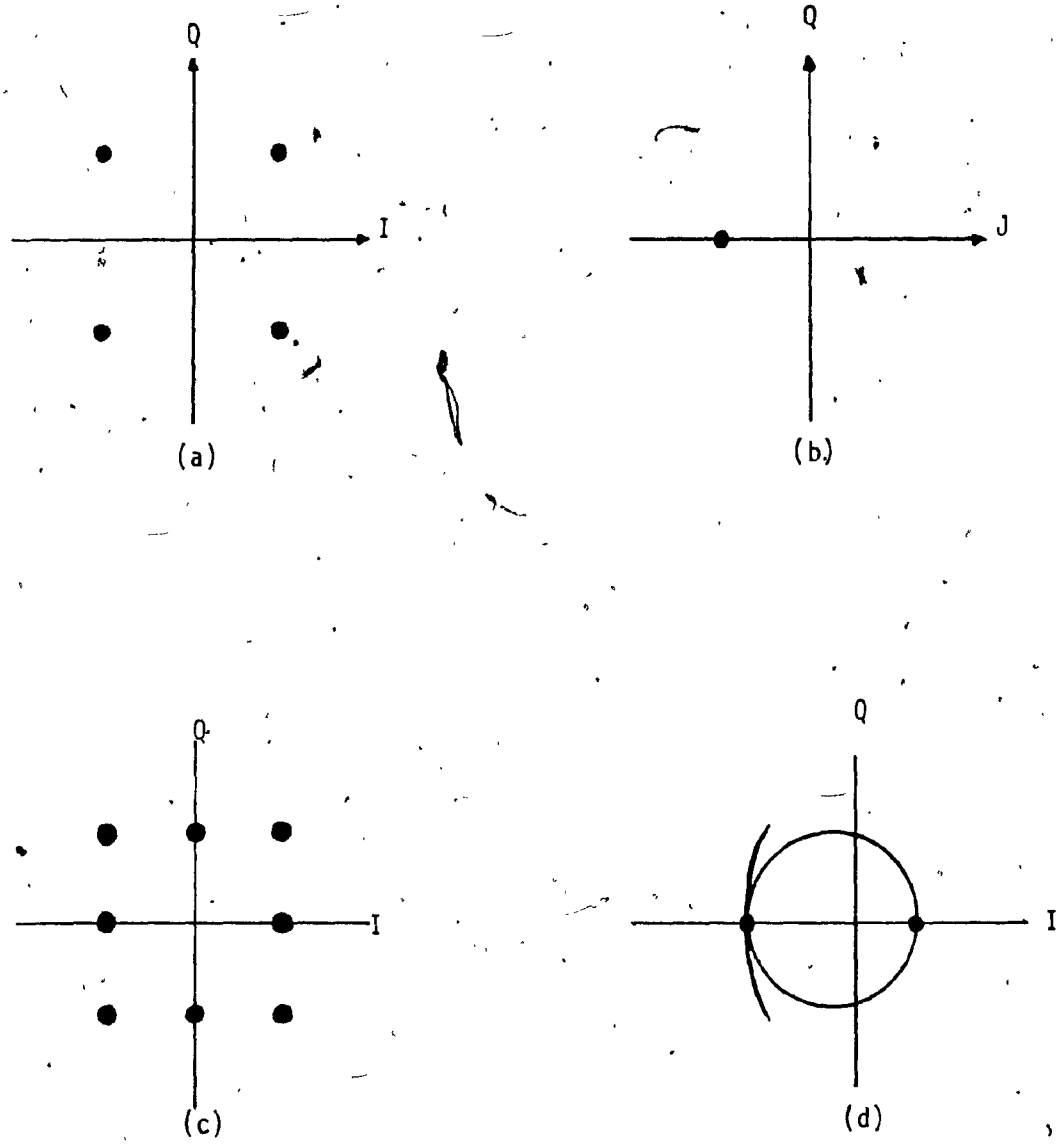

Fig. 5.1.3 Signal Constellation and its Fourth Power [1]

where $\theta = \pm 45°$ or $\pm 135°$. Passing this signal through a X4 multiplier, the output is given by equation (4.3.2).

$$S^4(t) = A^4 \cos^4(\omega_c t + \theta)$$

$$= A^4\left[\frac{3}{8} + \frac{1}{2}\cos(2\omega_c t + 2\theta) + \frac{1}{8}\cos(4\omega_c t + 4\theta)\right] \qquad (5.1.2)$$

Then, at the output of the PLL which separates the fourth harmonic of the desired carrier signal, as described in chapter four, the signal becomes

$$S^4(t) = \frac{A^4}{8}\cos(4\omega_c t + 4\theta) \qquad (5.1.3)$$

where $4\theta = \pm 180°$ or $\pm 540°$. Therefore, the fourth powered QPSK signal converges to one point.

For O-QPSK signals, however, since the sampling points in one channel are transition points in the other channel, the fourth powered O-QPSK signals at the sampling instants lie on a curve [1] as shown in Fig. 5.1.3 (b).

As a result, the O-QPSK has much larger amplitude fluctuations at the sampling instants than QPSK. These envelope variations can be reduced by shaping the modulating pulses such that zero crossings occur at half the symbol rate. By doing so, phase transitions are avoided altogether. This happens in a MSK system, where the amplitude of the pulses are constant, but the bandwidth of each individual pulse increases significantly as shown in Fig. 3.2.1. This type of signalling if it is used in closely spaced channels, because of its 50% wider transmitted spectrum relative to that of QPSK or O-QPSK, it must be severely filtered.

This would re-introduce envelope fluctuations in nonlinear environment, and for this reason, the use of MSK in narrowband nonlinear channels may be the worst of the three popular modulation schemes. On the other hand, the fact that the sampled signal amplitude of a QPSK signal is still concentrated about a fixed point even when it passes through a nonlinear channel, suggests that QPSK suffers less phase jitter in the recovered carrier than O-QPSK and MSK. Thus, in narrowband channels, O-QPSK and MSK whose signal is scattering at the sampling instants have larger overall system performance degradation than QPSK.

5.2 CARRIER PHASE OFFSET EFFECTS

Another important imperfection, other than the nonlinearity, that is present in a satellite channel is the offset in the phase of the carrier recovered at the receiver. In the following, the probability of error in one binary component is first calculated and the results are then doubled.

Let $P_S(e)$ represent the symbol error rate and $P_b(e)$ the bit error rate.

$$P_S(e) = 1 - [1-P_b(e)]^2 = 2\,P_b(e) - P_b^2(e) \qquad (5.2.1)$$

Since for practical values $P_b^2(e) << 2P_b(e)$, $P_s(e)$ can be computed in each symbol as the sum of the probabilities of crossing the two phase thresholds, as shown in Fig. 2.3.1 (a). That means, it can be assumed that

$$P_S(e) = 2\,P_b(e) \qquad (5.2.2)$$

The probability of each quadrature component of crossing the threshold is given by equation (2.1.20):

$$P_b(e) = \frac{1}{2}\,\mathrm{erfc}\,\sqrt{\frac{V^2T}{2N_o}} = \frac{1}{2}\,\mathrm{erfc}\,\sqrt{\frac{E_s}{2N_o}}$$

$$= \frac{1}{2}\,\mathrm{erfc}\,\sqrt{\frac{Z}{2}} \qquad (5.2.3)$$

where $Z = \frac{E_s}{N_o}$.

If the introduced carrier phase offset is $\pm\,\phi$, then

$$P_b(e) = \frac{1}{2}\,\mathrm{erfc}\left[\sqrt{\frac{Z}{2}}\cdot r(\phi)\right] \qquad (5.2.4)$$

The factor $r(\phi)$ represents any decrease in the demodulated signal voltage that results from a carrier phase offset of ϕ radius. This synchronization error ϕ introduces a correlation loss [17] in the demodulated signal that is equal to $\cos\phi$. When carrier synchronization is perfect, that is, when $r(\phi) = 1$ ($\phi = 0$), the two components of a QPSK signal are detected orthogonally. The orthogonality between the two binary components of a QPSK signal is lost by the introduction of a synchronization error ($\phi \neq 0$). In addition to the correlation loss in QPSK signalling, there is a further degradation due to phase error ϕ in carrier synchronization. Interchannel interference is introduced by crosscoupling between the binary symbol streams and it is proportional to $\pm\sin\phi$. Therefore, for a given phase error ϕ in carrier detection, the resulting decrease in the demodulated signal voltages is in accordance with

$$r(\phi) = \cos\phi \pm \sin\phi \qquad (5.2.5)$$

Thus, for QPSK signalling the error rate in each binary component, that is, the probability of crossing the threshold is

$$P_b(e) = \frac{1}{2}\,\mathrm{erfc}\left[\sqrt{\frac{Z}{2}}\,(\cos\phi \pm \sin\phi)\right] \qquad (5.2.6)$$

The choice of sign ($\pm$) in equation (5.2.6) is related to an increase or decrease in the component considered.

Assuming a random sequence, the two values of $P_b(e)$ have equal probabilities and consequently the conditional probability of decision error per detected bit in conventional QPSK waveforms is given by:

$$P_b(e) = \frac{1}{4}\left[\operatorname{erfc}\sqrt{\frac{Z}{2}}(\cos\phi + \sin\phi) + \operatorname{erfc}\sqrt{\frac{Z}{2}}(\cos\phi - \sin\phi)\right] \tag{5.2.7}$$

From this equation it is seen that during each quaternary symbol interval in QPSK signalling, one binary component suffers destructive interchannel interference ($\cos\phi + \sin\phi$), while the other binary component experiences constructive crosscoupling interference. It is also understood that because of the coincident alignment in QPSK signals, the interchannel interference is always constant during a bit interval.

In offset QPSK modulation the bit alignments are staggered. Because of the staggered alignment of the binary channels, the interchannel interference can change state at midbit. As a a result, the interference during the first half of the bit is cancelled by the interference of opposite polarity during the second half of the bit interval. Consequently, for O-QPSK modulation two different situations can occur:

a) One component is sampled while the other is changing. In this case the spurious component $\sin\phi$ is zero at the sampling instant because the crosscoupling changes state. Thus, the only degradation as a result of a synchronization error is the correlation loss $\cos\phi$, and the bit error rate of each binary channel becomes:

$$P_b(e) = \frac{1}{2} \operatorname{erfc} \sqrt{\frac{Z}{2}} \cos \phi \qquad (5.2.8)$$

b) One component is sampled while the other is not changing. In this case, the crosscoupling remains constant over the entire bit interval, and the bit error rate of each binary channel is given by equation (5.2.7).

Thus for a random sequence, the conditional probability of decision error for detected bit, in O-QPSK modulation, is given by:

$$P_b(e) = \frac{1}{8} \left[\operatorname{erfc} \sqrt{\frac{Z}{2}} (\cos \phi + \sin \phi)\right] + \operatorname{erfc} \left[\sqrt{\frac{Z}{2}} (\cos \phi - \sin \phi)\right] + 2 \operatorname{erfc} \left(\sqrt{\frac{Z}{2}} \cos \phi\right)] \qquad (5.2.9)$$

From equation (5.2.7) and (5.2.9) we have that:

$$P_b(\text{QPSK}) - P_b(\text{O-QPSK}) = \frac{1}{8}\left[\operatorname{erfc}\left[\sqrt{\frac{Z}{2}} (\cos \phi + \sin \phi)\right] + \operatorname{erfc} \left[\sqrt{\frac{Z}{2}} (\cos \phi - \sin \phi)\right] - 2 \operatorname{erfc} \left(\sqrt{\frac{Z}{2}} \cos \phi\right)\right] > 0 \qquad (5.2.10)$$

This concludes that O-QPSK is more resistive than QPSK in the face of carrier phase offsets.

5.3 PERFORMANCE STUDY BY COMPUTER SIMULATIONS

Comparative evaluations, based on computer simulations, about the behaviour of QPSK, O-QPSK and MSK over wide- and narrow-band nonlinear satellite channels have been conducted in [1],[2],[3],[4] and [16].

5.3.1 Comparative Performance Tests

A comparative evaluation of the performance of digital modulation techniques which can be used in data transmission at high bit rates over satellite channels, has been conducted in [4]. A single carrier wide-

band channel was analyzed.

In order to evaluate the systems performance degradation taking into account the nonlinear effects of the TWTA transponder, the inter-symbol interference due to time-spreading of filter responses, and additive noise, digital computer simulation was used. The block diagram of the system being simulated is shown in Fig. 5.3.1. The transmit and receive filters used were 4-pole, 0.5 dB ripple Chebyshev filters with a fixed 85 MHz 3 dB bandwidth. Only down-link noise was considered and perfect carrier references were assumed at the receiver. The TWTA which is represented by the combination of the two nonlinear effects, that is, the AM/AM and AM/PM conversion effects was modelled in quadrature form by the circuit of Fig. 3.3.3.

Bit error rate performance test results indicated that O-QPSK and MSK are relatively insensitive to the TWTA nonlinearities, as it would be expected, since both techniques retain their bandlimited spectra after passing through a nonlinear device. It was also found that operating the TWTA at 12 dB input power back-off (linear operation) the performance of QPSK, O-QPSK and MSK signals are closely identical to that of BPSK signal. However, with the TWTA operating at 1 dB input power back-off, that is essentially at saturation, the BER performance of O-QPSK was found better than QPSK and slightly better than MSK. This is shown in Fig. 5.3.2, where the BER performance curves correspond to 65.5 Mb/s transmission rate with the TWTA operated at 1 dB power back-off.

Another useful method to measure the performance of a digital modulation technique is the SNR degradation which is achieved by decreasing the B_ST product for a given BER. Figures 5.3.3 and 5.3.4 show the SNR degradation versus BT_S of different digital modulation schemes,

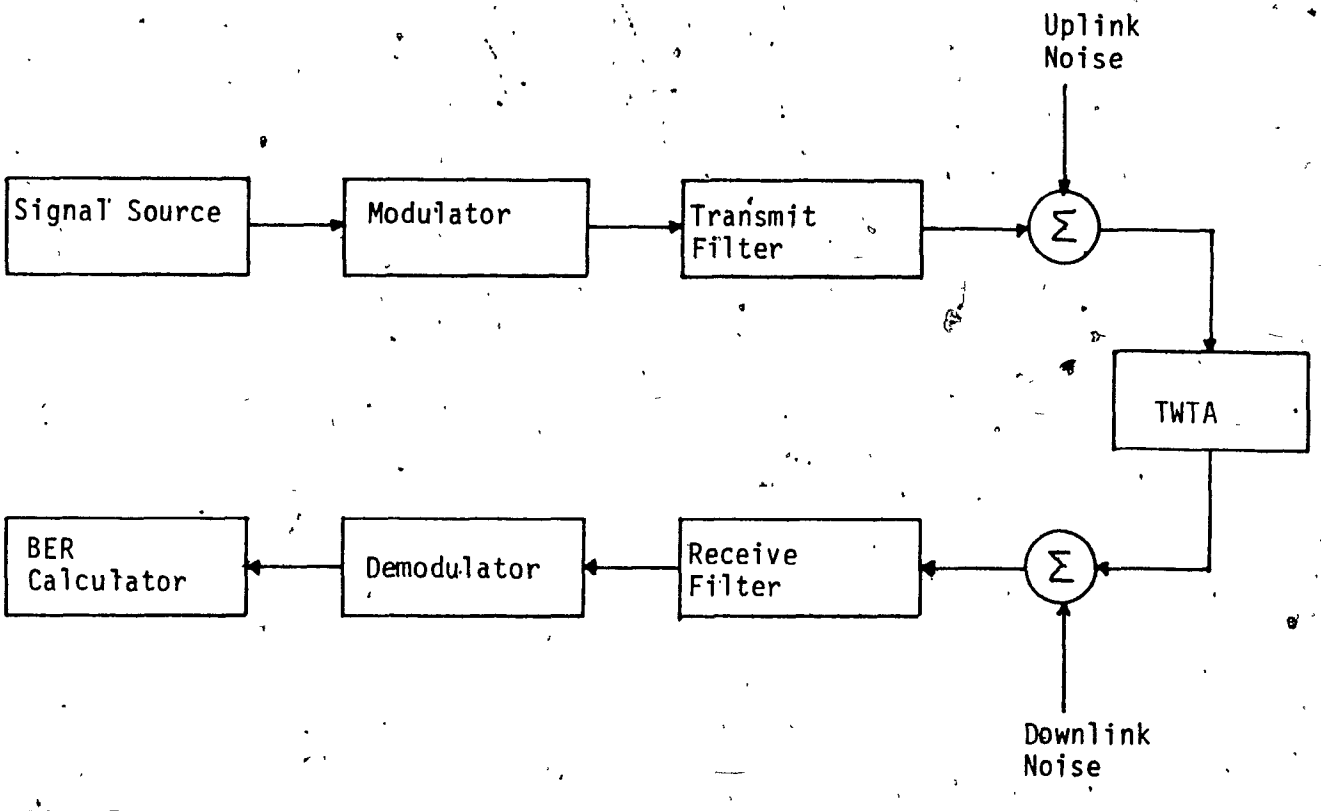

Fig. 5.3.1 Block Diagram of System Simulation[4]

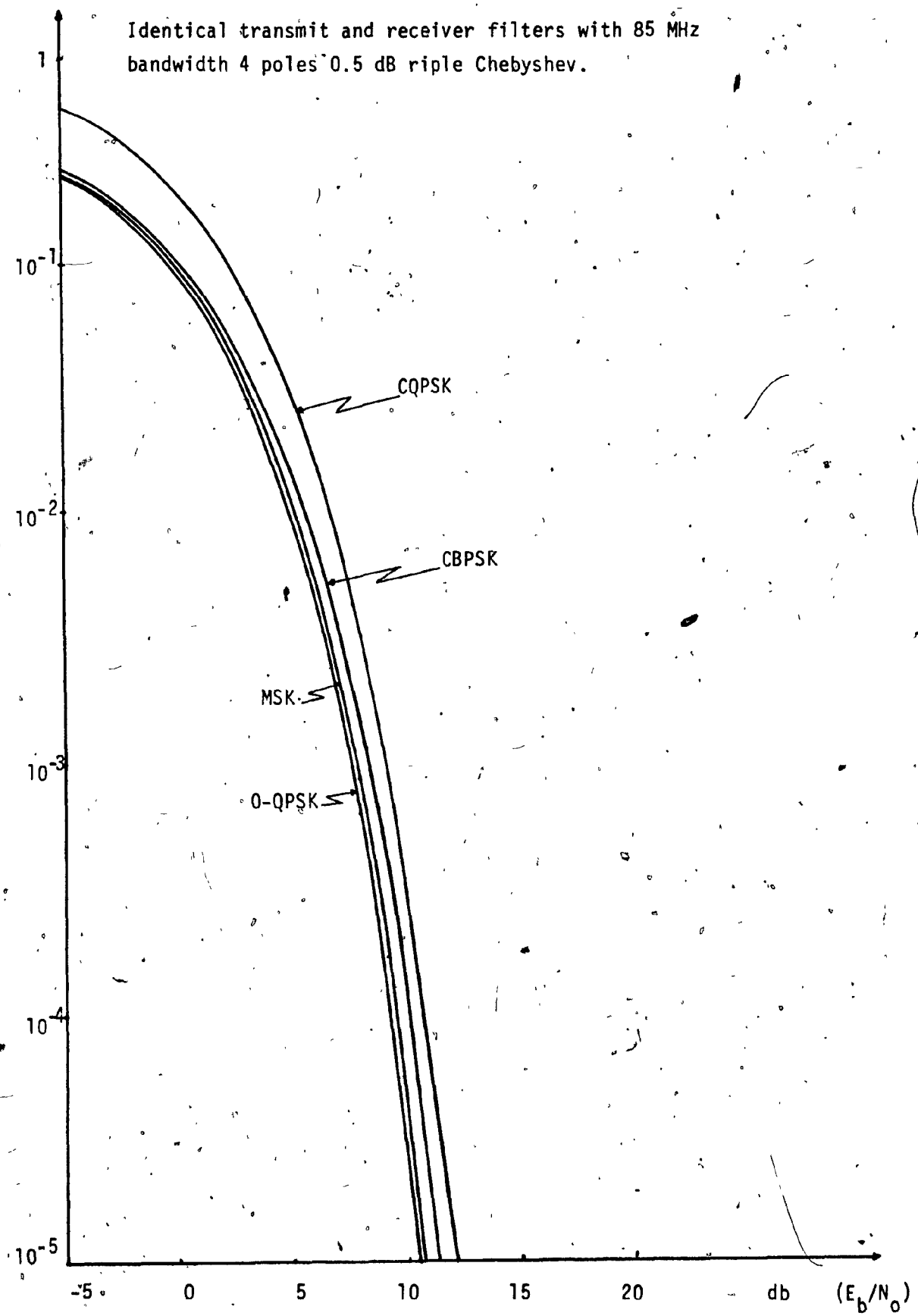

Fig. 5.3.2 Comparative Bit-Error Rates at 65.5 MBauds with a TWTA Input Back-off of 1 dB. [4]

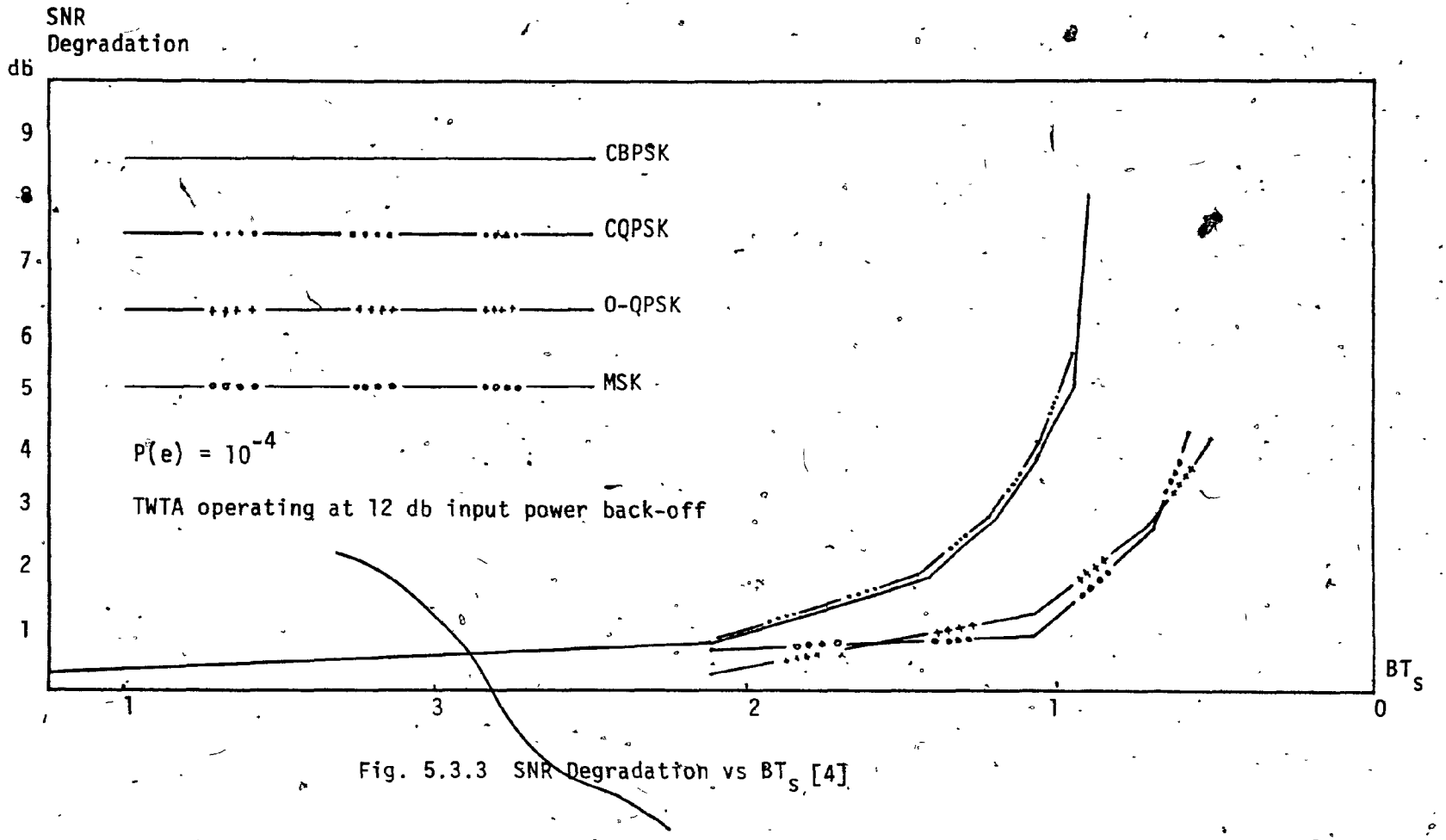

Fig. 5.3.3 SNR Degradation vs BT_s [4]

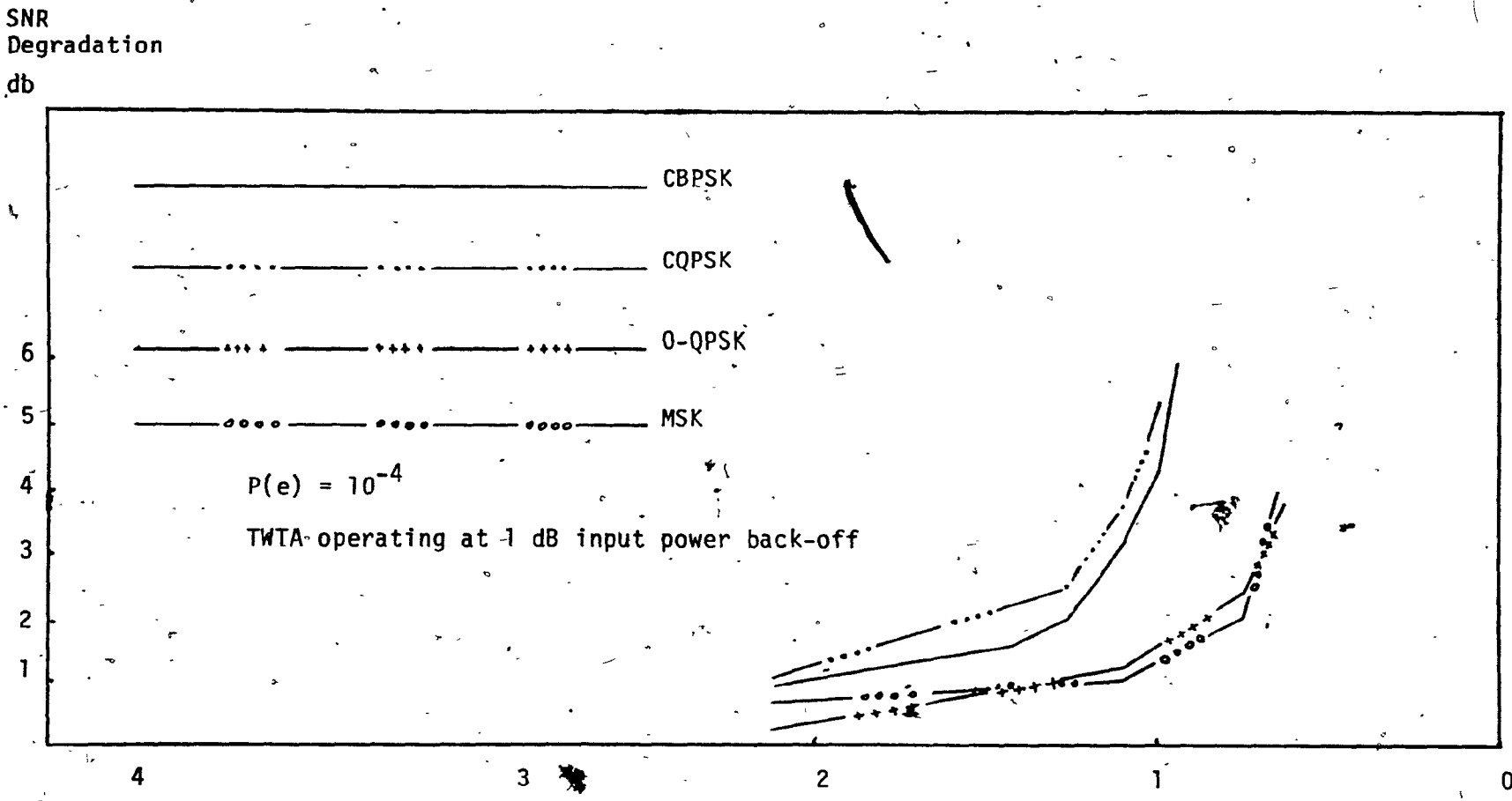

Fig. 5.3.4 SNR Dégradation vs BT_s [4]

for BER = 10^{-4} and with the TWTA operating at 12 dB and 1 dB input power back-off respectively. These figures indicate that O-QPSK and MSK perform better than QPSK for values of BT_S less than 2 with the superiority becoming greater as BT_S is reduced. The SNR degradation between O-QPSK and MSK is not significant while QPSK is about 0.5 to 1 dB worse than the previous two schemes.

5.3.2 Comparative Performance in Narrowband and Wideband Channels

In the design of an overall satellite system, two very important constraints must be considered. These are:first, the high power amplifier (HPA) at the transmitting station and the TWTA at the satellite transponder are usually operated as close to saturation as possible and second, the available transmitted bandwidth needs to be restricted to reduce adjacent channel interference.

A typical block diagram of a satellite channel model with upper and lower adjacent channel interference sources is shown in Fig. 5.3.5. Figure 5.3.6 shows the channel spacing of the two typical cases, i.e. narrowband and wideband channels. The transmitter filters eliminate adjacent channel interference signal components. However, since HPA operates in nonlinear mode, at its output some out-of-band spectra is reproduced. This power spectrum spreading interferes with adjacent channels in the up-link,especially when HPA output filters are not employed by the system. The interference in the down-link is minimal because the satellite transponder is usually equipped with separation filters. The combined signal passes through the input separation filter which suppresses the interference from adjacent channels. Noise is added at the TWTA output and the resultant signal passes through the receiver

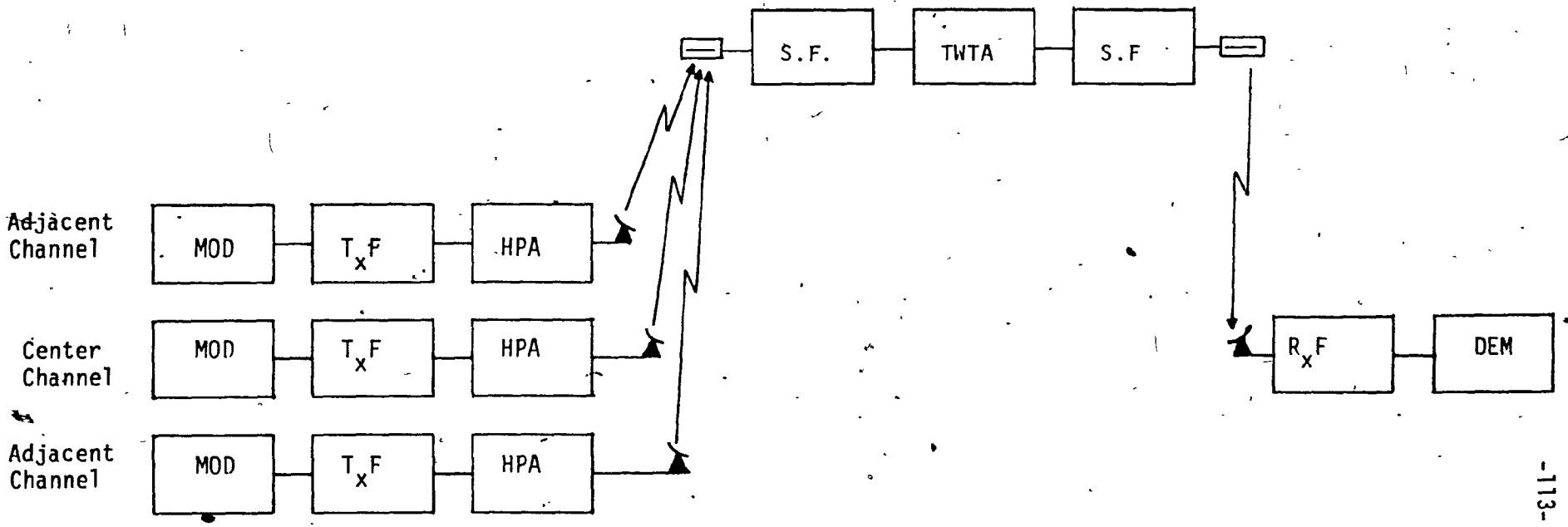

Fig. 5.3.5 Satellite Channel Model

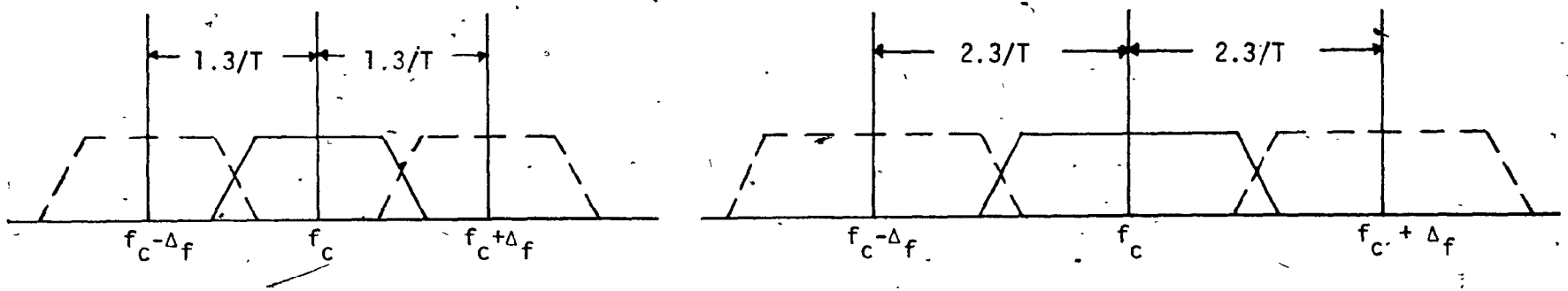

(a) Narrow-band Model

(b) Wide-band Model

Fig. 5.3.6 Channel Spacing

filter and demodulator.

Based on computer simulation results, it was found [1] that the best combination of filters for nonlinear channels is a sharp cut-off filter at the transmitter and a Nyquist shaping filter with equalizer at the receiver.

Equivalent power loss for various input back-offs for both HPA and TWTA is shown in Fig. 5.3.7. It can be seen that in narrowband nonlinear channels, QPSK is the best modulation technique. In wideband channels, O-QPSK is the best for small input back-off, while MSK becomes better as we move far from the saturation region. Fig. 5.3.8 shows the equivalent power loss when the TWTA input of the center channel is attenuated. It is seen that in the narrow band model, MSK degrades faster, followed by O-QPSK and with QPSK degrading slower. In a wideband model, however, the QPSK degrades most quickly, with the MSK next and with O-QPSK degrading scarcely. The carrier phase rms jitter was found to be 0.44°, 0.95° and 0.99° for QPSK, MSK and O-QPSK respectively in the wideband model with (6/4) dB back-off. In the narrowband case, the corresponding values are 0.98°, 4.0° and 4.3°. These values indicate that the carrier recovery in O-QPSK and MSK is much more difficult than in QPSK if a multiply by four (X4) multiplier is employed to recover the carrier. It should be noted, however, that the carrier in MSK can be also accomplished by squaring the received signal, and therefore the carrier phase rms jitter would be expected to be less than the aforementioned value. Figure 5.3.9 shows the rms phase jitter in recovered carrier for three back-off values. The reason that O-QPSK and MSK suffer more phase jitter in the recovered carrier is their large envelope fluctuations at the sampling instants. This was explained in Section 5.1.

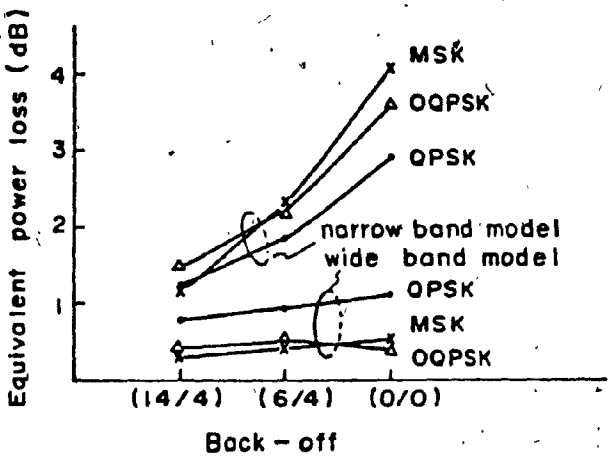

Fig. 5.3.7 Equivalent Power Loss vs HPA & TWTA Back-off [1]

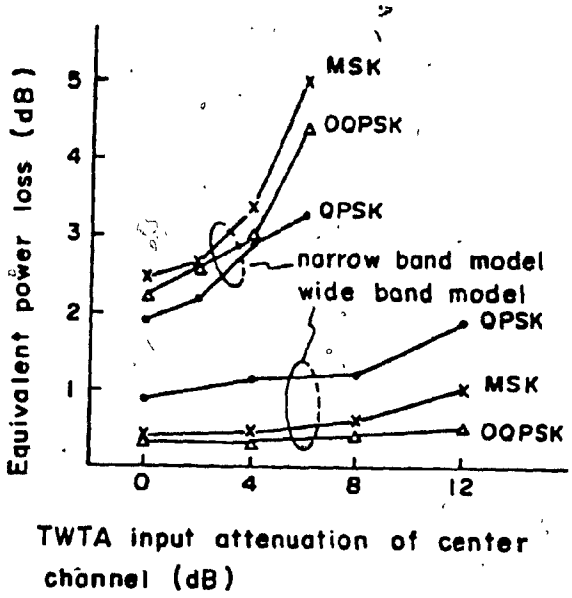

Fig. 5.3.8 Equivalent Power Loss vs TWTA Input Attenuation of Center Channel [1]

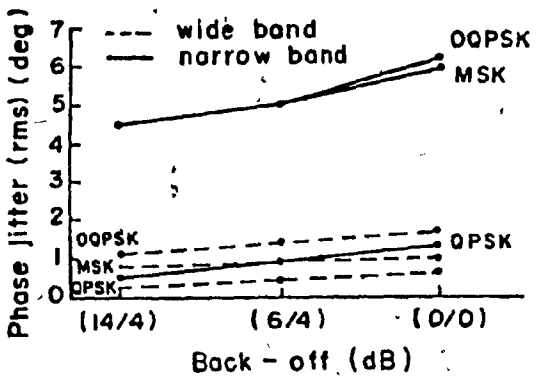

Fig. 5.3.9 Phase Jitter of Recovered Carrier [1]

5.3.3 Channel Performance With and Without ACI

Adjacent Channel Interference (ACI) occurs both on the up-link and on the down-link. Generally, it is caused by nonlinear spectrum spreading. Up-link adjacent channel interference can be controlled by backing off the transmitter or by filtering its output. Down-link adjacent channel interference is caused by the nonlinear TWTA spectrum spreading.

As discussed previously, when PSK signals are transmitted through bandlimited nonlinear satellite channels, the modulated carrier introduces amplitude variations of the envelope. In conjunction with the AM/PM conversions effect present in a nonlinear environment, this envelope fluctuation introduces spectrum spreading and additional intersymbol interference. Since the carrier and the clock in a coherent system are derived from the received spectrum, both are subjected to phase jitter caused by the spectrum distortion. All of these factors degrade more the performance of a system as nonlinearity increases.

For a typical narrowband satellite channel at an error rate of 10^{-4}, with no adjacent channel interference and phase/timing jitter, and with an input back-off of (14/4) dB, the equivalent power loss was measured in [3] as a function of BT_s. A Nyquist low-pass transmit filter and a receive filter with 45% roll-off were used. Fig. 5.3.10 illustrates the computed equivalent loss. It is seen that for QPSK the channel loss reaches a minimum of BT_S = 1.1 whereas for O-QPSK and MSK the channel losses indicate greater performance degradation than QPSK in the receiver product (BT_S) interval 0.9 to 1.4.

Taking into consideration adjacent channel interference the system performance degradation was also examined for three different

BT_S products. The HPA and TWTA were operating at (0/0) dB input back-off. Figures 5.3.11 to 5.3.13 show the bit error rate versus E_b/N_o performance of the channel with and without ACI. With tight transmit filtering, BT=1, the QPSK has better performance with and without ACI, than O-WPSK and MSK. On the other hand, for wider channel configuration ($BT \geq 1.5$) and ACI the O-QPSK outperforms the MSK and QPSK. Without ACI the order for better performance is reversed. Thus, in any event QPSK offers better performance in narrowband nonlinear channels.

Lundquist [2] in his study for the Intelsat V 60Mb/s satellite system through a 36 MHz bandwidth channel, with adjacent channels spaced 40 MHz apart, also concluded that in a narrowband nonlinear channel QPSK outperforms O-QPSK. In the same study, it was found that O-QPSK is more sensitive to the pulse shaping (Nyquist roll-off) than QPSK. In the study of the European Communication Satellite (ECS) 120 Mb/s system, Harris [16] showed that QPSK outperforms O-QPSK in the narrowband channel environment of ECS.

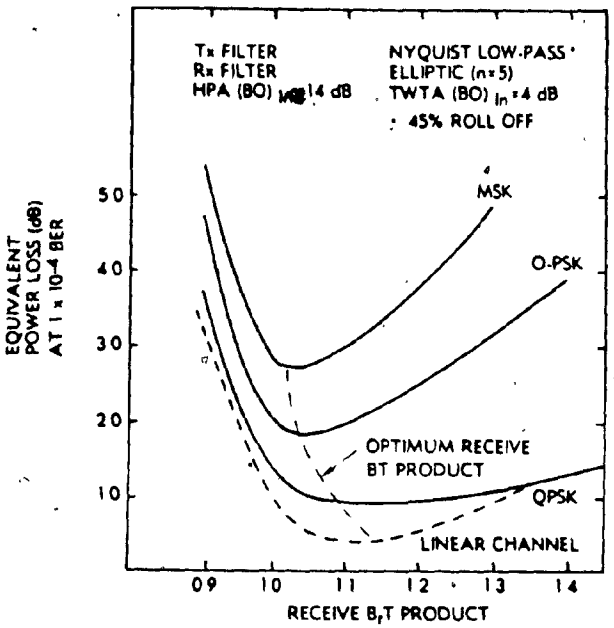

Fig. 5.3.10 Equivalent Power Loss vs BT_s [3]

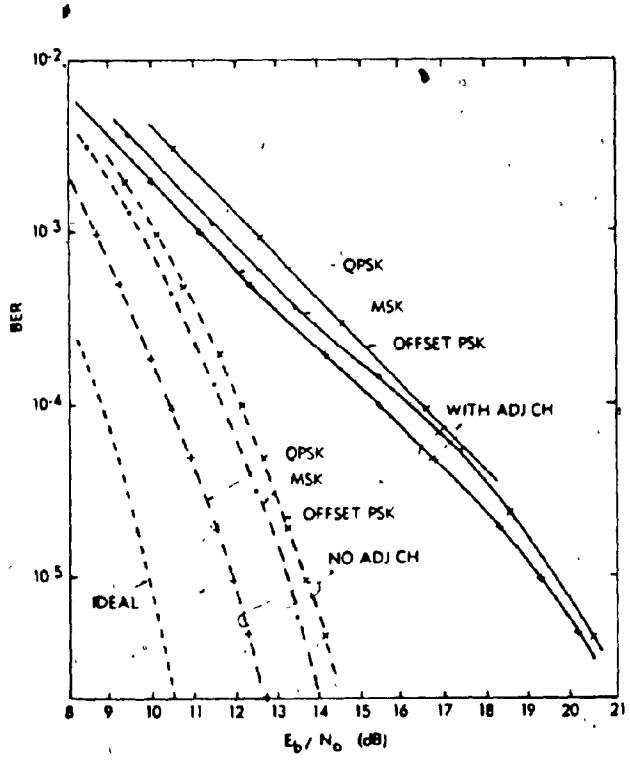

Fig. 5.3.11 BER Performance
(BT_s = 1, HPA & TWTA Back-off = 0dB) [3]

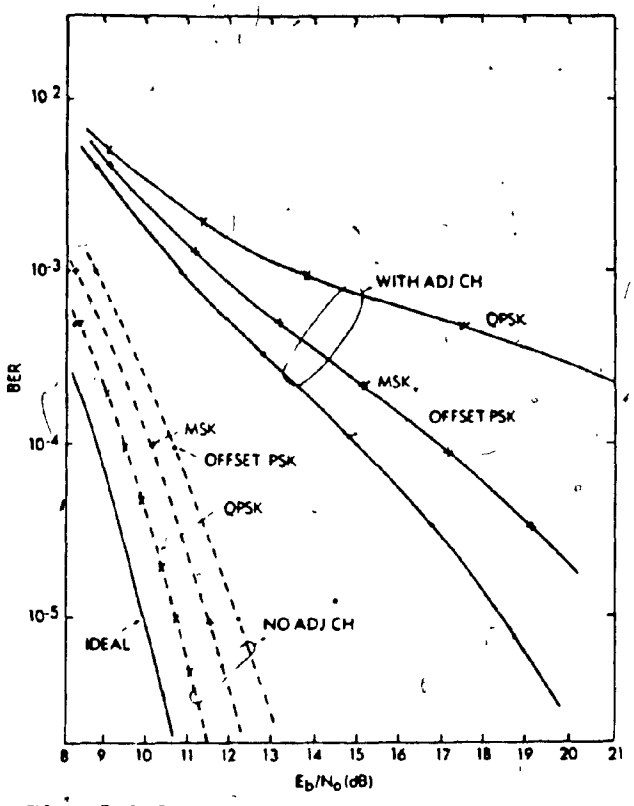

Fig. 5.3.12 BER Performance

(BT_s = 1.5, HPA & TWTA Back-off = 0dB) [3]

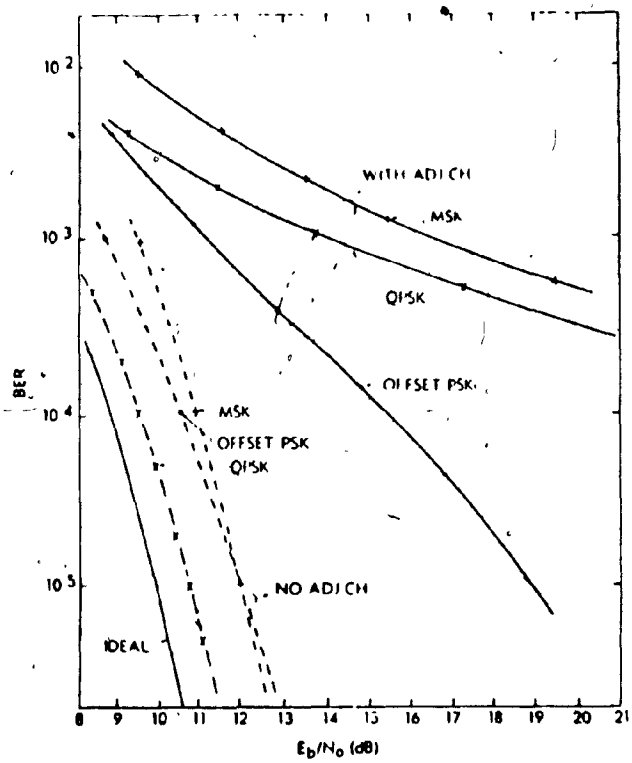

Fig. 5.3.13 BER Performance

(BT_s = 2, HPA & TWTA Back-off = 0dB) [3]

CHAPTER SIX

CONCLUSION

In this report, the two most popular modulation techniques of the PSK family, that is, the conventional QPSK and the offset (or staggered) QPSK have been analytically presented along with their behavior when transmitted through a bandlimited nonlinear satellite environment.

As was shown, QPSK and O-QPSK consist of two quadrature carrier components which are binary phase modulated by rectangular pulses of rate equal to half the data rate. The difference between the two singalling techniques is that in O-QPSK, the two binary modulation sequences are shifted in the relative alignment of an amount equal to the data bit period. In QPSK modulation, the carrier can assume one of the following phase conditions at a given instant: 0°, 90°, 180° and -90°. A carrier phase shift of 180°, however, results in the most severe amplitude depression of the modulated signal envelope caused by bandlimiting. When both quadrature channel data change phase simultaneously, the envelope goes through zero amplitude. This envelope fluctuation is deleterious to the system in a a nonlinear environment because it causes distortion and out-of-band spectrum restoration at the output of the TWTA by its AM/AM and AM/PM conversion effects. As was mentioned in Chapter Three, this results in adjacent channel interference. The 180° carrier shifts are avoided in O-QPSK modulation, by delaying one quadrature channel by one bit time interval. Thus when only one channel data change phase at the keying instant and ± 90° carrier phase shifts arise the maximum envelope fluctuation in O-QPSK is only 3 dB. Therefore,

less spectrum spreading will occur when the signal passes through a nonlinear device. This property is very desirable for communications in nonlinear channels, and because of this, O-QPSK has been foreseen to be more acceptable than QPSK in a nonlinear environment.

One special case of O-QPSK is MSK (or FFSK) which avoids phase transitions altogether due to half cosine shape of the data modulating pulses, and further suppression of out-of-band interference can be obtained in bandlimiting-hardlimiting applications. Although, however, MSK has a smoother phase transition than that of O-QPSK, its main spectral lobe, single-sided bandwidth, is 50% wider than that of QPSK or O-QPSK, as illustrated in Chapter Three. Because of this, the best way to utilize the spectral characteristics of MSK is to use wideband filters, except that this is of no great use for communications satellites due to large number of applications with closely spaced channels.

Although O-QPSK has smaller overall amplitude fluctuations than QPSK, at the critical sampling instants it has much larger amplitude variations than QPSK. Thus, after passing through a nonlinear device the fact that the I channel sampling point coincides with the transition of the Q channel, and vice versa, causes scattering of the signal at the sampling point, which in turn is translated into intersymbol interference. On the other hand, the QPSK signal due to the relatively smaller amplitude fluctuation at the sampling instant, after passing through a nonlinear device, the sampling point is still concentrated at a fixed point and hence correspondingly less intersymbol interference is caused. As a result, larger degradations in the overall system performance of O-QPSK are inherent, in comparison to QPSK.

The generation and detection process for QPSK and O-QPSK

signals were presented. The three most popular methods of recovering the carrier reference using nonlinear signal processing were also described as well as the NRZ to RZ digital code conversion and pre-demodulation methods for the bit timing recovery. It was shown that for QPSK the data coding which takes care of the phase ambiguities of the recovered carrier references can be implemented by means of differential coding on pairs of bits. This is not possible for O-QPSK where differential encoding can be performed by alternating exclusive-OR and exclusive-NOR operations applied to the outputs of the serial-to-parallel converter which incorporates the one half symbol delay to one of its two outputs. The data decoding in O-QPSK is accomplished by exclusive-ORing the demodulated I- and Q- data, and then gating the output with a clock at the baud rate the desired data stream is recovered. The use of an exclusive-OR gate also resolves the uncertainty of the I and Q channel identification.

The QPSK and O-QPSK signal analysis and behaviour in bandlimited nonlinear satellite channels was shown that in severely bandlimited channels, O-QPSK recovered carrier has much larger phase jitter than that of QPSK, resulting in large overall system performance degradation. However, O-QPSK is more resistant to carrier phase error than QPSK. Comparative performance studies based on simulation results indicate that QPSK is the optimum modulation format for narrowband nonlinear channels. For relaxed bandwidth channels O-QPSK and MSK are more preferable.

REFERENCES

1. S. Murakami, Y. Furuya, Y. Matsuo and M. Sugiyano, "Modulation schemes comparative study for nonlinear satellite channel", Conference Proceedings, ICC '78, Toronto, Canada, June 1978, pp. 19.2.1 - 19.2.5.

2. L. Lundquist, "Modulation techniques for band and power limited satellite channels", 4th International Conference on Digital Satellite Communications, Montreal, Canada, Oct. 1978, pp.94 - 100.

3. D. Chakraborty, T. Noguchi, S.J. Campanella and C.J. Wolejsza, "Digital modem design for nonlinear satellite channels", 4th International Conference on Digital Satellite Communications, Montreal, Canada, Oct. 1978, pp. 123-130.

4. H.C. Chan, D.P. Taylor and S.S. Haykin,"Comparative Evaluation of Digital Modulation Techniques: Executive Summary", CRL-18 Part I, McMaster University, Hamilton, Canada.

5. D.P. Taylor, S.S. Haykin and H.C. Chan,"Comparative Evaluation of Digital Modulation Techniques: Literature Survey" CRL-18 part II, McMaster University, Hamilton, Canada, April 1974.

6. R.E. Ziemer and W.H. Tranter,"Principles of Communications", Houghton-Mifflin Company, 1976.

7. R.W. Lucky, J. Salz and E.J. Weldon, "Principles of Data Communication", McGraw-Hill Book Company, 1968.

8. W.R. Bennett and J.R. Davey,"Data Transmission", McGraw-Hill Book Company, 1965.

9. S. Gromeyer and A. McBride,"MSK and OFFset QPSK modulation", IEEE Transactions on Communications, August 1976, pp. 809-819.

10. S.A. Rhodes,"Effects of Hard Limiting on Bandlimited Transmissions with Conventional and Offset QPSK Modulation", NTC '72, 20F1-20F7, 1972.

11. M.J. Eric,"Intermodulation Analysis of Non-linear Devices for Multiple-Carrier Inputs", CRC Report No. 1234, Ottawa, Nov. 1972.

12. G. Robinson, O. Shimbo and R. Fang,"PSK Power Spectrum Spreading Produced by Memoryless Nonlinear TWT's" COMSAT Technical Review, Vol.3, No.2, Fall 1973, pp. 227-255.

13. T. Mizumo, N. Morina and T. Bamekawa, "Transmission Characteristics of an M-ary Coherent PSK Signal via a Cascade of N Bandpass Hard Limiters", IEEE Trans. on Comm.,Vol. COM-24, No.5, May 1976, pp. 540-545.

14. D.G. Leeper,"A Universal Digital Data Scrambler", BSTJ, Vol. 52, No. 10, Dec. 1973.

15. H. Yamamoto, K. Hirade and Y. Watanabe,"Carrier Synchronizer for Coherent Detection of High-Speed Four-Phase-Shift-Keyed Signals", IEEE Trans. on Comm., Vol. COM-20, No.4, Aug. 1972.

16. R.A. Harris, "Transmission Analysis and Design for the ECS System", 4th International Conference on Digital Satellite Communications, Montreal, Canada, Oct. 1978, pp. 81-93.

17. A.J. Viterbi, "Principles of Coherent Communication",McGraw Hill Book Company, 1966, pp. 198-204.

18. E. Constellano,"Relative Performance of Conventional QPSK and Staggered QPSK Modulation in a Nonlinear Channel", ESA, Vol.2, 1978, pp. 37-47.

19. C. Devieux, Jr., "QPSK Bit Error Rate Performance as Affected by Cascaded Linear and Nonlinear Elements", COMSAT Technical Review, Vol. 8, No.1, Spring 1978, pp. 205-218.

20. J.J. Spilker, "Digital Communications by Satellite", Prentice Hall Inc., 1977.

21. H. Taub and D.L. Schilling, "Principles of Communication Systems", McGraw-Hill Book Company, 1971.

22. J.C.Y. Huang and K. Feher,"Performance of Bandlimited QPSK, OKQPSK and MSK Signals Through Cascaded Nonlinearities", ICC'79, pp.34.4.1 to 34.4.5.

23. K. Feher, "Digital Modulation Techniques in an Interference Environment" Don White Consultants, Inc. 1977.

24. P.P. Giusto, "L-PSK: A New Type of PSK Modulation", Alta Frequenza, Vol. 18, Dec. 1974.

25. R.K. Kwan,"The Effects of Filtering and Limiting A Double-Binary PSK Signal", IEEE Trans. on Aerospace and Electronic Systems, Vol. AES-5, No.4, July 1969.

26. S.A. Rhodes,"Effect of Noisy Phase Reference on Coherent Detection of Offset-QPSK Signals", IEEE Trans. on Comm., Vol. COM-22, No.8, August 1974.

27. L. Lundquist, M. Lopriore and F.M. Gardner", Transmisstion of 4ϕ-Phase-Shift Keyed Time-Division Multiple Access over Satellite Channels", IEEE Trans. on Comm., Vol. COM-22, No.9, Sept. 1974.

28. L. Lundquist, M. Shum, and S. Fredricsson,"Pulse Shaping in Bandlimited Digital Satellite Systems", IEEE Trans. on Comm., Vol. COM-26, No.4, April 1978.

29. S.A. Fredricsson,"Optimum Receiver Filters in Digital Quadrature Phase-Shift-Keyed Systems with a Nonlinear Repeater", IEEE Trans. on Comm., Vol. COM-23, No.12, December 1975.

30. F.M. Gardner,"Clock Recovery from a Nonlinear Channel", ESA, Vol.2, 1978.

31. A. Berman and C.E.Mahle,"Nonlinear Phase Shift in Traveling-Wave Tubes as Applied to Multiple Access Communications Satellites", IEEE Trans. on Comm., Vol. COM-18, No.1, Feb. 1970.

32. B.E. Tyree and J.F. Bailey,"An Investigation of the Effects of the Error Rate of Multiple Phase-Shift-Keyed Signals Through a Hard Limited", IEEE Trans. on Comm., June 1972.

33. I. Kalet,"A Look at Crosstalk in Quadrature-Carrier Modualtion Systems", IEEE Trans. on Comm., Vol. COM-25, No.9, Sept. 1977.

34. "Seminar Notes on Digital Communication and Signal Processing" University of Ottawa, Ottawa, Canada, Dec. 1978.

35. H. Nyquist, "Certain Topics in Telegraph Transmission Theory", AIEE Transactions, April 1928.

36. J.P. Costas,"Synchronous Communications", Proceedings of IRE, Vol.44, 1956, pp. 1713-1718.

37. S. Pasupathy,"Minimum Shift Keying: A Spectrally Efficient Modulation", IEEE Communications Magazine, Vol. 17, No. 4, July 1979.

38. R. de Buda, Fast FSK Signals and Their Demodulation Canadian Electrical Eng. Journal, Vol. 1, No. 1, pp. 591-596, 1976.

39. S. Stein and J.J. Jones,"Modem Communication Principles with Application to Digital Signaling", McGraw-Hill Book Company, 1967.